

AD-A152 244

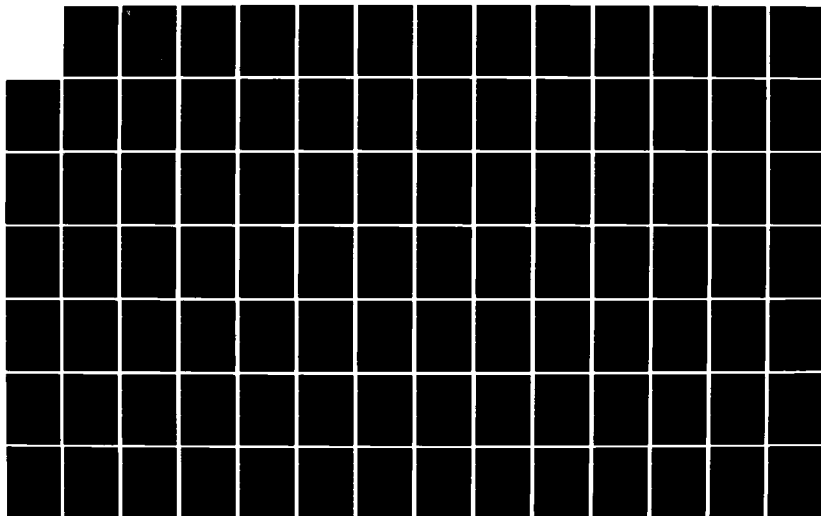
ADVANCED ENERGY STORAGE SYSTEMS(U) IAP RESEARCH INC
DAYTON OH A CHALLITA ET AL JAN 85 IAP-TR-83-7
AFRPL-TR-84-899 F04611-82-C-0029

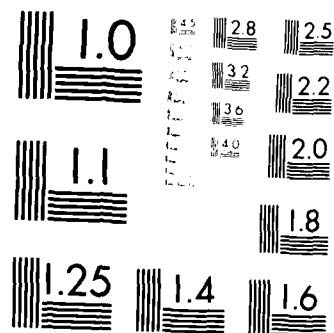
1/3

UNCLASSIFIED

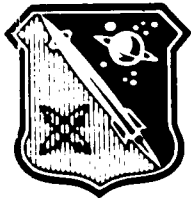
F/G 21/3

NL





MICROCOPY RESOLUTION TEST CHART
NATIONAL BUREAU OF STANDARDS-1963-A



AFRPL TR-84-099

AD:

Final Report
for the period
1 June 1982 to
1 September 1984

Advanced Energy Storage Systems

January 1985

Authors:
A. Challita
J. P. Barber
T. J. McCormick

IAP Research, Incorporated
7546 McEwen Road
Dayton, Ohio 45429-3723

IAP-TR-83-7
F04611-82-C-0029

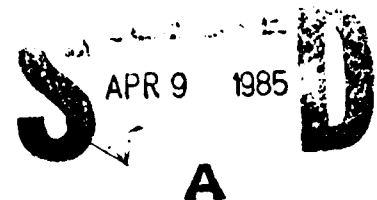
Approved for Public Release

Distribution unlimited. The AFRPL Technical Services Office has reviewed this report, and it is releasable to the National Technical Information Service, where it will be available to the general public, including foreign nationals.

prepared for the:

**Air Force
Rocket Propulsion
Laboratory**

Air Force Space Technology Center
Space Division, Air Force Systems Command
Edwards Air Force Base,
California 93523



AD-A152 244

DTIC FILE COPY

NOTICE

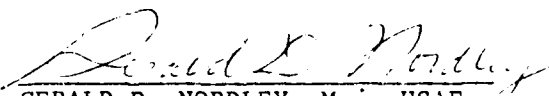
When U.S. Government drawings, specifications, or other data are used for any purpose other than a definitely related government procurement operation, the government thereby incurs no responsibility nor any obligation whatsoever, and the fact that the government may have formulated, furnished, or in any way supplied the said drawings, specifications, or other data, is not to be regarded by implication or otherwise, or conveying any rights or permission to manufacture, use, or sell any patented invention that may in any way be related thereto.

FOREWORD

This final technical report was submitted by IAP Research, Inc., 7546 McEwen Road, Dayton, OH 45459 under Air Force Rocket Propulsion Laboratory contract No. F04611-82-C-0029.

This technical report has been reviewed and is approved for publication and distribution in accordance with the distribution statement on the cover and on the DD Form 1473.


CURTIS C. SELPH
Project Manager


GERALD D. NORDLEY, Maj, USAF
Chief, Advanced Propulsion
Branch

FOR THE DIRECTOR


CLARK W. HAWK
Chief, Liquid Rocket Division

REPORT DOCUMENTATION PAGE

1a REPORT SECURITY CLASSIFICATION UNCLASSIFIED			1b RESTRICTIVE MARKINGS	
2a SECURITY CLASSIFICATION AUTHORITY			3 DISTRIBUTION/AVAILABILITY OF REPORT	
2b DECLASSIFICATION/DOWNGRADING SCHEDULE			Approved for Public Release. Distribution Unlimited.	
4 PERFORMING ORGANIZATION REPORT NUMBER(S) IAP-TR-83-7			5. MONITORING ORGANIZATION REPORT NUMBER(S) AFRPL-TR-84-099	
6a NAME OF PERFORMING ORGANIZATION IAP Research, Inc.		6b. OFFICE SYMBOL (If applicable)	7a. NAME OF MONITORING ORGANIZATION Air Force Rocket Propulsion Laboratory	
6c ADDRESS (City, State and ZIP Code) 7546 McEwen Rd Dayton, Ohio 45429-3723		7b. ADDRESS (City, State and ZIP Code) AFRPL/LKCS, Stop 24 Edwards Air Force Base, CA 93523-5000		
8a NAME OF FUNDING/SPONSORING ORGANIZATION		8b OFFICE SYMBOL (If applicable)	9. PROCUREMENT INSTRUMENT IDENTIFICATION NUMBER F04611-82-C-0029	
8c ADDRESS (City, State and ZIP Code)		10 SOURCE OF FUNDING NOS		
		PROGRAM ELEMENT NO	PROJECT NO	TASK NO
11 TITLE (Include Security Classification) ADVANCED ENERGY STORAGE SYSTEMS (U)		62302F	5730	05
12 PERSONAL AUTHOR(S) Challita, A., Barber, J. P., and McCormick, T. J.				
13a. TYPE OF REPORT Final		13b TIME COVERED FROM 82/6/1 TO 84/9/1		14 DATE OF REPORT (Yr., Mo., Day) 85/01
15 PAGE COUNT 201				
16 SUPPLEMENTARY NOTATION				
17 COSATI CODES			18 SUBJECT TERMS (Continue on reverse if necessary and identify by block number)	
FIELD	GROUP	SUB GR		
10	03		Electromagnetic Propulsion, Orbit Transfer, Stationkeeping, Optimization, Energy Storage/Power Conditioning (ES/PC), Pulsed Inductive Thruster (PIT), Teflon Pulsed Plasma Thruster (TPP), Magnetoplasmadynamic Thruster (MPD).	
19 ABSTRACT (Continue on reverse if necessary and identify by block number)				
<p>This report describes the selection, sizing, and optimization of energy storage/power conditioning systems (ES/PC) for the electromagnetic propulsion systems. An ES/PC is the interface between an electromagnetic thruster and a primary power source. The ES/PC accepts the relatively low, continuous power output from the primary power source, and converts it to a series of high power pulses and delivers it to the thruster. The ES/PC minimizes the primary power requirements while maximizing the thruster performance.</p> <p>A selection, sizing, and optimization can be achieved if an optimization criterion exists, and if the ES/PC is examined within the context of the integrated propulsion system. We selected mass minimization as the optimization criterion. To develop the selection methodology, we identified the requirements imposed on the ES/PC and parametrically related the ES/PC performance to the propulsion system outputs.</p>				
20 DISTRIBUTION AVAILABILITY OF ABSTRACT UNCLASSIFIED-UNLIMITED <input type="checkbox"/> SAME AS RPT <input checked="" type="checkbox"/> DTIC USERS <input type="checkbox"/>			21 ABSTRACT SECURITY CLASSIFICATION UNCLASSIFIED	
22a NAME OF RESPONSIBLE INDIVIDUAL Curtis C. Selph			22b TELEPHONE NUMBER (Include Area Code) (805) 277-5168	22c OFFICE SYMBOL LKCS

Block 18 (Continued): Electric Rail Gun Thruster (ERG), Inductors, Capacitors, Compulsators.

Block 19 (Continued): The propulsion systems considered covered a range of missions, thrusters, primary power options, and ES/PC options. The missions were: ten year stationkeeping and orbit transfer from lower earth orbit (LEO) to geosynchronous orbit (GEO) of large payloads (up to 25 metric tons). The thrusters considered were: the Teflon inductive thruster (TIP), and the electric rail gun (ERG). The primary power options were: solar cell arrays, solar thermophotovoltaic, nuclear thermonic, nuclear thermoelectric, nuclear Brayton cycle, nuclear Rankine cycle, and nuclear magnetohydrodynamic (MHD). The ES/PC options were: capacitive, normal inductive, superconducting inductive, and inertial based systems.

We exercised the selection method over the range of missions, thrusters, and primary power sources, and found that for each mission/thruster combination, there is one ES/PC system which minimizes the mass of the propulsion system.

Table of Contents

1	INTRODUCTION	1
2	ES/PC ANALYSES APPROACH	3
	2.1 MISSION CHARACTERISTICS	3
	2.1.1 Stationkeeping	3
	2.1.2 Orbit Transfer	5
	2.2 INTEGRATED ELECTROMAGNETIC PROPULSION SYSTEM	7
	2.2.1 The Primary Power System	8
	2.2.2 The ES/PC	9
	2.2.3 The Propellant System	10
	2.2.4 The Thruster	11
	2.3 PROPULSION SYSTEM SELECTION AND SIZING	12
	2.3.1 The Mission	12
	2.3.2 Propulsion System Optimization	13
	2.3.3 Summary	14
3	INTEGRATED PROPULSION SYSTEM PERFORMANCE AND MODELING	15
	3.1 PRIMARY POWER CHARACTERISTICS	15
	3.2 THRUSTER CHARACTERISTICS	17
	3.2.1 Pulsed Inductive Thruster (PIT)	17
	3.2.2 Teflon Pulsed Plasma Thruster (TPP)	18
	3.2.3 Magnetoplasmadynamic Thruster (MPD)	19
	3.2.4 Electric Rail Gun Thruster (ERG)	20
	3.2.5 Thruster Performance Modeling	20
	3.2.5.1 Pulse Energy	21
	3.2.5.2 Current/Pulse Time	24
	3.2.5.3 Voltage	25
	3.2.5.4 Summary	26
	3.3 PROPELLANT SYSTEM CHARACTERISTICS	26
	3.4 ES/PC CHARACTERISTICS	27
	3.4.1 ES/PC Input/Output Constraints	28
	3.4.2 ES/PC Concepts	28
	3.4.3 Energy Store Models	31
	3.4.3.1 Capacitors	31
	3.4.3.2 Normal Inductors	36
	3.4.3.3 Superconducting Inductors	37
	3.4.3.4 The Compulsator	39
	3.4.4 Input Conditioner Models	44
	3.4.4.1 DC-DC Converters	44
	3.4.4.2 Electric Motors	46
	3.4.4.3 Series-Parallel Switching of Primary Power Modules	47
	3.4.5 Output Conditioner Models	50
	3.4.5.1 SCR'S	50
	3.4.5.2 Thyratrons	51
	3.4.5.3 Spark Gaps	54
	3.4.6 Heat Rejection System Model	57

Table of Contents (concluded)

3.5	SYSTEM INTEGRATION	58
4	RESULTS	60
4.1	EPSDES VALIDATION	60
4.1.1	EPSDES Optimization	60
4.1.2	Optimum Propulsion Systems	62
4.1.3	Comparison of EPSDES with Martin Marietta Results	62
4.1.3.1	The Stationkeeping System	63
4.1.3.2	The Orbit Transfer System	64
4.2	SENSITIVITY ANALYSIS	67
4.2.1	Payload Mass	67
4.2.2	Mission Duration	67
4.2.3	Velocity Increment	70
4.2.4	Primary Power Options	70
4.2.5	ES/PC Options	70
4.3	POINT DESIGNS	72
4.3.1	Stationkeeping Mission	73
4.3.2	Orbit Transfer Mission	75
5	CONCLUSIONS AND RECOMMENDATIONS	79
5.1	CONCLUSIONS	79
5.2	RECOMMENDATIONS	80
	REFERENCES	81
	APPENDICES	
A	PRIMARY POWER FOR ELECTROMAGNETIC PROPULSION	
B	ELECTROMAGNETIC THRUSTER MODELS	
C	INDUCTORS IN PULSE POWER SYSTEMS	
D	PARAMETRIC MODEL OF SUPERCONDUCTING ENERGY STORE FOR SPACE PROPULSION	

List of Figures

Figure		Page
1	Velocity Increment Per Year Required To Correct Eccentricity Changes By Solar Radiation	6
2	Generic Electromagnetic Propulsion System	7
3	Generic ES/PC	9
4	Power Level Range of Primary Power Systems	16
5	Power Output Voltage Range of Primary Power Systems	17
6	Cross-sectional View of Pulsed Inductive Thruster (PIT)	18
7	Teflon Pulsed Plasma Thruster (TPP)	19
8	Magnetoplasmadynamic Thruster (MPD)	20
9	Electric Rail Gun (ERG)	21
10	Generic ES/PC Functions	27
11	ES/PC Concept Using a Simple Capacitor as the Energy Store	29
12	ES/PC Concept Using an LC Circuit	29
13	ES/PC Concept Using a Multi-Stage Pulse Forming Network	29
14	ES/PC Concept Using a Normal Inductor as the Energy Store	30
15	ES/PC Concept Using a Superconducting Inductor as the Energy Store	30
16	ES/PC Concept Using a Compulsator	30
17	Parallel Plate Capacitor	32
18	Specific Energy of Capacitors Using Polypropylene Film	35
19	Specific Energy of Minimum Mass Inductors	37
20	Compensated Pulsed Alternator (Compulsator)	39
21	Compulsator Cross Section	40
22	Specific Energy of Compulsators as a Function of Pulse Energy ($f = 10$ Hz and $t_p = 1$ ms)	43
23	Specific Energy of Compulsators as a Function of the Pulse Duration ($f = 10$ Hz and $E_p = 100$ kJ)	43

List of Figures (concluded)

24	DC-DC Converter Block Diagram	45
25	DC-DC Converter Mass	45
26	DC-DC Converter Specific Mass	46
27	Specific Power of Electric Motors	48
28	Series-Parallel Switching Concept	49
29	I-V Characteristics of S-P Switched Solar Arrays	49
30	SCR's Mass Models	51
31	Thyratron Schematic	52
32	Thyratron Specific Power	54
33	Spark Gap Mass	57
34	Flowchart of the Electric Propulsion System DESign (EPSDES) Computer Program	58
35	Propulsion System Optimization (Orbit Transfer, TPP)	61
36	Optimum Propulsion System Mass (Orbit Transfer, TPP)	61
37	Optimum Propulsion System Mass for Different Payload Mass for Stationkeeping Missions	68
38	Optimum Propulsion System Mass for Different Payload Mass for Orbit Transfer Missions	68
39	Optimum Propulsion System Mass for Different Mission Duration for Stationkeeping Missions	69
40	Optimum Propulsion System Mass for Different Mission Duration for Orbit Transfer Missions	69
41	Velocity Increment Effects on Optimum Propulsion System Mass	70
42	Effects of Primary Power Options on Optimum Propulsion System Mass for Stationkeeping Missions	71
43	Effects of Primary Power Options on Optimum Propulsion System Mass for Orbit Transfer Missions	71
44	Propulsion System Mass for Different ES/PC Options for Stationkeeping Missions	72
45	Propulsion System Mass for Orbit Transfer Missions Using Different ES/PC Options	73

List of Tables

Table		Page
1	Characteristics of a Generic Class of Space Structures . . .	5
2	ΔV Required for LEO to GEO Transfer	6
3	Summary of Mission Characteristics	7
4	Specific Mass of the Primary Power Systems	16
5	Pulse Energy Coefficients	23
6	ES/PC Input Constraints and Output Requirements	28
7	Summary of ES/PC Concepts	31
8	Dielectric Properties	34
9	Stationkeeping Performance Comparison	64
10	Stationkeeping Performance Comparison (The specific energy of capacitors was assumed to be 1.7 J/kg)	65
11	Orbit Transfer Performance Comparison	66
12	Orbit Transfer Performance Comparison (The specific energy of capacitors was assumed to be 1.7 J/kg)	66
13	Stationkeeping Optimum Propulsion System for a Point Design.	74
14	Thruster Size and Characteristics for Stationkeeping Point Design	75
15	ES/PC Size and Characteristics for Stationkeeping Point Design	76
16	Orbit Transfer Propulsion System	77
17	Thruster Size and Characteristics for Orbit Transfer Mission	77
18	ES/PC Size and Characteristics for Orbit Transfer Mission .	78

List of Symbols

b	length of rotor
d	dist. separating the plates
e_p	peak eccentricity
f	operating frequency
f_e	electrical frequency
f_m	mechanical rotor speed
k	constants
k_1	constants
k_2	constants
m	mass, kg
m_{dew}	mass of dewar
m_p	propellant pulse mass
m_{ref}	mass of refrigerator
m_{sp}	specific mass
\dot{m}_p	mass flow rate
s	solar constant at 1 AU
t_d	total time (thrusting)
t_m	mission time, duration
t_p	pulse duration
v	rotor tip speed
v_e	avg. exhaust velocity
w	specific energy
w	specific power in W/kg
w_{ind}	specific energy of inductor
A	constant
A	surface area of one of the plates in a parallel plate capacitor
A_{dew}	surface area of dewar
A/M	area-to-mass ratio
C	capacitance
C	total charge, coulombs
E	electric field
E_b	breakdown strength of dielectric
E_{dis}	dissipation energy

List of Symbols (continued)

E_{ion}	ionization energy
E_p	pulse energy
E_s	energy stored
E_{KE}	kinetic energy
I	current
J	current
J_{avg}	average current
J_{th}	current, thruster
K	relative dielectric constant
L'	axial inductance gradient
M_{comp}	mass, compulsator
M_{espc}	Mass of ES/PC system
M_{pay}	payload mass
M_{pp}	primary power mass
$M_{prp\ sys}$	Mass of propellant system
M_{rot}	mass, rotor
M_{tank}	Mass of storage tank
M_{tot}	Total Mass
N	number of cycles
P	average power, W
P	number of field poles
P_o	refrigeration power
P_{pp}	average power level
R	voltage reversal experienced by capacitors
V	voltage
V_{avg}	average voltage
V_f	electrode fall
V_{th}	voltage, thruster
β	eccentricity ratio
α	duty cycle
ΔV	velocity increment
ΔV_{GEO}	tangential velocity of GEO payload
$\Delta \theta$	change in payload orbital plane inclination

List of Symbols (concluded)

ϵ_0	permittivity of free space
η	efficiency
η_{espc}	efficiency of ES/PC
η_{th}	efficiency of thruster
θ	inclination of equatorial plane with respect to ecliptic or lunar orbital plane
λ	longitude, $^{\circ}\text{E}$ of Greenwich
$\dot{\lambda}$	mean angular velocity of earth motion around sun
ρ	density
ω	rotational speed, rad/s

M_{tot} is minimized by taking partial derivatives and setting them equal to zero. Since only two equations are needed, we can select which partial derivatives to use. We used the partial derivatives with respect to v_e and f given by:

$$\begin{aligned} M_{tot}/\partial v_e &= 0 \\ M_{tot}/\partial f &= 0 \end{aligned} \quad (24)$$

These equations are complex and numerical methods were used to solve them.

2.3.3 Summary

The process of selecting, sizing, and designing an integrated electromagnetic propulsion system can be summarized as follows:

- a. The mission must be defined (ΔV , M_{pay} , t_m , α).
- b. The thruster and primary power types must be chosen.
- c. The outputs of the propulsion system (m_p , v_e , f , and t_d) are selected to minimize the propulsion system and to satisfy the mission requirements (i.e., solving equations 20, 21, and 24 simultaneously).

To accomplish this selection methodology we need to develop:

- a. Thruster performance models,
- b. Primary power source mass functions,
- c. Propellant system mass functions, and
- d. ES/PC mass functions.

All mass and performance models must be developed as functions of the propulsion system outputs.

$$M_{pay} + M_{pp} + M_{espc} + M_{prp\ sys} = M_{prp} / (\exp(\Delta V / v_e) - 1) \quad (20)$$

In order to solve this equation, the mass of the propellant and the dry engine mass must be related to the thruster output parameters as described by Equations 17 to 19.

The second equation derived from the mission requirements is that the total thrust time, t_d , is related to the mission time, t_m , by:

$$t_d = \alpha t_m \quad (21)$$

where α = the thruster duty cycle.

The thruster duty cycle is defined by the mission, and Equation 21 uniquely defines the total thrust time.

No further independent relations among the thruster output parameters can be derived from the mission. The two remaining equations must be derived from propulsion system optimization.

2.3.2 Propulsion System Optimization

Optimized design of electromagnetic propulsion systems involves the minimization of deployed mass. The criterion of mass minimization applied to system selection and sizing is illustrated as follows.

Mathematically, minimization of the total propulsion system mass may be thought of as minimizing a function (the propulsion system mass) of several independent variables (the propulsion system outputs) subject to certain auxiliary restrictions (the mission requirements). The propulsion system mass is the sum of the subsystem masses:

$$M_{tot} = M_{pp} + M_{espc} + M_{prp\ sys} \quad (22)$$

which can be expressed as a function of the propulsion system outputs since all the subsystem masses are uniquely related to these variables (Equations 17 to 19). Then M_{tot} can be written as:

$$M_{tot} = F(m_p, v_e, f, t_d) \quad (23)$$

If these relations were known, inspection of Equations 5, 8 and 12 shows that all the major propulsion subsystem masses (and other performance requirements) are uniquely related to the propulsion system outputs as:

$$M_{pp} = M_{pp}(m_p, v_e, f, t_d) \quad (17)$$

$$M_{espc} = M_{espc}(m_p, v_e, f, t_d) \quad (18)$$

$$M_{prp\ sys} = M_{prp\ sys}(m_p, f, t_d) \quad (19)$$

Therefore, the performance characteristics of the major subsystems must be known before an integrated propulsion system can be selected, sized, or designed in an optimal manner. In order to illustrate this more clearly we next examine the generic problem of propulsion system selection and sizing.

2.3 PROPULSION SYSTEM SELECTION AND SIZING

The selection and sizing of an optimal propulsion system for a specific mission is a complex task. The basic principles are simple. Propulsion system selection and sizing may be thought of as the process of choosing a combination of m_p , v_e , f and t_d which meet the mission objectives and satisfy the optimization criteria. Also, the process of choosing the propulsion system outputs results in a unique definition of the size and performance of each of the propulsion subsystems.

Mathematically, the process may be thought of as simultaneously solving four equations with four unknowns (i.e., the propulsion system outputs). In order to find unique solutions for these output parameters, four independent equations which relate the parameters to one another must be developed. The process by which this is accomplished is illustrated in the following paragraphs.

2.3.1 The Mission

The mission provides us with two of the four required equations. The first equation is derived from the momentum change which must be imparted to the payload mass. Momentum must also be imparted to the dry engine mass and the propellant. The complete equation is:

$$M_{\text{tank}} = k_1 M_{\text{prp}} \quad (11)$$

and the propellant system mass can be written as:

$$M_{\text{prp sys}} = k_2 m_p f t_d \quad (12)$$

where $k_2 > 1$. As can be seen from equation 12, thruster characteristics do not directly affect propellant mass requirements.

2.2.4 The Thruster

The thruster converts the electrical energy delivered to it from the ES/PC into kinetic energy of the pulse mass. The thruster is required to do this at a frequency and for a total time consistent with the mission requirements. The manner in which the thruster accomplishes this task has a major impact on the other subsystems in the propulsion system. Thruster performance has a first order effect on the ES/PC and primary power systems. The efficiency of the thruster will determine the energy storage and average power requirements of the system. The physics of thruster operation will determine the current and voltage levels and pulse duration required of the ES/PC.

Under 'steady' average thrusting conditions the thruster produces identical pulses and its performance should be largely independent of the pulse frequency or the total operating time. This implies that thruster performance is only dependent on pulse mass and exhaust velocity. The modeling relationships which are required may then be expressed as

$$\eta_{th} = \eta_{th}(m_p, v_e) \quad (13)$$

$$J_{th} = J_{th}(m_p, v_e) \quad (14)$$

$$V_{th} = V_{th}(m_p, v_e) \quad (15)$$

$$t_p = t_p(m_p, v_e) \quad (16)$$

$$M_{espc} = M_{espc}(E_p, J, V, f, t_p, t_d) \quad (8)$$

where J = ES/PC output current

V = ES/PC output voltage

f = operating frequency

t_p = pulse duration

t_d = thrusting time

The efficiency of the ES/PC system will also depend on these factors and may be expressed as:

$$\eta_{espc} = \eta_{espc}(E_p, J, V, f, t_p, t_d) \quad (9)$$

The relationships described by Equations 8 and 9 have not been extensively investigated. The determination of these relationships was one of the primary goals of this program.

Examination of Equations 8 and 9 indicates that four of the six parameters on which ES/PC performance depends are determined by thruster performance. These four parameters are E_p , J , V and t_p . Thruster modeling must, therefore, not only address pulse energy requirements (or efficiency) but must also treat current, voltage, and pulse duration.

2.2.3 The Propellant System

The primary functions of the propellant system are to store the propellant and to provide the reaction mass for the propulsion system. The propellant mass is a significant mass component of the total propulsion system and in some missions will dominate propulsion system mass. The propellant mass is related to propulsion system outputs by:

$$M_{prp} = m_p f t_d \quad (10)$$

The propellant storage container mass may be a considerable fraction of the propellant system mass, depending on the propellant type (gas or solid) and on the way it is stored (i.e., gas propellant may be stored cryogenically or in high pressure tanks). In general, the container mass is expressed as a function of the propellant mass as:

Inspection of Equations 5, 6, and 7 indicates that the mass of the primary power system and the output power requirements are directly related to the propulsion system output parameters, m_p , v_e , f and t_d , plus the thruster and ES/PC efficiencies. The ES/PC efficiency is usually high (>80%) and has a small effect on the primary power. The thruster efficiency is not as high (<60%) and has a major impact on system performance. Thruster efficiency is an important aspect of thruster performance which must be analyzed, understood, and modeled.

2.2.2 The ES/PC

A generic ES/PC is presented in Figure 3. The primary function of the ES/PC is to store energy for each thruster pulse. In addition, the ES/PC system must condition the output to deliver an optimum pulse to the thruster (i.e., the correct current and voltage profiles). Input conditioning may also be required of the ES/PC to permit efficient charging of the energy store from the primary power source.

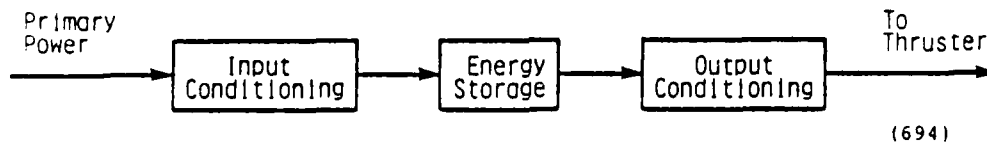


Figure 3. Generic ES/PC.

The mass of the ES/PC is dominated by the mass of the energy storage component. The mass of energy storage devices is directly related to the energy stored. Therefore, it is expected that the mass of the ES/PC will primarily depend upon the pulse energy requirements. The masses of the input and output conditioning systems depend on current and voltage levels and to some extent on frequency, pulse duration, and total propulsion system operating time (i.e., component life). Total ES/PC mass may then be expressed as:

Each of the major subsystems plays an important part in propulsion system performance. The performance characteristics of each subsystem, particularly subsystem mass, must be investigated and understood in order to optimally select, size, and design integrated propulsion systems. The generic characteristics of each subsystem and the implications these characteristics have on the propulsion system performance modeling are examined in the following paragraphs.

2.2.1 The Primary Power System

The primary power system is the basic source of energy for the propulsion system. The output of the source is electrical power at some characteristic voltage and current level. The power is delivered at a constant level to maximize the efficiency of the primary power source and minimize its mass.

The mass of the primary power source is primarily a function of the average power level required. Primary power sources for space application have been investigated extensively, and their mass can be expressed as:

$$M_{pp} = M_{pp}(P_{pp}) \quad (5)$$

where M_{pp} = primary power mass
 P_{pp} = average power level

P_{pp} is related to the pulse energy, E_p , (i.e., the energy required by the thruster for each pulse) by:

$$P_{pp} = E_p f / \eta_{espc} \quad (6)$$

where f = propulsion system operating frequency
 η_{espc} = the efficiency of the ES/PC.

E_p is determined by the kinetic energy output and the efficiency of the thruster, and is:

$$E_p = m_p v_e^2 / 2 \eta_{th} \quad (7)$$

where η_{th} = thruster efficiency.

The range of mission parameters used in this study is summarized in Table 3.

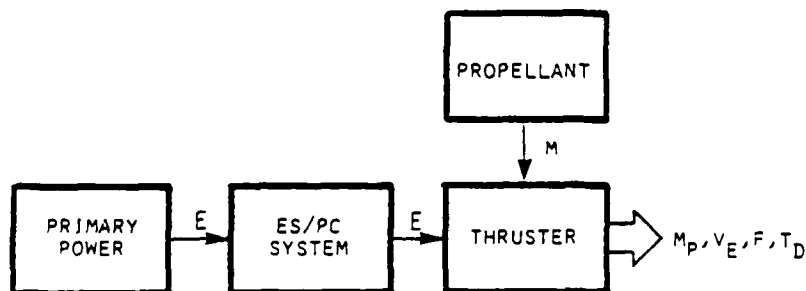
TABLE 3
SUMMARY OF MISSION CHARACTERISTICS

	Payload Mass (kg)	ΔV (m/s)	Mission Time	Duty Cycle
Stationkeeping	2000-25000	50-185/yr.	1-10 yrs	0.1-1
Orbit Transfer	2000-25000	5800	30-300 days	1

2.2 INTEGRATED ELECTROMAGNETIC PROPULSION SYSTEM

A generic electromagnetic propulsion system is illustrated in Figure 2. It consists of four major subsystems or mass components: a primary power source, an ES/PC, a propellant system (propellant and its storage containers) and the thruster itself. All of these subsystems are required to produce the thruster output, a pulse of propellant mass, m_p , at an average exhaust velocity, v_e . The propulsion system produces these mass pulses repetitively at frequency, f , for a total time, t_d .

The parameters m_p , v_e , f and t_d are the propulsion system outputs. Therefore, system performance must be modeled with these parameters as the independent variables.



(594)

Figure 2. Generic Electromagnetic Propulsion System.

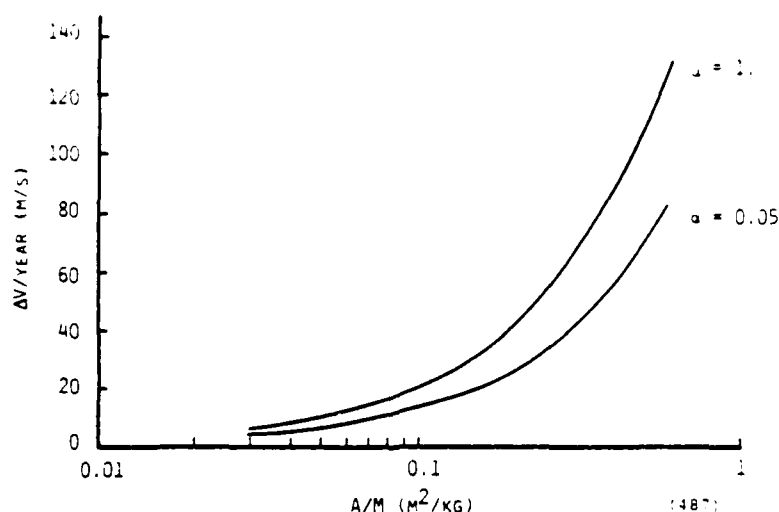


Figure 1. Velocity Increment Per Year Required To Correct Eccentricity Changes Caused By Solar Radiation.

possible (about 30 days) to 300 days. The payload mass of interest is similar to stationkeeping payload mass (2000 to 25000 kg).

TABLE 2

ΔV REQUIRED FOR LEO TO GEO TRANSFER²

Transfer	Parameter	Analytic Prediction	SECKSPOT Results	
			w/o Shadow	w/Shadow
No Inclination Change	Δu (km/sec)	4.674	4.674	4.811
	t _f (days)	40.0	40.0	51.5
Inclination Change	Δu (km/sec)	5.757	5.802	5.814
	t _f (days)	40.0	40.3	49.6

²Bauer, David P., Barber, John P., Swift, Hallock F., Vahlberg, C. Julian, 'Electric Rail Gun Propulsion Study (Advanced Electric Propulsion Technology—High Thrust)', AFRPL-TR-81-02, 1981.

A/M for a generic class of space structures which can be deployed in a single shuttle launch is presented in Table 1 and ranges from 0.08 to 0.598 m²/kg. The ΔV requirements calculated for this generic class of space structures are presented in Figure 1.

TABLE 1
CHARACTERISTICS OF A GENERIC CLASS OF SPACE STRUCTURES¹

SINGLE SHUTTLE LAUNCH			MASS	AREA/MASS	EFFECTIVE
GENERIC CLASS	SIZE		(kg)	(m ² /kg)	A/M(m ² /kg)
I PLATE STRUCTURE W/O BLANKET	MEDIUM (100 m)		1618	4.014	0.201
	LARGE (250 m)		3672	11.055	0.553
II PLATE STRUCTURE W/ BLANKET	SMALL (30 m)		1334	0.430	0.438
	MEDIUM (100 m)		11350	0.572	0.572
	LARGE (150 m)		24420	0.598	0.598
III MODULAR ANTENNA	SMALL (15 m)		2300	0.165	0.091
	MEDIUM (60 m)		8375	0.433	0.113
	LARGE (200 m)		18017	1.980	0.236
IV SERIES OF ANTENNAS	SMALL (2)		7500	0.826	0.085
	MEDIUM (3)		11250	0.802	0.085
	LARGE (4)		15000	0.764	0.084

The total ΔV requirements for all stationkeeping functions range from 50 to 184 m/s/yr mission times ranging from 1 to 10 years.

2.1.2 Orbit Transfer

The ΔV for orbit transfer is 5800 m/s. The ΔV required for LEO to GEO transfer was investigated in a previous program and the results are presented in Table 2. The mission times of interest range from the minimum

¹Smith, W. W. and Clark, J. P., 'Study of Electrical and Chemical Propulsion Systems for Auxiliary Propulsion of Large Space Systems,' NASA CR-165502, 1981.

The ΔV required to correct the payload inclination caused by solar and lunar perturbations is given by:

$$\Delta V/\text{year} = \Delta\theta \Delta V_{\text{GEO}} \quad (2)$$

where $\Delta\theta$ = required payload orbital plane inclination change (rad/yr)
 $\Delta\theta = A \sin \theta \cos \theta$
 A = constant whose value depends on the body creating the effect (0.74 for solar and 1.615 for lunar)
 θ = inclination of equatorial plane with respect to the ecliptic or lunar orbital planes
 ΔV_{GEO} = tangential velocity of GEO payload (3074.7 m/s)

Substituting back into Equation 2 we get:

$$\begin{aligned} \Delta V/\text{year} = & -(3074.7/(360/2\pi))[(0.74 \sin \theta \cos \theta)_{\text{solar}} \\ & + (1.615 \sin \theta \cos \theta)_{\text{lunar}}] \end{aligned} \quad (3)$$

The ΔV ranges from 41.2 to 51.8 m/s/yr.

The ΔV required to correct eccentricity changes caused by solar radiation effects is given by:

$$\Delta V/\text{year} = (3sk\pi/2\lambda)(\alpha\pi/2 \sin(\alpha\pi/2))(\beta/\sin^{-1} \beta) \quad (4)$$

where s = solar constant at 1 AU = $4.5 \times 10^{-6} \text{ kg}/(\text{m} \cdot \text{s}^2)$
 $k = (1+\sigma)(A/M)$
 σ = average reflectivity of payload ~ 0.3
 A/M = area-to-mass ratio (m^2/kg)
 λ = mean angular velocity of earth motion around sun
 $= 1.99 \times 10^{-7} \text{ rad/s}$
 α = duty cycle
 β = eccentricity ratio
 $= \frac{e^*}{e_p}$, e^* = maximum allowable eccentricity
 e_p = peak eccentricity that would occur if initial orbit was circular and no stationkeeping corrections were applied.

β defines the stationkeeping accuracy required and is set to zero to calculate the maximum ΔV . ΔV is a function of α and A/M ; α may be as high as 1.

SECTION 2

ES/PC ANALYSES APPROACH

The ES/PC will be examined within the context of an integrated propulsion system. The process of propulsion system selection begins with identification of the mission. The propulsion system is then sized to accomplish that mission in the most economical manner (the propulsion system is optimized for the mission). Optimized design can, in principle, always be accomplished if criteria for optimization are established. We assumed that the optimization criterion is minimization of the integrated propulsion system mass.

2.1 MISSION CHARACTERISTICS

All space propulsion systems are required to accomplish the same generic task: imparting a velocity increment, ΔV , to a payload mass, M_{pay} , in some mission time, t_m . These mission parameters are the basic, independent variables which constrain propulsion system selection and sizing, and to which propulsion system performance must be related. The range of mission parameters of interest must be identified.

2.1.1 Stationkeeping

On-orbit stationkeeping of geosynchronous payloads is required to remove accumulated disturbances caused by: longitude drift caused by triaxiality of the earth, long term increase in inclination of the payload orbital plane due to lunar and solar perturbations, and change in eccentricity caused by solar radiation effects. Stationkeeping is accomplished by supplying external torques which are provided by the propulsion system. The ΔV imposed on the propulsion system by these disturbances were calculated.

The ΔV due to longitudinal drift is expressed as:

$$\Delta V/\text{year} = (1.72 \sin (2\lambda+15)) \quad (1)$$

where λ is the longitude in degrees East of Greenwich. The ΔV range is from 0 to 1.8 m/s/yr.

We exercised the selection method over the range of missions, thrusters, and primary power sources and found that for each mission/thruster combination, there is one ES/PC system which minimizes the mass of the propulsion system.

SECTION 1

INTRODUCTION

An energy storage/power conditioning system (ES/PC) is the interface between an electromagnetic thruster and a primary power source in a space propulsion system. An ES/PC accepts the relatively low, continuous power output from a primary source, converts it to a series of high power pulses and delivers it to the thrusters. Electromagnetic thrusters require peak power levels well above the average power level required to accomplish mission objectives. The ES/PC is required to minimize the primary power source requirements while maximizing thruster performance.

Development of electromagnetic propulsion systems has continued for over twenty years. Most of the work has concentrated on the thrusters. As thruster technology matures, more emphasis must be placed on the ES/PC and on system integration. This report describes the results of a program conducted at IAP Research, Inc. to establish guidelines by which program planners can optimally select and evaluate the performance of integrated propulsion systems. The guidelines allow the program planner to make tradeoffs among the propulsion system components and compare alternative concepts.

The propulsion systems considered in this program covered a range of missions, thrusters, and primary power options. The missions were: ten year stationkeeping and orbit transfer from low earth orbit (LEO) to geosynchronous orbit (GEO) of large payloads (up to 25 metric ton). The thrusters were: the Teflon pulsed plasma (TPP), the magnetoplasmadynamic (MPD), the pulsed inductive (PIT), and the electric rail gun (ERG). The primary power options were: solar cell arrays, solar thermophotovoltaic, nuclear thermionic, nuclear thermoelectric, nuclear Rankine cycle, nuclear Brayton cycle and nuclear magnetohydrodynamic (MHD).

Selection, sizing, and optimization of an ES/PC can be achieved if an optimization criterion is established and if the ES/PC is examined within the context of an integrated propulsion system. To develop the selection guidelines, we identified the requirements imposed on the ES/PC and parametrically related the ES/PC performance to the propulsion system outputs.

SECTION 3

INTEGRATED PROPULSION SYSTEM PERFORMANCE AND MODELING

In this section we describe the characteristics of the subsystems in the integrated propulsion system and present the performance and mass models of these subsystems.

3.1 PRIMARY POWER CHARACTERISTICS

The primary power source was assumed to contain all the components necessary to deliver electrical power, at some characteristic voltage and current level, to the ES/PC. The performance characteristics of several power sources were studied and mass models were developed. The characteristics and mass models are described in detail in Appendix A. A summary is presented in this section.

The characteristics of interest are the output constraints (current and voltage), the minimum and maximum power levels available, and the mass. The characteristics were determined by conducting a literature survey and contacting technical experts to confirm the results and make refinements where needed. The literature contained considerable point design data but very little parametric or limit data. The primary power mass is best described as:

$$M_{pp} = m_{sp} P_{pp} \quad (25)$$

where m_{sp} is the specific mass. The specific mass was modeled by curve-fitting the data gathered in the literature search for power levels ranging from 2 kW to 7 MW. The results are presented in Table 4. All power sources investigated in this study can be theoretically designed for any power level. If a power level lower than the minimum specified in Table 4 is required, the mass is set to the minimum. For high power levels (>500 kW) multiple shuttle launches may be required. These effects are shown in Figure 4.

The output voltage range of these systems is presented in Figure 5. There is a tradeoff between ohmic losses in the busses and insulation degradation due to the high voltage. The optimum output voltage cannot be determined until the mission is defined.

TABLE 4
SPECIFIC MASS OF THE PRIMARY POWER SYSTEMS

POWER SOURCE	SPECIFIC MASS (m_{sp}) MODEL *	MINIMUM MASS (kg)
Solar Cell Arrays	$0.013 + 40.61/P_{pp}$, $P_{pp} > 1000$ W	54
Solar Thermophotovoltaic	$0.005 + 4.6 \times 10^{-7} P_{pp}$, 1000 W $< P_{pp} < 10,000$ W	6
Nuclear Thermoelectric	$0.021 + 370.3/P_{pp}$, $P_{pp} > 1000$ W	392
Nuclear Thermionic	$0.018 + 514/P_{pp}$, $P_{pp} > 10,000$ W	700
Nuclear Brayton Cycle	$0.019 + 190.6/P_{pp}$, $P_{pp} > 1500$ W	220
Nuclear Rankine Cycle	$0.013 + 178.6/P_{pp}$, $P_{pp} > 1000$ W	191
Nuclear MHD	$10^{-4} + 1990.1/P_{pp}$, $P_{pp} > 100,000$ W	2000

*Specific mass is in kg/W and primary power in W.

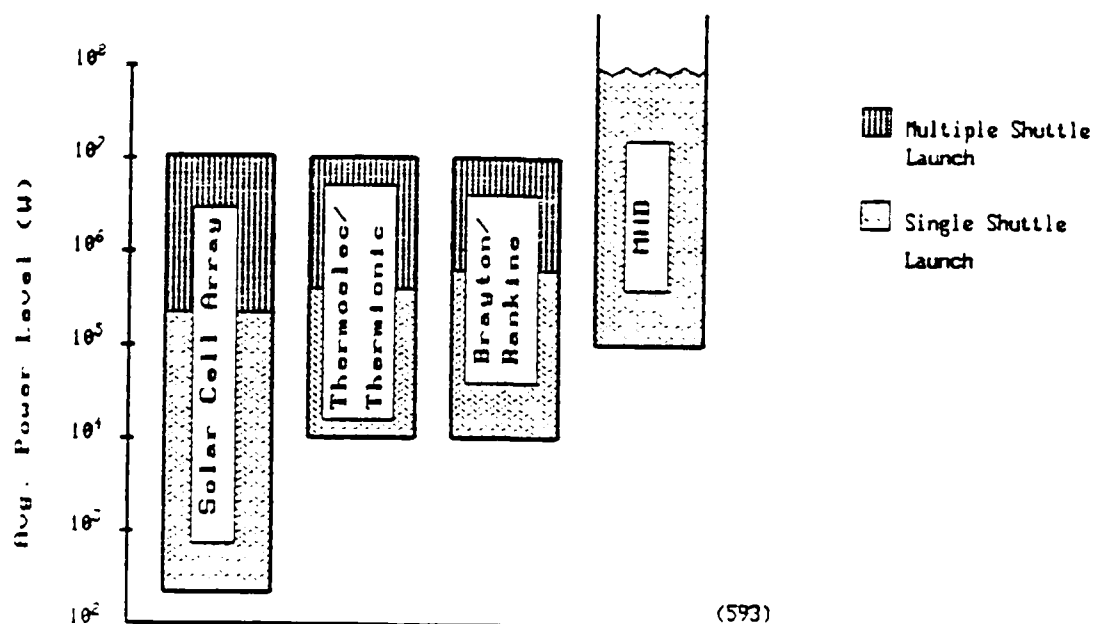


Figure 4. Power Level Range of Primary Power Systems.

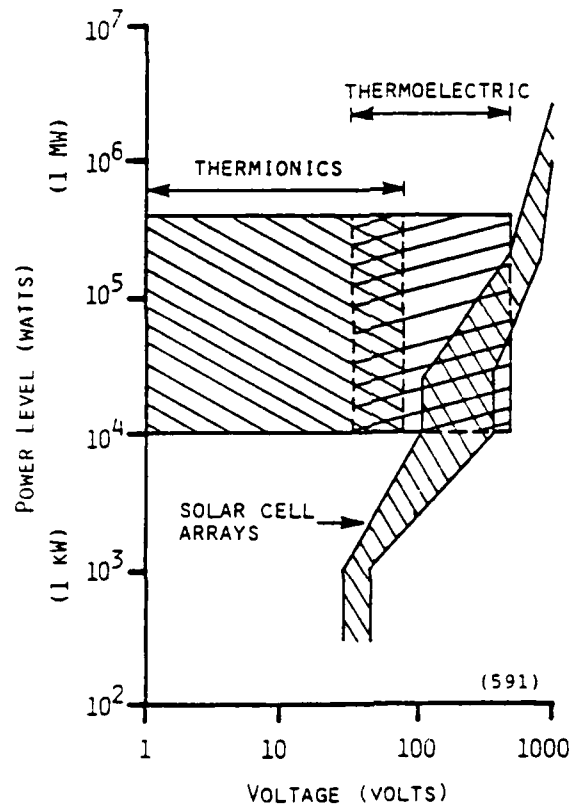


Figure 5. Power Output Voltage Range of Primary Power Systems.

3.2 THRUSTER CHARACTERISTICS

The performance characteristics of the four electromagnetic thrusters were identified and their inputs were modeled. The characteristics and models are described in detail in Appendix B. A summary of the characteristics and a brief description of the operation of each thruster is presented in the following paragraphs.

3.2.1 Pulsed Inductive Thruster (PIT)

The PIT consists of a flat, spiral coil through which an energy supply is discharged. A cross-sectional view is shown in Figure 6. A thin layer of propellant gas is injected over the face of the coil. When this propellant layer has achieved the desired density, the energy supply is discharged through the coil.

A magnetic field is produced from the current flowing in the coil and induces a sheet of current to form in the gas. Current in this sheet flows

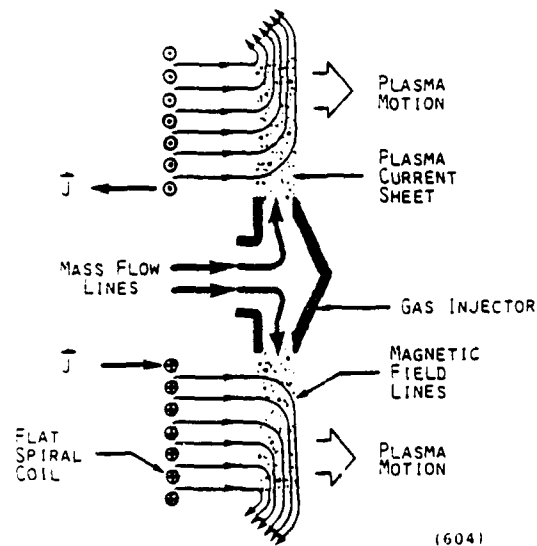


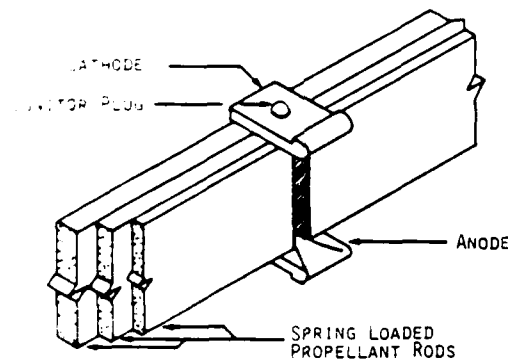
Figure 6. Cross-sectional View of Pulsed Inductive Thruster (PIT).

in the opposite direction to current flow in the coil, and the two repel each other. The sheet accelerates away from the coil in the axial direction and produces the desired impulse. The acceleration of the propellant ceases at some distance from the primary coil, when the magnitude of the primary magnetic field is insufficient to induce current flow in the propellant.

3.2.2 Teflon Pulsed Plasma Thruster (TPP)

The TPP thruster is illustrated in Figure 7, and consists of a set of parallel electrodes separated by several Teflon fuel bars. The Teflon propellant is held against the electrodes by a constant force spring. A solid state ignitor plug is located in the cathode of the thruster, between the Teflon bars, and an energy supply is connected directly to the thruster electrodes.

In operation, the energy supply is charged and supplies a potential to the thruster electrodes. This applied voltage is sustained by the thruster until a pulse is supplied to the ignitor plug initiating a discharge between the electrodes. The mini-discharge from the ignitor plug produces enough electrical conductivity between the thruster electrodes for the main energy supply to discharge. An arc forms between the electrodes, ablates and



(601)

Figure 7. Teflon Pulsed Plasma Thruster (TPP).

ionizes material from the face of the Teflon fuel bars. The ionized propellant is then accelerated by gas dynamic and electromagnetic forces produced from the interaction of the arc current and its self-generated magnetic field. After the energy supply has discharged, the cycle can be repeated.

3.2.3 Magnetoplasma dynamic Thruster (MPD)

The MPD thruster has a coaxial cylindrical geometry as shown in Figure 8. It consists of an outer cylindrical anode and an axial cathode. The back wall of the thruster chamber is an insulating backplate which contains propellant injection holes. A power supply is connected across the electrodes. Propellant is injected into the chamber through the backplate at a constant flow rate. The presence of the propellant gas between the electrodes causes a breakdown, forming a plasma. The high radial plasma current (10^4A) induces a toroidal self-generated magnetic field which accelerates the ionized gas. After a short time into the discharge ($10\text{ }\mu\text{s}$), the current distribution in the plasma becomes constant. The stable current then continues to ionize and accelerate propellant gas as it enters the chamber. Very high power ($>1\text{ MW}$) is required to operate this thruster efficiently, and only pulsed (or repetitive) operation has been considered here. The term 'quasi-steady' is used to describe this thruster operation.

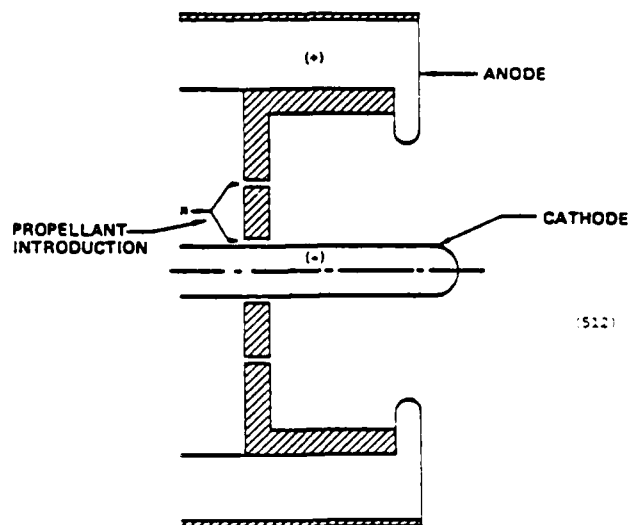


Figure 8. Magnetoplasmadynamic Thruster (MPD).

3.2.4 Electric Rail Gun Thruster (ERG)

The acceleration process of an electric rail gun is very similar to that of a Teflon pulsed plasma thruster. It is a parallel rail device as shown in Figure 9. The mass to be accelerated, a 'pellet' which contains an electrically conducting armature at its rear, is placed in the bore of the gun. The presence of the pellet is the major difference between the ERG and TPP. The electric rail gun does not rely on mass ablation for arc (or armature) formation or for reaction mass.

In operation, an electric potential is applied across the electrodes at the breech end of the gun. Current flows down one rail, across the conducting armature, and back down the other rail. The interaction of the armature current with the self-generated magnetic field caused by current flowing in the rails, accelerates the armature and projectile down the bore and out of the gun producing the desired impulse. The cycle is repeated as required.

3.2.5 Thruster Performance Modeling

For each combination of pulse mass and exhaust velocity, there is only one thruster geometry which has maximum efficiency. It is this thruster which is of interest here. Thruster performance modeling could be readily

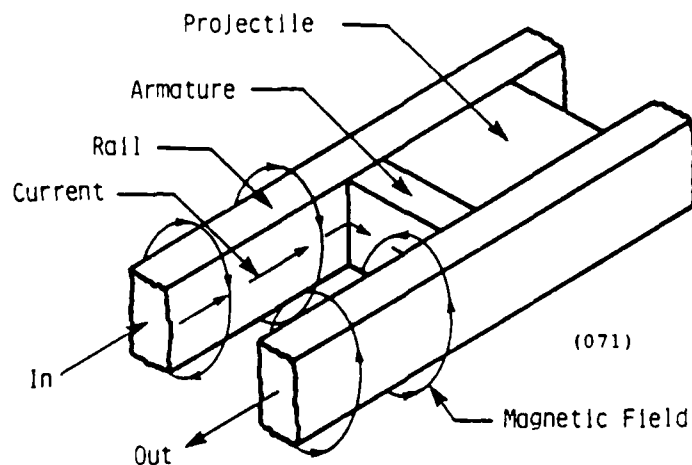


Figure 9. Electric Rail Gun (ERG).

accomplished if a large body of data existed (either experimental or analytical) for maximum efficiency thrusters and if this data contained values for the input requirements over a wide range of m_p and v_e . A simple multivariate curve fitting technique could then be used to develop the required relationships for E_p , J , V and t_p . This was the approach used for modeling the electric rail gun.³ This simple data-based approach could not be applied to the other thrusters, because not enough data was available over a wide range of m_p and v_e . An alternate approach was developed based on methods of extrapolating thruster performance from existing performance data using physically reasonable assumptions concerning thruster operation. Using these methods we were able to develop the required relationships between the thrusters input requirements and the propulsion system outputs. The results of thruster performance modeling are presented in paragraphs 3.2.5.1 through 3.2.5.4, along with the assumptions made to develop the models.

3.2.5.1 Pulse Energy

We assumed that the pulse energy required (for any of the thrusters) is the sum of three components: (1) kinetic energy, E_{KE} ; (2) ionization

³Bauer, D. P., Barber, J. P. and Vahlberg, C.J., 'The Electric Rail Gun for Space Propulsion,' NASA-CR-165312, Final Report, February 1981.

energy', E_{ion} , and (3) dissipation energy, E_{dis} . Then the pulse energy can be expressed as:

$$E_p = E_{KE} + E_{ion} + E_{dis} \quad (26)$$

The kinetic energy is the useful energy imparted to the pulse mass during the pulse and is given by:

$$E_{KE} = m_p v_e^2 / 2 \quad (27)$$

The ionization energy includes all energy that is 'frozen' into the propellant. This term is not strictly ionization but includes depolymerization, ionization, and heating of the gas. This term can be written as:

$$E_{ion} = m_p e_i \quad (28)$$

where e_i is a 'specific ionization energy' characteristic of the state of the plasma at the thruster exit and has units of energy/mass.

The dissipative energy loss term includes both electrode losses and radiative losses from the plasma. This term includes only those 'steady' losses that occur during gas acceleration. The dissipative energy is required to maintain the plasma at temperature and does not include ionization and other one time penalties. The energy loss mechanism was characterized as a resistance for both the TPP and PIT and as a resistance and 'electrode fall' for the MPD. The dissipative loss term can be written as:

$$E_{dis} = \int R I^2 dt + \int V_f J dt \quad (29)$$

where V_f is the electrode fall or voltage penalty which must be paid to remove current from the electrodes. V_f was assumed to be zero for the TPP and PIT. Using the definition of the dissipation energy and assuming that:

- (a) The resistive dissipation in the thruster is primarily due to plasma resistance,
- (b) The apparent dissipative resistance remains constant during acceleration,
- (c) The acceleration of the plasma is primarily magnetic, and

- (d) The plasma body scales geometrically with pulse mass (i.e., ratios of dimensions remain fixed as the thruster size is varied).

the dissipation energy for the PIT and TPP can be written as

$$E_{dis} = k m_p^{2/3} v_e \quad (30)$$

and for the MPD as:

$$E_{dis} = k_1 \dot{m}_p^{1/2} v_e t_p + k_2 (\dot{m}_p v_e)^{1/2} t_p \quad (31)$$

See Appendix B for the complete derivation of Equations 30 and 31. The terms k , k_1 , and k_2 are constants which were determined from available performance data and are shown in Table 5.

TABLE 5
PULSE ENERGY COEFFICIENTS

	e_i (MJ/kg)	CONSTANTS	1st IONIZATION (MJ / kg)
PIT ⁴	88.8	$k = 145$	Argon 40
TPP ^{5,6}	120.0	$k = 140$	Teflon 90
MPD ⁷	28.0	$k_1 = 1206$ $k_2 = 68,600$	Argon 40

⁴Lovberg, R. H. and Dailey, C. L., 'Large Inductive Thruster Performance Measurement', AIAA-81-0708R, 1981.

⁵Huberman, M. N. and Zafran, S., 'Pulsed Plasma Propulsion System/Spacecraft Design Guide', AFRPL-TR-80-38, Final Report, September 1980, ADA091006.

⁶Personal Communication - Dominic Palumbo - Fairchild Industries, Inc.

⁷Personal Communication - Kenn Clark - Princeton University.

The efficiency of the thruster is defined as the kinetic energy divided by the pulse energy. For the PIT and TPP, the efficiency is:

$$\eta = 1/(1 + 2 e_i/v_e^2 + 2k/(m_p^{1/3} v_e)) \quad (32)$$

The efficiency for the MPD is:

$$\eta = 1/(1 + 2e_i/v_e^2 + 2k_1/(\dot{m}_p^{1/2} v_e) + 2k_2/(\dot{m}_p^{1/2} v_e^{3/2})) \quad (33)$$

The efficiency for the ERG³ is:

$$\eta = 13.67 m_p^{0.104} v_e^{-0.299} \quad (34)$$

3.2.5.2 Current/Pulse Time

An average current can be defined as:

$$J_{avg} = [\int_0^{t_p} J^2 dt / t_p]^{1/2} \quad (35)$$

which can be further reduced by using the electromagnetic impulse equation:

$$m_p v_e = (L' \int J^2 dt) / 2, \quad (36)$$

where L' is the axial inductance gradient for the device. Combining Equations 35 and 36 we obtain:

$$J_{avg} = (2 m_p v_e / (L' t_p))^{1/2} \quad (37)$$

Equation 37 must be reduced further to obtain the model of interest (a function of m_p and v_e only). Therefore L' and t_p have to be expressed as functions of m_p and v_e . This is discussed in Appendix B. The resulting average current and pulse durations are

$$t_p = 13 m_p^{1/3} / v_e \quad (38)$$

and

$$J_{avg} = 148.25 m_p^{1/3} v_e \quad (39)$$

for the PIT.

For the TPP, the expressions are:

$$t_p = 1.5 \times 10^{-11} m_p^{1/3} v_e \quad (40)$$

and

$$J_{avg} = 1.07 \times 10^7 m_p^{1/3} \quad (41)$$

For the MPD, the pulse duration (t_p) is an independent parameter since the MPD is operated in a quasi-steady mode. The MPD current is:

$$J_{avg} = 2.42 \times 10^3 (\dot{m}_p v_e)^{1/2} \quad (42)$$

For the ERG³, the expressions are:

$$t_p = 4.45 \times 10^{-6} m_p^{1/3} v_e \quad (43)$$

and

$$J_{avg} = 2.2 \times 10^6 m_p^{1/3} \quad (44)$$

3.2.5.3 Voltage

The thrusters considered in this study are all electromagnetic and are 'current driven' devices (i.e., the acceleration forces are related to current, not voltage). These devices do not require a high voltage to accelerate the pulse mass (although some require a relatively high voltage for the formation of the current carrying plasma and to produce the required short pulses). The voltage is, therefore, a derived parameter in electromagnetic thrusters and is indicative of the impedance of the device.

The average voltage, V_{avg} , is computed from the pulse energy, the pulse time, and the average current and can be written as:

$$V_{avg} = E_p / (t_p J_{avg}) \quad (45)$$

Substituting E_p , t_p and J_{avg} by the corresponding equation for each thruster we obtain the following.

For the PIT,

$$V_{avg} = 2.59 \times 10^{-4} m_p^{1/3} v_e^2 + 4.61 \times 10^4 m_p^{1/3} + 7.52 \times 10^{-2} v_e \quad (46)$$

For the TPP,

$$V_{avg} = 0.311 m_p^{1/3} v_e + 7.5 \times 10^7 m_p^{1/3} / v_e + 87.2 \quad (47)$$

For the MPD,

$$V_{avg} = 2.07 \times 10^{-4} m_p^{1/2} v_e^{3/2} + 1.16 \times 10^4 m_p^{1/2} v_e^{-1/2} + 0.498 v_e^{1/2} + 28.3 \quad (48)$$

For the ERG,

$$V_{avg} = 0.032 m_p^{0.896} v_e^{2.229} \quad (49)$$

3.2.5.4 Summary

Thruster characteristics and performance were related to the propulsion system outputs. The models developed for the thrusters (except for the ERG) were based on an understanding of the physical principles of operation and a number of assumptions concerning the performance of optimized thrusters combined with available performance data. The models are extremely versatile, permitting rapid evaluation of thruster input requirements over a wide range of output conditions.

3.3 PROPELLANT SYSTEM CHARACTERISTICS

The propellant system mass is expressed as

$$M_{prp\ sys} = K m_p f t_d \quad (12)$$

where K is a constant greater than one and accounts for the storage containers and propellant feed system. The storage container mass varies over a wide range, depending on the propellant type (gas/solid) and the storage media (gas propellant may be stored cryogenically or in high pressure tanks). Thus, the exact storage container mass cannot be determined until

the mission is specified. We assumed that the container mass is 20% of the propellant. The propellant system mass can be written as:

$$M_{prp\ sys} = 1.2m_{pft_d} \quad (50)$$

3.4 ES/PC CHARACTERISTICS

The generic ES/PC functions which were analyzed are presented in Figure 10. The approach used was as follows:

- (1) Define the input constraints and output requirements of the ES/PC.
- (2) Conduct a literature search and identify ES/PC concepts and components capable of performing the defined functions.
- (3) Analyze each component independently and identify the critical parameters and any operational constraints.
- (4) Generate 'skeletal' performance models based on fundamental understanding of how each component operates.
- (5) 'Calibrate' the skeletal models by using existing data to form parametric models which describe the operational capabilities and limits of each component.
- (6) Combine the component models to develop ES/PC concept models.
- (7) Integrate the concept models with the propulsion system selecting and sizing technique.

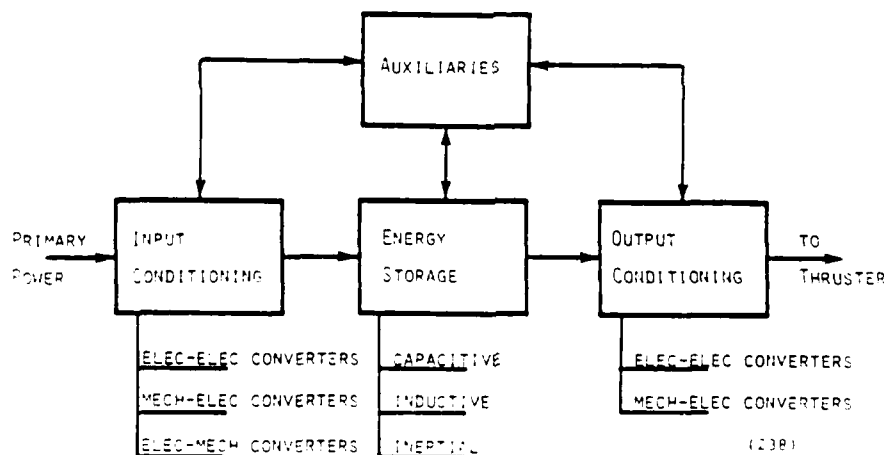


Figure 10. Generic ES/PC Functions.

The results of this approach are presented in the following paragraphs.

3.4.1 ES/PC Input/Output Constraints

The input constraints and output requirements of the ES/PC are essential in identifying the concepts and components capable of performing the required functions. The constraints and requirements are presented in Table 6. These were computed from the primary power output and thruster input requirements. More than one mass, size, and efficiency model may be required for the ES/PC concepts and components, because the parameter values span such a wide range (up to 5 order of magnitude).

TABLE 6
ES/PC INPUT CONSTRAINTS AND OUTPUT REQUIREMENTS

	PARAMETER	VALUE
Output	E_p (kJ)	0.1 - 400
	V (kV)	0.06 - 27.5
	I (kA)	15.0 - 1170
	t_p (μ s)	1.0 - 5800
	f (Hz)	0.04 - 19
Input	P_{pp} (kW)	0.2 - 7800
	V (V)	28 - 1000

3.4.2 ES/PC Concepts

The energy store in an ES/PC is the main component of the system. The input conditioners are selected to charge it efficiently and the output conditioners are selected to deliver the stored energy in the required form (i.e., to shape the pulse). Three types of energy stores were considered: capacitive, inductive, and inertial.

Three capacitive-based ES/PC concepts were considered. The first concept consisted of a simple capacitor with a closing switch as the output conditioner (Figure 11). This concept is ideal for thrusters requiring short pulses (on the order of few microseconds). The second concept was an LC circuit (Figure 12). This concept can be used with thrusters requiring a

assumed the total compulsator mass to be 2.5 times the rotor mass, which can be expressed as:

$$M_{\text{comp}} = 10 E_p / (av^2) \quad (69)$$

The compulsator size can be derived from the rotor size. It will have the same length and twice the radius. The rotor radius, r , is related to the rotor tip speed by:

$$v = 2\pi f_m r \quad (70)$$

Combining Equations 65, 67, and 70 we obtain:

$$r = 8Pvt_p / \pi \quad (71)$$

The length (b) of the rotor can be calculated from the rotor mass and radius and is given by:

$$b = M_{\text{rot}} / (\rho \pi r^2) \quad (72)$$

These equations can be used to calculate the mass and size of a compulsator optimized for a set of independent parameters (t_p , E_p , and f) specified by the mission. During selection and sizing of a compulsator, it should be kept in mind that:

- (1) a short pulse requirement may lead to an impractically small rotor radius. A practical minimum pulse duration is 100 μ s to 500 μ s.
- (2) a long pulse, on the other hand, may lead to a short rotor (thin disk) which is dynamically unstable. In this case, the tip speed must be decreased until the length-to-diameter ratio is satisfactory (say 1) and the mass and radius of the rotor must be recalculated.
- (3) Finally, surface current density must not exceed the maximum allowable limit of 10 MA/m in order to control the armature winding bond shear stress. If the current density exceeds this value, the length of the rotor must be increased and the mass and rotor radius must be recalculated.

We exercised this methodology over the range of independent parameters of interest and some of the results are presented in Figures 22 and 23. The

The pulse width is related to the electrical frequency, f_e , of the alternator by:

$$t_p = 1/(16f_e) \quad (65)$$

because the compulsator compresses the half cycle pulse width of the alternator by a factor of 8 (assuming electromagnetic thrusters act resistively). The electrical frequency is related to rotational speed by:

$$f_e = f_m P/2 \quad (66)$$

where f_m is the mechanical rotor speed and P is the number of field poles. The factor of 2 can be removed from Equation 66 if either polarity can be used. The electrical frequency becomes:

$$f_e = f_m P \quad (67)$$

The minimum pulse width can be decreased by increasing either the rotor speed or the number of poles or both. The maximum rotor speed is stress limited to 150 m/s. The maximum number of poles is limited by the air gap distance between the rotor and stator. As the pole-to-pole separation approaches the air gap distance, the excitation field leakage increases. At some point, the leakage becomes so great that the addition of poles is futile.

The mass components of a compulsator are: the rotor (the energy store), the back iron (return path of the magnetic flux) and the field coils (generate the magnetic field). The mass of the rotor is given by:

$$M_{rot} = 4 E_s / v^2 \quad (68)$$

where v is the rotor tip speed. The energy stored is calculated from the ratio of pulsed to stored energy (α) and is limited to less than 5 percent by peak power constraints. The back iron has the same cross-sectional area as the rotor and its mass should be approximately equal to the rotor (both are ferromagnetic and have similar densities). The field coils are sized to deliver the required output voltage and their mass is relatively small. We

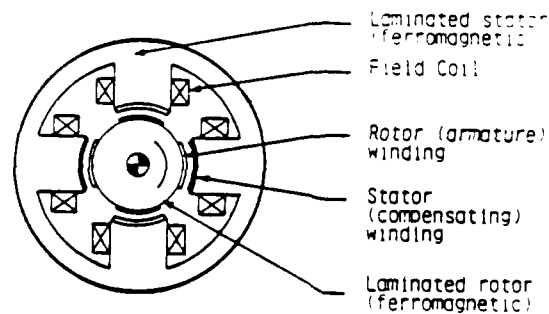


Figure 21. Compulsator Cross Section.¹⁴

We conducted a literature survey and developed a methodology to calculate the size and mass of a compulsator. The methodology and the limitations of the compulsator are discussed below.

The fundamental limitations to the compulsator were investigated by Weldon et al.¹⁴ The limits can be divided into three groups: those dealing with the effects of load characteristics, those limiting output power, and those limiting minimum pulse width.

The load affects the ability of the compulsator to compress flux and produce short pulses. The compulsator was found to reduce the basic alternator half cycle pulse width by a factor of 8 for a resistive load and by a factor of 4 for a capacitive load.

The peak output power is limited by several factors. The thickness and dielectric strength of the air gap between the rotor and stator windings have a significant effect on peak power. The air gap must be minimized in order to minimize the inductance and thereby maximize output current. This reduces the voltage breakdown strength of the gap (and the maximum permissible output voltage of the machine). A second limitation on the output power is the shear strength of the insulation system used to bond the stator windings to the stator and rotor windings to the rotor. The interaction between the compulsator discharge current and the excitation field causes a tangential force on the conductors. This force slows the rotor, converting inertial energy to electrical energy, and results in a tangential shear stress on the insulation bond. The maximum strength of the insulation was found to be 28 MPa (4 ksi) which corresponds to a maximum surface current density of 10 MA/m.

$$m_{\text{ref}} = 60 P_0^{0.7} \quad (64)$$

where P_0 = refrigeration power.

This does not include the mass of radiators required to reject the heat.

3.4.3.4 The Compulsator

The compensated pulsed alternator (compulsator) is an inertial energy store. It combines both the energy store and the output conditioning functions in one device. It provides high-voltage, high-current pulses by utilizing the principles of magnetic induction and flux compression. The compulsator is a single-phase alternator with a stationary field and a rotating armature. The armature winding and an identical stationary (or compensating) winding are connected in series. At at least one point per cycle the inductance of the armature circuit is minimized. The variable armature inductance leads to a flux compression action. When coupled with alternator action this produces high current pulses into the load. The basic operation is illustrated in Figure 20. A simplified cross-sectional view of a compulsator is presented in Figure 21.

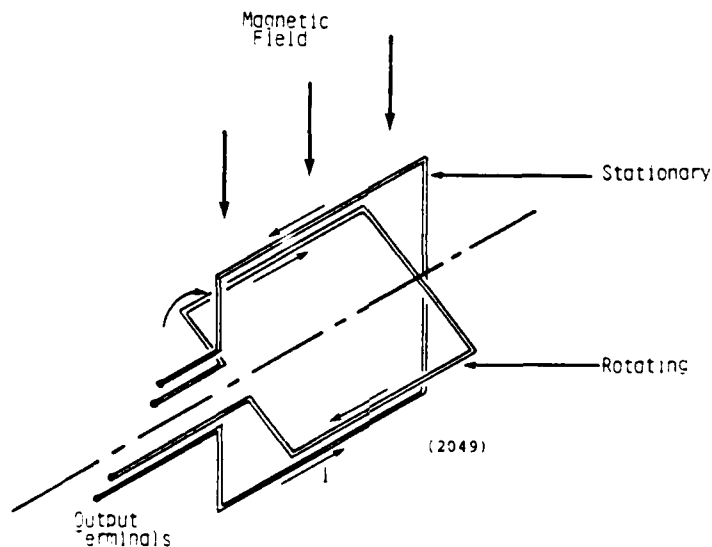


Figure 20. Compensated Pulsed Alternator (Compulsator).¹⁴

¹⁴Weldon, W. F., Bird, W. L., Driga, M. D., Tolk, K. M., Rylander, H. G., and Woodson, H. H., 'Fundamental Limitations and Design Considerations for Compensated Pulsed Alternators', CEM University of Texas at Austin.

auxiliary equipment. The analysis and characterization of superconducting systems is described in detail in Appendix D.

Superconducting systems have four major components, the inductor, the current leads, the dewar, and the refrigerator. The mass of the inductor is determined by the choice of geometry, the materials, the magnetic field, and the structural support system. When suitable choices are made for these parameters the specific energy of the inductor is found to be:

$$w_{ind} = 3.33 \times 10^3 \text{ J/kg} \quad (61)$$

The current leads carry current from the normal environment into the cryogenic environment of the inductor. The current leads are a major mass component. The size of current leads is determined by a tradeoff between lead mass and resistive losses. The lead mass is then related only to the current carried and is given by:

$$m_{lead} = 200 I \quad (62)$$

The dewar provides the cryogenic environment for the inductor and is designed to limit heat flow from ambient to cryogenic. The mass of the dewar is determined by the size of the inductor and by the loads it must carry. The mass of the dewar and insulation is given by:

$$m_{dew} = 16.2 A_{dew} \quad (63)$$

where A_{dew} = the surface area of the dewar.

The remaining component in a superconducting system is the refrigerator. The long duration of propulsion missions requires that a closed cycle refrigeration system be used. The size of the refrigeration system is primarily dependent on the heat losses into the cryogenic system. The losses result from the 'downleads,' the dewar, and the pulse losses in the superconductor. This energy must be removed by the refrigeration system at cryogenic temperature and rejected at ambient temperature. The mass of the refrigerator is primarily related to the refrigeration power required at the cryogen temperature. The mass is:

program are the mass, resistance, number of turns, dimensions, and efficiency of the inductor.

The minimum mass constraint results in maximum resistance and minimum efficiency. For some applications the efficiency may be unacceptably low. Therefore a tradeoff study must be conducted to find the optimum size. A higher efficiency can be obtained but there is a mass penalty. The tradeoff in an integrated propulsion system is between the additional inductor mass, radiator mass, and primary power mass. Our electromagnetic propulsion system optimization and sizing computer program conduct this tradeoff analysis every time an inductor size is required.

An example of specific energy of minimum mass (minimum efficiency) inductors is presented in Figure 19. At low current, the specific energy is proportional to the current and has a slight dependence on the inductance. At high current, the energy density is independent of current and inductance.

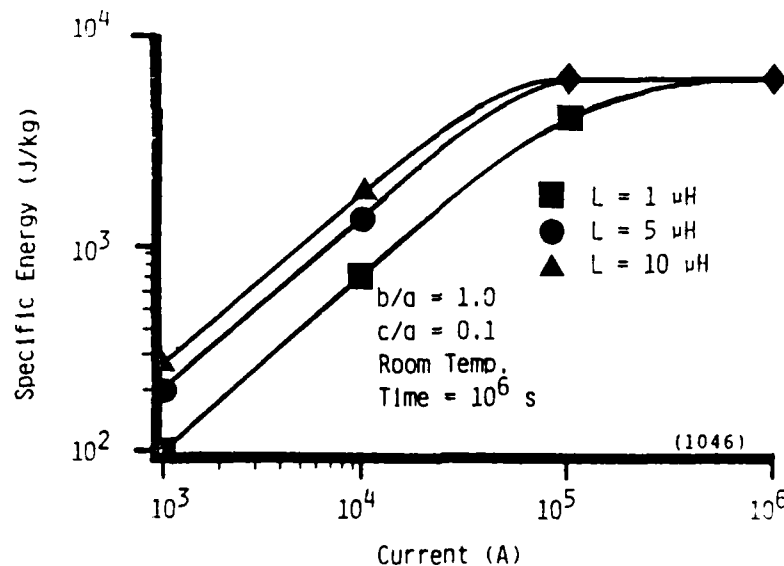


Figure 19. Specific Energy of Minimum Mass Inductors.

3.4.3.3 Superconducting Inductors

The high resistive losses characteristic of normal inductors can be overcome by using superconducting materials. Superconducting energy storage systems are more complex than normal systems and require substantial

The characteristic dimensions of a capacitor can be calculated from the mass. The mass of the dielectric is half the capacitor mass. The density and volume of the dielectric are known. Assuming the capacitor is a cube, the characteristic dimension will be the cube root of the volume.

The dielectric thickness can be calculated from Equations 53, 56, 57. The minimum possible dielectric thickness was assumed to be 2.5 microns.¹³ If the calculated dielectric thickness is less than the minimum specified, then it is set to the minimum and the mass of the capacitor recalculated.

The efficiency of capacitors was assumed to be 90%, that is 10% of the energy stored is dissipated in the terminations and bus bars.

3.4.3.2 Normal Inductors

Inductors are used in pulse power systems either as energy stores or as pulse-forming components. When used as energy stores, inductors are attractive because they provide a constant current source characteristic. This characteristic is very important for some electromagnetic thrusters. The disadvantage of inductors is that they are 'lossy' and inefficient. When used as pulse-forming components, inductors control the shape and duration of pulses delivered from capacitors. They can be used either in a normal 'LC' combination or in a multi-staged pulse-forming network. As pulse-forming components, inductors carry current for a short time and therefore the resistive losses inherent in inductors, are not so important.

Sizing inductors for either function (energy storage or pulse forming) is complex and must account for thermal, mechanical, and geometrical constraints. The effects of these constraints on the size, mass, and efficiency of normal inductors are discussed in detail in Appendix C.

We are primarily interested in minimum-mass inductors. The minimum mass configuration is found by simultaneous solution of the equations describing the constraints (thermal, mechanical, and geometrical). A closed form solution is not possible and a numerical approach must be used. A computer program was developed to find the solution. The inductance, current, and conduction time were treated as the independent variables and input to the computer program. The material properties such as resistivity, density, and maximum stress must also be supplied. The outputs of the

Equation 59 does not account for the mass of the capacitor case, the terminations, or the impregnating fluid (if required). The mass of these elements was estimated to range from 20% to 80% of the total capacitor mass.^{12,13} We selected a factor of 50% to provide the specific energy of a capacitor as:

$$w (\text{capacitor}) = 3985 N^{-0.241}$$

and for $R < 20\%$ and

(60)

$$w (\text{capacitor}) = 3985 (N \cdot e^{0.046/2.5})^{-0.241}$$

for $R > 20\%$.

The specific energy is presented in Figure 18.

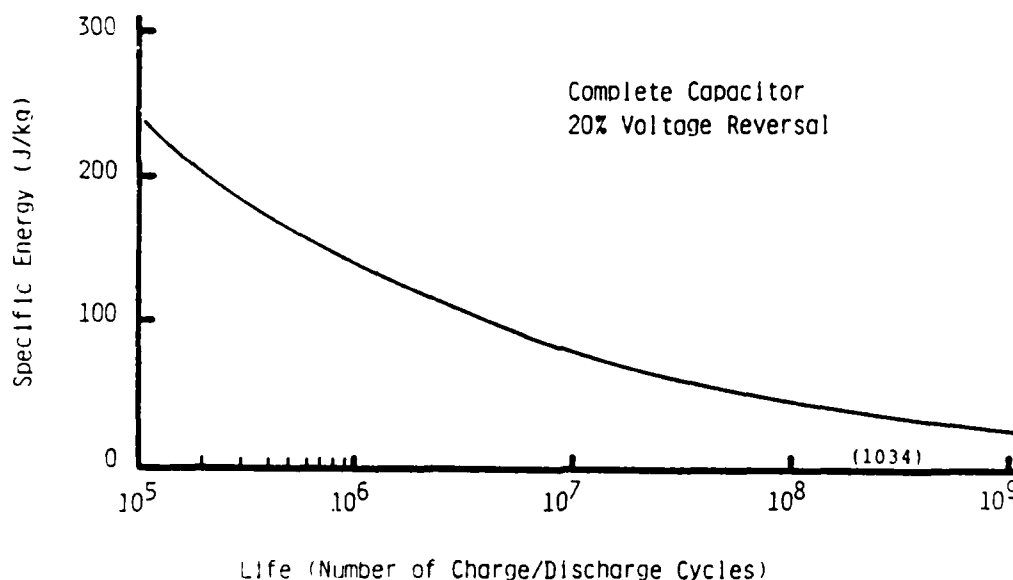


Figure 18. Specific Energy of Capacitors Using Polypropylene Film.

¹²Personal Communication - A. S. Gilmour, SUNYAB, April 1983.

¹³Personal Communication - Howard Mauldin, Sandia National Laboratory, August 1983.

$$N = (E/E_b)^{-8.3} (2.5e^{-0.046R}) \quad (57)$$

Substituting Equation 57 into Equation 55, we get the specific energy of dielectric for voltage reversal greater than 20 percent:

$$w = \epsilon_0 (k/\rho) (N.e^{0.046R/2.5})^{-0.241} E_b^2/2$$

and for voltage reversal less than 20 percent: (58)

$$w = \epsilon_0 (k/\rho) N^{-0.241} E_b^2/2$$

To maximize the specific energy (minimize the mass), Equation 58 shows that kE_b^2/ρ should be maximum. An evaluation of the commonly used dielectric materials in capacitors is presented in Table 8. The most attractive dielectric is polypropylene film.

TABLE 8
DIELECTRIC PROPERTIES

MATERIAL	k	ρ Kg/m ³	E_b V/m	kE_b^2/ρ V-m/kg
K-Film	10	1750	2.75×10^8	4.32×10^{14}
POLYIMIDE	3.6	1420	2.75×10^8	1.9×10^{14}
POLYSULFONE	3.1	1240	2.95×10^8	2.17×10^{14}
POLYCARBONATE	2.8	1210	2.75×10^8	1.75×10^{14}
POLYPROPYLENE	2.2	900	8.66×10^8	1.8×10^{15}
TEFLON	2.1	2300	5.9×10^7	3.2×10^{12}

Substituting values for polypropylene in Equation 58 yields the optimum specific energy of the dielectric which is expressed as:

$$w = 7970 (N.e^{0.046R/2.5})^{-0.241}$$

and for $R > 20\%$ and (59)

$$w = 7970 N^{-0.241}$$

for $R < 20\%$.

The parameters k and ρ are material properties. For a given dielectric, the energy density is directly proportional to the square of the applied electric field on the dielectric. To maximize the energy density, the dielectric must be stressed to the maximum allowable electric field determined by the breakdown strength (E_b).

The maximum allowable field is a quantity which depends on the required number of cycles, N , (number of charge/discharge cycles), and the voltage reversal (R) experienced during the capacitor operation.⁸ The allowable ratio of charging to breakdown voltage reflects the limit on capacitor life due to corona formation.⁹ When the applied electric field is greater than the allowable field, small currents may arise in the dielectric and may degrade the dielectric or lead to a complete breakdown.¹⁰ Voltage reversal affects the capacitor life because it leads to degradation of the dielectric and corona formation.

Data for high-energy-density capacitors¹¹ were used to determine the relationship between capacitor life and the applied electric field. This relationship is

$$N = (E/E_b)^{-8.3} \quad (56)$$

Equation 56 shows that the life of the capacitor is equal to one cycle when the applied field equals the breakdown strength and that life increases exponentially as the applied field is decreased.

The effect of voltage reversal on the capacitor life was analyzed in Reference 9 and was found to have a negligible effect if the voltage reversal is less than 20%. Voltage reversal greater than 20% reduces the life by:

⁸Sargent, W. J. 'Energy Storage Capacitors', Los Alamos National Scientific Laboratory.

⁹Dailey, C. L., White, C. W., 'Capacitors for Aircraft High Power', AFAPL-TR-74-79.

¹⁰Kunhardt, E. E., 'Electric and Magnetic Properties of Materials', Texas Tech University.

¹¹Maxwell, Data Sheets - Series M Capacitors

$$E_s = CV^2/2 \quad (51)$$

where C is the capacitance and V is the voltage to which the capacitor is charged. For a parallel-plate capacitor, the capacitance can be written as

$$C = k\epsilon_0(A/d) \quad (52)$$

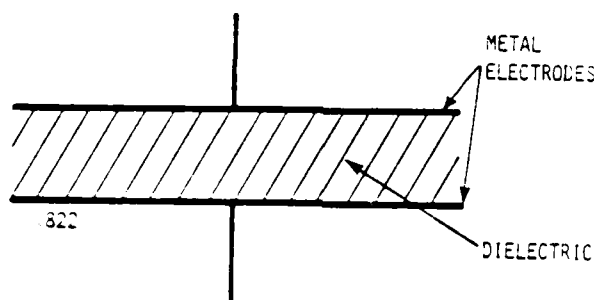


Figure 17. Parallel Plate Capacitor.

where ϵ_0 is the permittivity of free space, k is the relative dielectric constant, A is the surface area of one of the plates, and d is the distance separating the plates. (This assumes that the linear dimensions of the plates are much greater than the plate separation distance.)

The voltage can be written as

$$V = Ed \quad (53)$$

where E is the electric field between the plates.

Substituting C and V into equation 51 we obtain:

$$E_s = \epsilon_0 kAdE^2/2 \quad (54)$$

' Ad ' is simply the volume of the dielectric. Using the density of the dielectric (ρ), the specific energy (w) of the dielectric can then be written as

$$w = \epsilon_0(k/\rho)E^2/2 \quad (55)$$

Permutations of the input conditioners, energy stores, and output conditioners will give the possible ES/PC concepts. This is illustrated in Table 7. The type of input and output conditioner is also constrained by the primary power source selected and the thruster (e.g., Series/Parallel switching of the primary power sources is only feasible when modular power sources are used). No input conditioner may be required when thermocycles such as Rankine or Brayton are the primary power sources and they are used with an inertial energy store. The thruster requirements will limit the type of energy store and output conditioner which can be selected.

TABLE 7
SUMMARY OF ES/PC CONCEPTS

INPUT CONDITIONER	ENERGY STORE	OUTPUT CONDITIONER
DC/DC Converter S/P Switching	CAPACITOR	Thyratron Spark Gap SCR (as closing switch) LC Circuit PFN Circuit
	Normal Inductor Superconducting Inductor	SCR (As opening switch)
DC/DC Converter and Electric Motor o None	Compulsator	SCR (As closing switch)

The next step is to characterize the ES/PC components and develop the mass, size, and efficiency models. The models will be presented in paragraphs 3.4.3 through 3.4.6 and they will be grouped by generic function.

3.4.3 Energy Store Models

3.4.3.1 Capacitors

Two conducting bodies (electrodes) are separated by a dielectric to form a capacitor. The energy is stored electrostatically in the dielectric. A parallel plate capacitor is shown in Figure 17. The energy stored in an ideal capacitor is given by:

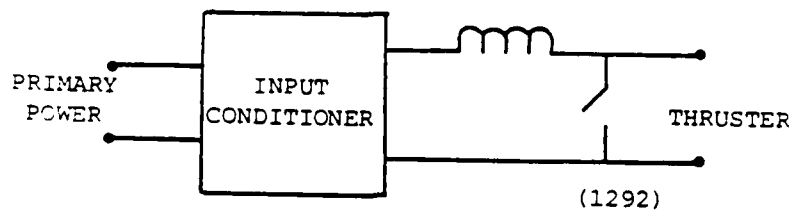


Figure 14. ES/PC Concept Using a Normal Inductor as the Energy Store.

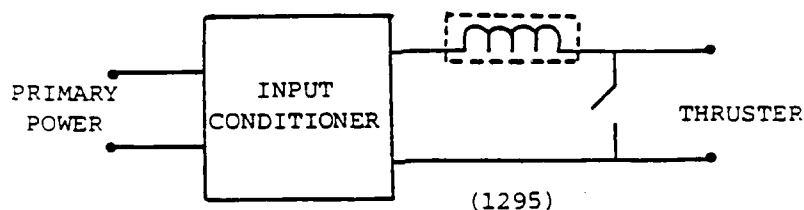


Figure 15. ES/PC Concept Using a Superconducting Inductors as the Energy Store.

store (Figure 16). A homopolar generator was also considered but was not feasible because of the relatively short pulses required by the thrusters.

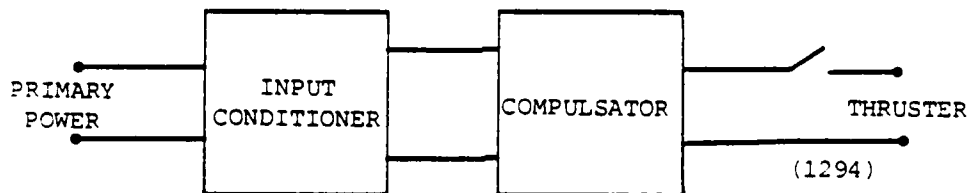


Figure 16. ES/PC Concept Using a Compulsator.

The input conditioners considered for these concepts were: DC/DC converters, series/parallel switching of primary power modules, and electric motors.

The output conditioners were switches and inductors. Inductors are a part of the capacitive-based concepts (LC and PFN). The switches considered were SCR's, Thyratrons, and spark gaps.

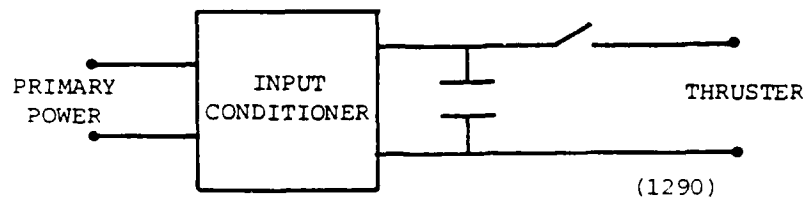


Figure 11. ES/PC Concept Using a Simple Capacitor as the Energy Store.

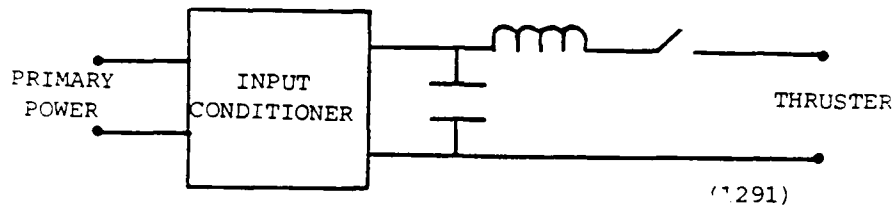


Figure 12. ES/PC Concept Using an LC Circuit.

pulse duration of a few hundred microseconds. The third concept was a multi-stage pulse-forming network (PFN) (Figure 13). This concept is ideal for thrusters requiring long pulses (on the order of milliseconds).

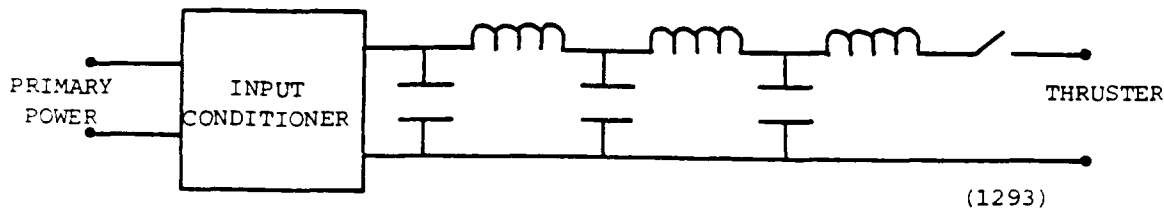


Figure 13. ES/PC Concept Using a Multi-Stage Pulse Forming Network.

Two inductive-based ES/PC concepts were considered: one using a normal inductor as the energy store (Figure 14) and the second using a superconducting inductor as the energy store (Figure 15). Both systems are attractive for pulse durations on the order of milliseconds. The major difference between the two is that the superconducting inductor offers a higher efficiency than a normal inductor. Superconducting inductors require a refrigeration system which offsets the saving from higher efficiency. A tradeoff evaluation must be conducted before a selection can be made.

The third type of energy storage is inertial. Inertial stores have the advantage of storing large amounts of energy in a small volume. The system considered used a compensated pulsed alternator (compulsator) as the energy

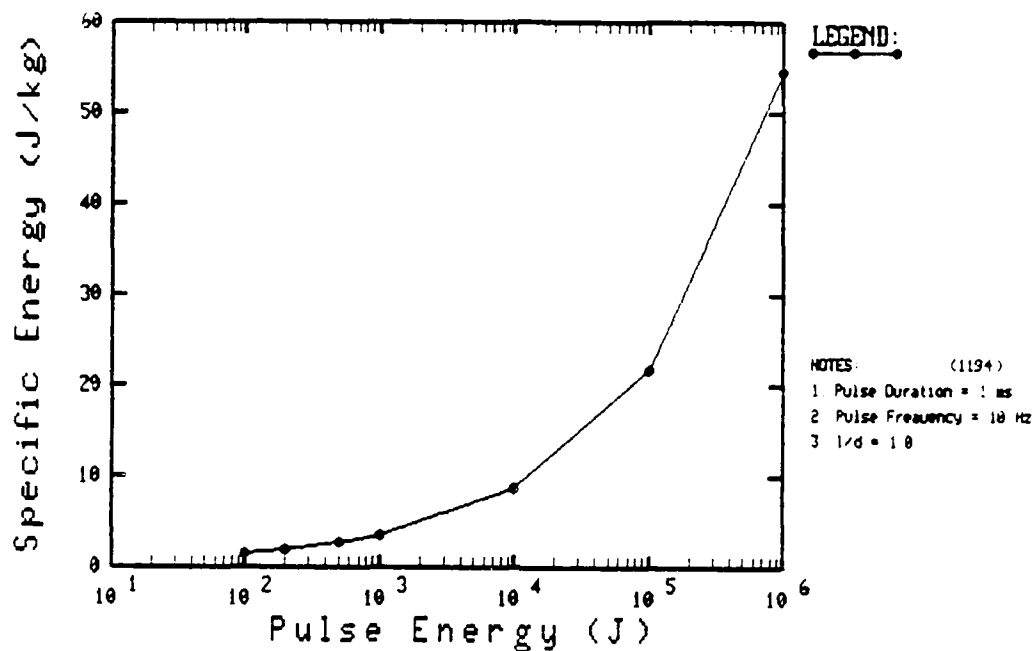


Figure 22. Specific Energy of Compulsators as a Function of Pulse Energy ($f = 10$ Hz and $t_p = 1$ ms).

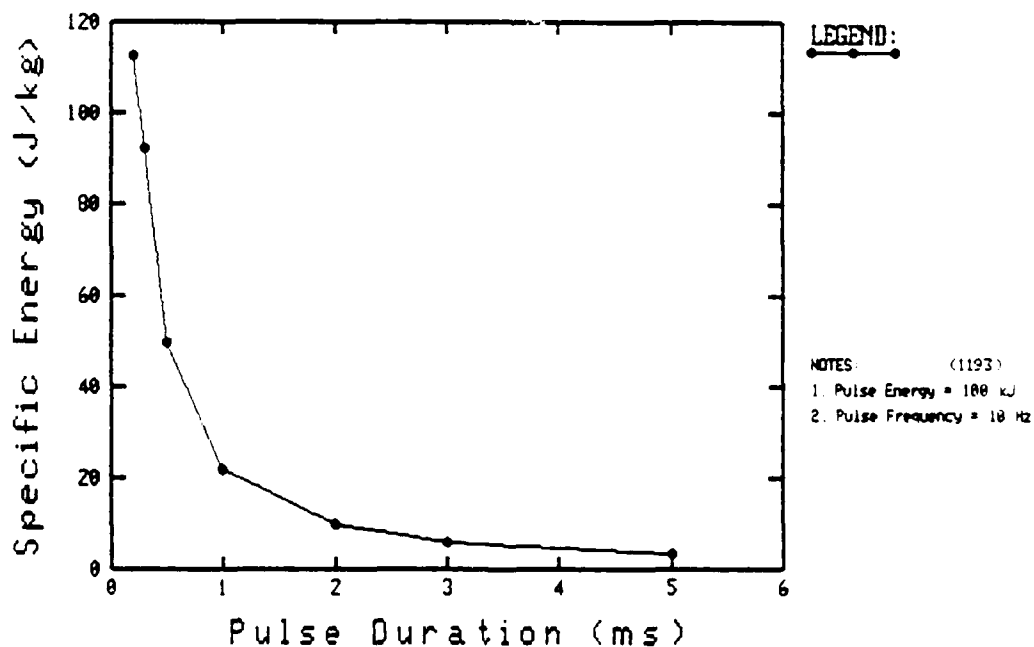


Figure 23. Specific Energy of Compulsators as a Function of the Pulse Duration ($f = 10$ Hz and $E_p = 100$ kJ).

results are displayed as specific energy (pulse energy divided by machine mass) to permit comparison with alternatives. Figure 22 shows the specific energy as a function of pulse energy for a frequency of 10 Hz and pulse width of 1 ms. Specific energy increases with pulse energy and is an order of magnitude lower than that of dielectric capacitors.

Figure 23 shows the specific energy as a function of the pulse duration for a pulse energy of 10^5 J and a frequency of 10 Hz. The specific energy decreases with increasing pulse duration for a fixed pulsed energy. For long pulse durations the rotor length becomes too short unless the tip speed is decreased. When the tip speed decreases the rotor mass must increase for a fixed stored energy (Equation 68). The result is increased rotor mass and decreased specific energy.

3.4.4 Input Conditioner Models

3.4.4.1 DC-DC Converters

DC-DC converters are used: (1) to perform voltage scaling to allow high voltage power transmission, (2) to operate with near-constant input impedance to provide maximum power-point operation of the source, (3) to provide constant power, variable voltage and current, energy store charging, (4) to protect the system from electrical transients generated by the source, and (5) to perform all above functions for the entire range of power level of interest.

In a previous Air Force contract, we modeled a DC-DC converter that satisfies all these requirements.² An actively controlled series resonant inverter-converter is required. A block diagram of a DC-DC converter is presented in Figure 24. The electric energy from the DC source is passed through a high frequency input filter which protects the source and the DC-DC converter from electrical transients. The next stage of the converter is a series resonant inverter with active pulse modulation. The inverter generates high frequency power which is modulated in frequency and amplitude during generation. Active modulation control provides system stabilization, maximum power point tracking, and load voltage tracking. The high frequency transformer performs the voltage scaling function and a diode bridge rectifies the power. The high frequency output filter removes the harmonic content of the internally generated AC power.

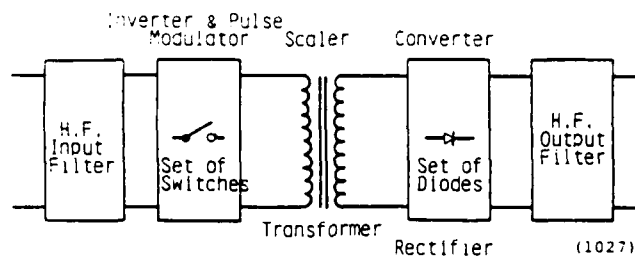


Figure 24. DC-DC Converter Block Diagram.

The mass of this DC-DC converter was found to be:

$$m = 10 + 0.057P^{0.5} + 0.014P^{0.75} + 10^{-4}P \quad (73)$$

where m is the mass in kg, and P the input power in W. This model is valid for power levels ranging from 5 kW to 1 MW. The mass and specific mass of DC-DC converters are presented in Figures 25 and 26 respectively. The efficiency of DC-DC converters was reported to range from 88% to 97% and to depend on the specific design, not on the power level handled. We assumed an efficiency of 92% for all power levels.

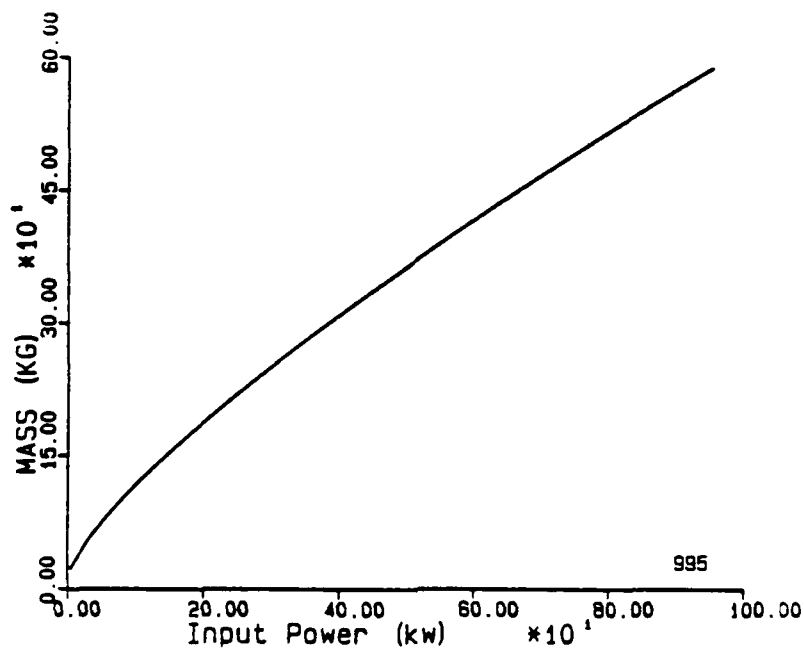


Figure 25. DC-DC Converter Mass.

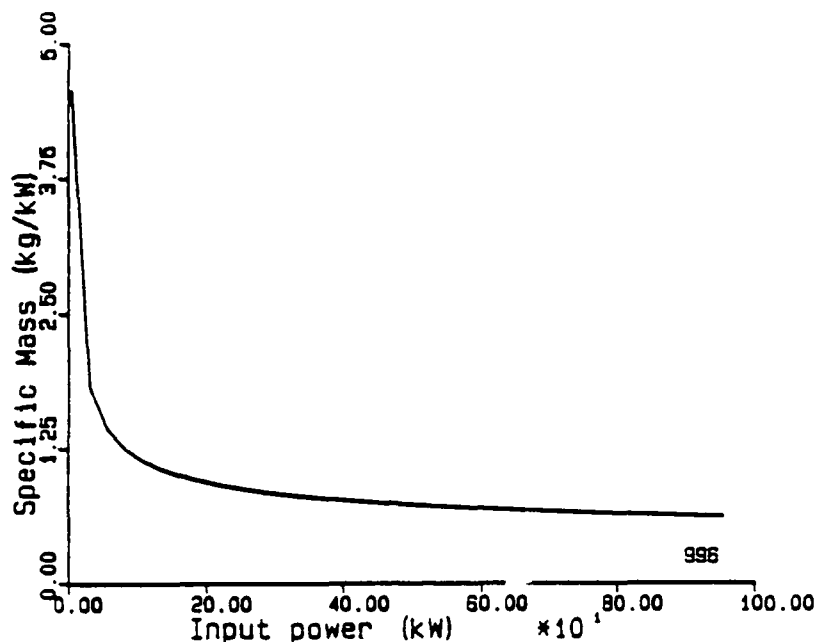


Figure 26. DC-DC Converter Specific Mass.

3.4.4.2 Electric Motors

Electric motors are required to convert electrical energy from the primary power source to mechanical energy for inertial energy stores.

We investigated electric motors to determine which type is best suited for space applications, and to develop mass models over the power range of interest. We conducted a literature search and contacted motor manufacturers. Only motors in the low power range (150 W - 75 kW) have been developed for space/aerospace applications. No data was found for power levels above 75 kW. At these low power levels, permanent magnet brushless DC motors and variable frequency AC induction motors have the highest specific power. The available performance data for space-qualified motors were curve-fitted and the resulting equation is:

$$w = P(0.046 + 0.21 \omega/P) \quad (74)$$

where w is the specific power in W/kg, ω is the rotational speed in rad/s and P is the average power in Watts. The efficiency of these motors was estimated to be 90%. The efficiency of electric motors generally increases with power level and rotational speed.

Electric motor performance data for terrestrial application were used to project the performance of space qualified motors to power levels higher than 75 kW. The available performance data for motors for terrestrial applications were curve-fitted to obtain the specific power and efficiency. The specific power is:

$$w = 4.706P^{0.2926} \quad (75)$$

and the efficiency:

$$\eta = 67.96P^{0.0252} \quad (76)$$

The projected specific power for space-qualified motors is:

$$w = 19.18P^{0.2368} \quad (77)$$

This model has the same 'slope' as the data for motors for terrestrial applications and is presented as a dashed line in Figure 27. This model results in a conservative estimate for the mass of electric motors for space applications.

3.4.4.3 Series-Parallel Switching of Primary Power Modules

Series-Parallel Switching (S-P) of primary power modules is an input conditioning method which allows constant power charging of either capacitive or inductive energy stores, and eliminates the need for voltage scaling. S-P can be designed to deliver any required current/voltage level to the energy store.¹⁵ S-P can only be used with modular power sources such as photovoltaic, thermoelectric, and thermionic.

¹⁵ Ijichi, K., and Billerbeck, W. J., 'Capacitor Bank Charging by Series-Parallel Switching of Solar Arrays', 16th International Electric Propulsion Conference, 1982, AIAA-82-1879.

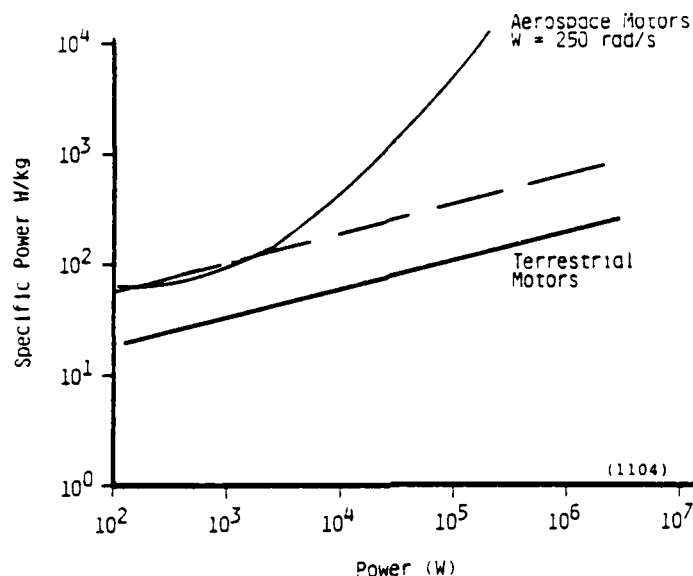


Figure 27. Specific Power of Electric Motors.

To illustrate this concept, consider a solar array which is used to charge a capacitor bank. The solar array can be divided in N modules where N is an even integer. All the modules are connected in parallel at the beginning of the charging cycle (configuration A in Figure 28). The I-V characteristic of configuration A is curve 'a' in Figure 29. The charging proceeds from point A to point B along curve 'a'. When the voltage reaches point B, the modules are switched to configuration B in Figure 28. The I-V characteristic of the array is then curve 'b' in Figure 29. The charging proceeds along curve 'b' to point C. Similar switchings are repeated until the voltage reaches the required value with the solar array in configuration D. Depending on the number of modules and switches, S-P will result in capacitor charging which closely approaches the constant power curve, 'e'.

We assumed that the modular power source had eight modules and that the switches used were SCR's. To model the mass we need an SCR mass model and a method to determine the number of SCR's required. For eight modules, the switches required and their characteristics are: 8 SCR's capable of $1/8$ the capacitor voltage and eight times the capacitor current, 4 SCR's capable of $1/4$ the voltage and 4 times the current, 2 SCR's capable of $1/2$ the voltage and twice the current, and 7 SCR's capable of the full voltage and current.

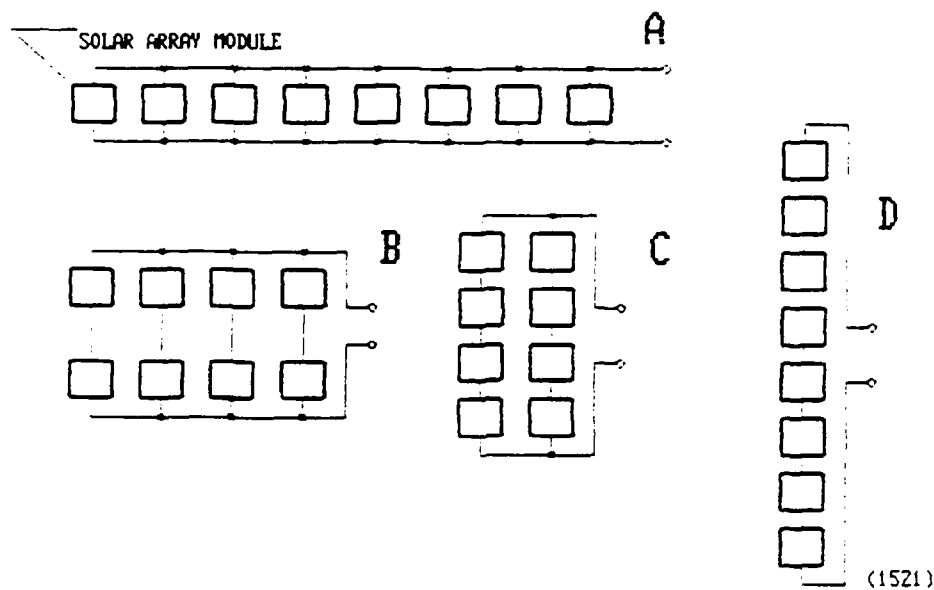


Figure 28. Series-Parallel Switching Concept.¹⁵

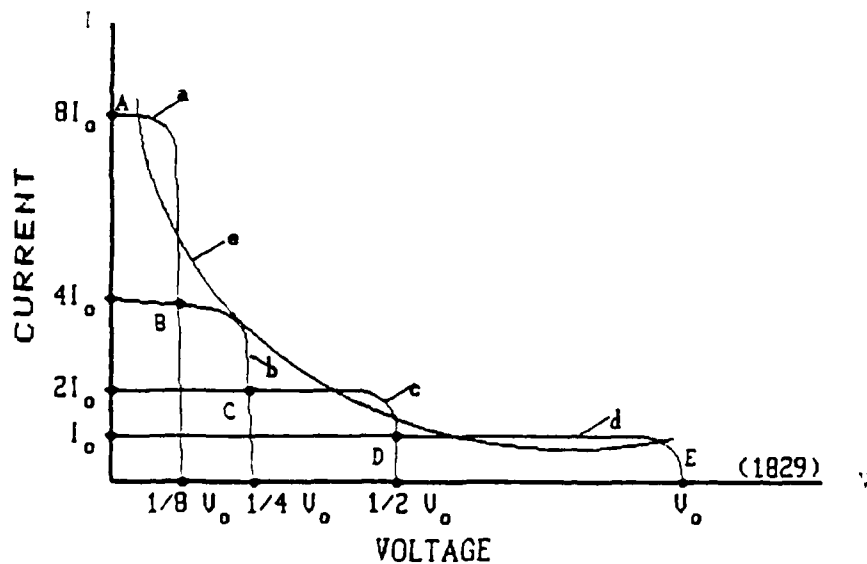


Figure 29. I-V Characteristics of S-P Switched Solar Arrays.¹⁵

This is a total of 21 switches. The mass and efficiency of each switch is calculated separately. The mass of the S-P system is the sum of the individual masses and the efficiency is the product of the individual efficiencies.

3.4.5 Output Conditioner Models

3.4.5.1 SCR'S

SCR's are semiconductor switches which have demonstrated long life and reliability. The mass, efficiency and operating constraints of SCR's are discussed below.

Fast switching SCR's capable of switching up to 17000 amperes and 2000 volts in a pulsed mode are available. For higher power requirements, SCR's can be placed in a series or parallel arrangement to switch the required current and voltage. SCR's have a life higher than the 10^9 cycles and an efficiency of better than 98%.

SCR current and voltage capabilities are limited by the breakdown voltage of the junction and by power dissipation in the on-state. Assemblies with cooling systems capable of keeping the SCR's at a safe temperature (175°C) are available.

Manufacturer's specification data¹⁶ were used to model the mass and efficiency of the SCR's. Two mass models were generated: one for SCR's used as closing switches (pulse rated data were used), and one for SCR's used as opening switches (RMS data were used). The mass models are presented in Figure 30. The mass of SCR's can be best modeled as normalized to the maximum safe conduction current (m/I). By normalizing the mass, we were able to account for the modularity of SCR's. For a specific application, the mass of the SCR (and assembly) is the product of the normalized mass and the required current. The normalized mass models for the SCR's as closing switches are:

$$m/I = 1.36 \times 10^{-3} \text{ for: } V < 1200\text{V}$$

and

$$m/I = 0.67 \times 10^{-6} V \times 5.6 \times 10^{-4} \text{ for: } V > 1200\text{V}$$

(78)

¹⁶Westinghouse Power Semiconductor User's Manual and Data Book.

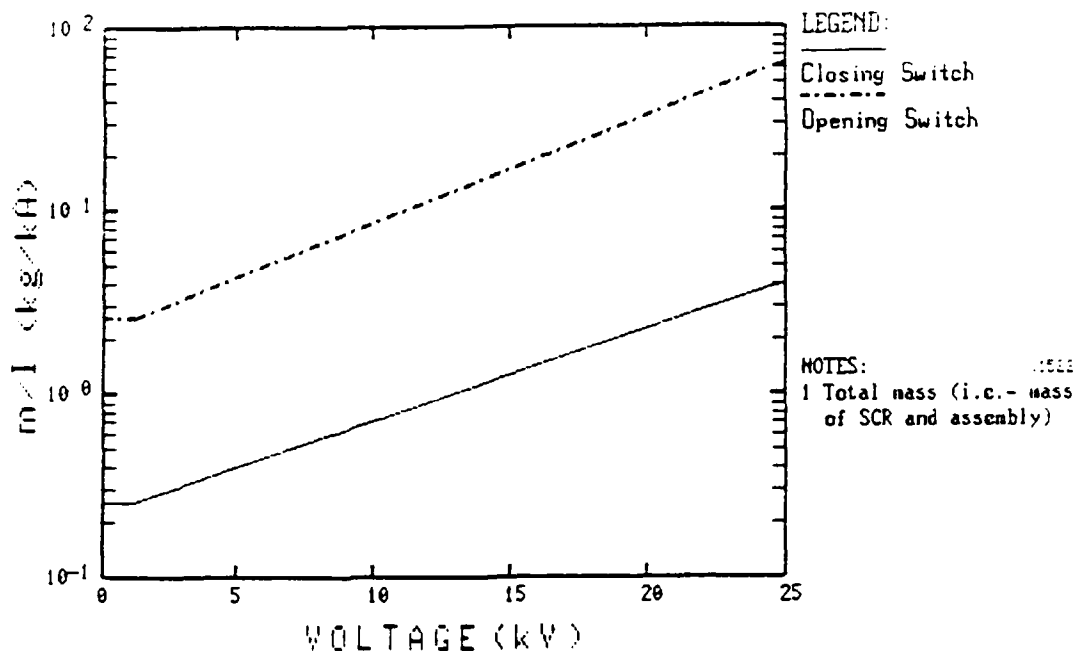


Figure 30. SCR's Mass Models.

The models for the SCR's as opening switches are:

$$m/I = 2.51 \times 10^{-3} \text{ for: } V < 1200V$$

and

$$m/I = 2.47 \times 10^{-6}V - 4.5 \times 10^{-4} \text{ for: } V > 1200V$$

(79)

The efficiency of the SCR's as modelled was about 99%.

3.4.5.2 Thyratrons

A thyatron is a gas-filled closing switch used in many applications which require high peak-power levels (MW or greater) for very short durations (10's of μs or less). A thyatron is shown schematically in Figure 31. It consists of two electrodes: an anode and a cathode. A third electrode, the control grid, is placed between the main electrodes. These three elements are contained in a sealed tube (typically ceramic) which is filled with a gas.

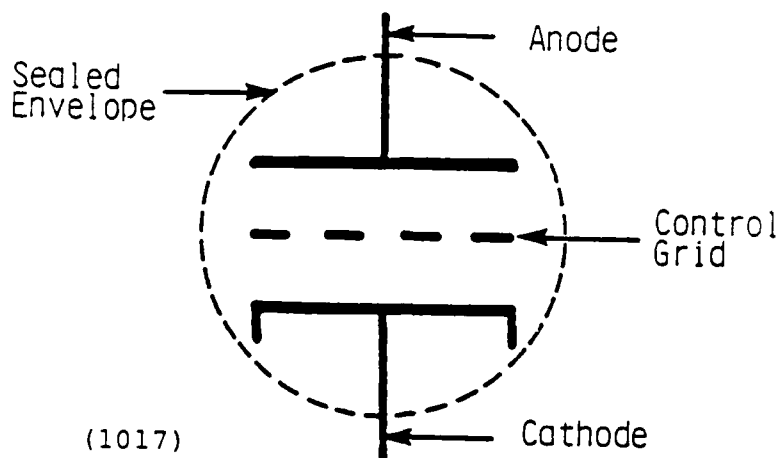


Figure 31. Thyratron Schematic.

Tube conduction is controlled by the grid voltage. When a positive signal is applied to the grid, the gas in the cathode-grid space becomes ionized. Ions near the grid are then accelerated by the anode field, causing the entire volume to become ionized. The tube then acts as a closed switch. A thyratron will continue to conduct as long as the gas remains ionized. During conduction, a positive space charge forms around the grid and effectively removes it from the circuit. Additional potentials applied to the grid will not control the anode-to-cathode current. In order to restore the tube to its 'open' condition, the anode voltage must be removed or made slightly negative for a time sufficient to allow the gas to deionize.

Thyratrons are used with mercury, rare gases, or hydrogen as the filler gas. Hydrogen is the most commonly used filler gas. Hydrogen provides a lower recombination (recovery) time and the voltage drop across its plasma is low enough to keep the ion velocities low. Ions with high velocities can damage the electrodes.

The parameters affecting thyratron performance are: peak current, peak voltage, pulse width, recovery time, pulse frequency (rep-rate), forward voltage drop, and lifetime (total number of pulses).

The peak current is limited by cathode arcing and grid quenching. When the peak current exceeds some allowable limit, an arc forms between the anode or grid and the cathode and damages the cathode. High peak currents can also cause localized heating (only a small part of the cathode is used

for conduction in each pulse) which degrades the performance of the thyatron. Thyratrons with a peak current capacity of 120 kA have been built.¹⁷

The peak voltage which a thyatron is capable of 'standing off' is determined by the distance between the anode and the control grid. Under repetitive pulse operation, more complex mechanisms begin to limit the stand-off voltage, such as charge accumulation on the tube walls. One way to increase the stand-off capabilities is to increase the number of control grids. Manufacturing procedures and tube packaging constraints place a practical limit of 40-50 kV/gap on the stand-off voltage.

The pulse width is limited by the peak current and the desired life of the tube. High currents for long times can result in arc formation and a high rate of cathode vaporization. Typical pulse lengths at peak currents are on the order of tens of microseconds.

The pulse rep-rate and the recovery time are inter-related. The maximum rep-rate is limited by the recovery time (time required for a gas to recombine and regain its stand-off capabilities). Thyratrons with rep-rates on the order of kHz have been built. High rep-rates increase the average heating of the tube and affect the tube performance and life.

The voltage drop in hydrogen thyratrons must be limited to keep the ion velocity below the critical velocity which damages the electrodes. Typical voltage drops are about 100 volts.

Thyatron life is strongly related to the allowable peak current, pulse width, and rep-rate in high frequency applications. The end of the tube life occurs when the cathode can no longer emit electrons into the neutral plasma to begin conduction. Typical hydrogen thyatron life is greater than 10^{11} pulses.

A mass model of the hydrogen thyatron was developed by curve-fitting available data. The data was derived from manufacturers' specification sheets. The mass of thyratrons can best be presented as specific power (w) versus peak power (P). The relationship is:

$$w = 5.31 \times 10^8 P^{-0.21} \quad (80)$$

¹⁷ EG and G Ceramic Metal Grounded Grid Thyratrons Data Sheet, H5003-1.

and is illustrated in Figure 32.

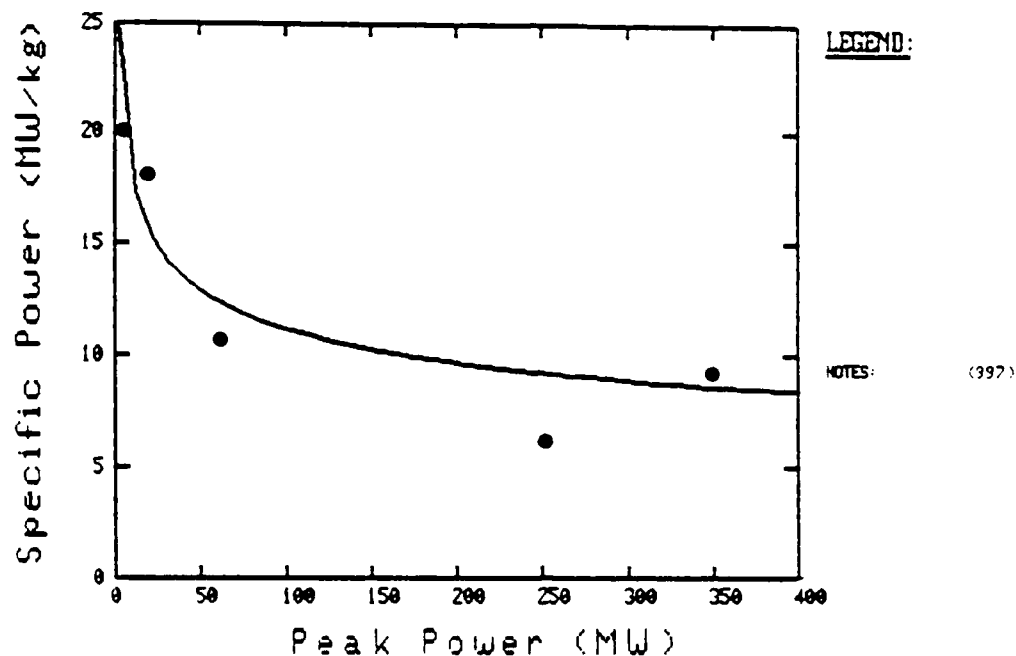


Figure 32. Thyatron Specific Power.

The efficiency of the thyatron can be calculated using the voltage drop (V_{drop}). The energy dissipated is:

$$E_{\text{dis}} = V_{\text{drop}} I / t_p \quad (81)$$

and the efficiency is given by:

$$\eta = (E_p - E_{\text{dis}}) / E_p \quad (82)$$

In most cases the efficiency is better than 95%.

3.4.5.3 Spark Gaps

A spark gap is a high-voltage, high-peak-current switch used in many pulse power applications. The major feature of this switch is that it is capable of transferring many coulombs of charge per pulse. The three most common types of spark gaps are the direct over-volted spark gap, the triggered spark gap, and the field distortion gap. All spark gaps consist of

two electrodes (an anode and cathode) separated by some distance (called the inter-electrode spacing). The elements are enclosed in a sealed envelope which is either evacuated or filled with a pressurized gas.

The direct over-volted spark gap breaks down when the stress in the inter-electrode gap exceeds some critical value. This critical value is called the self-breakdown voltage (SBV). The self-breakdown voltage is a very strong function of the inter-electrode spacing, the electrode shape, and the filler gas conditions (if a gas is present).

The triggered spark gap has a third electrode placed inside, but separate from, one of the main electrodes. An electrical pulse is applied to the third electrode generating an arc between it and the nearby electrode. The resultant 'mini discharge' causes the main electrodes to break down. The breakdown time is a function of the voltage across the gap. The closer the gap voltage is to the SBV, the faster the gap will break down.

The field distortion gap has a third element (usually a ring shaped device) placed between the two main electrodes. This 'trigger' is placed at a point where it is not normally distorting the electric field lines in the gap. When an electrical pulse is applied to the trigger electrode, the field in the gap is distorted and a breakdown occurs.

The parameters which affect spark gap performance are: peak current, peak voltage, pulse width, pulse rep-rate, total coulomb transfer, recovery time, and lifetime.⁸

The peak current is limited by the required pulse width, the resultant charge transfer per pulse, and the total number of pulses. Peak currents of hundreds of kA are not uncommon in typical spark gap applications.

The voltage which a spark gap can stand off is a complex function of the filler gas type (if a gas is present), the electrode material, and the electrode spacing. For extremely high voltage applications, the maximum standoff voltage is, in practice, limited by surface flashover outside of the gap rather than by the gap design itself. Peak voltages of millions of volts have been achieved and values as high as 100 kV are typical.

The maximum pulse width that a spark gap is capable of is a function of the required current and life. Pulse widths of tens of microseconds are common. The maximum single-shot pulse width is limited by electrode

cooling. The minimum pulse width is set by external circuit parameters. Pulse widths less than 1 ns have been achieved.

The allowable pulse rep-rate is limited by the recovery time and the rated voltage standoff. The recovery time is a fundamental limit to the maximum pulse rep-rate. The recovery time is limited by the plasma recombination time and the gas and electrode cooling rates. For 100% voltage standoff, a practical limit on pulse rep-rate is a few hundred pulses per second.

The total charge transferred during the life of a switch is equal to the charge transferred per pulse multiplied by the total number of pulses. The charge transferred per pulse is directly related to the current and pulse width. Spark gaps transfer a relatively large charge per pulse. This changes the surface microstructure of the main electrodes and affects operation. Very large charges per pulse have been transferred in single-shot devices.

The life of spark gaps is an area of considerable uncertainty. Nearly all manufacturers estimate spark gap life at 10,000 pulses at maximum rated conditions. Very little work on extrapolation of life data has been performed. The charge transferred per pulse must be decreased to increase life (a spark gap can only transfer a finite total charge during its life). Increased life can also be obtained by preionizing the gas with an external source to reduce the charge transfer load imposed on the electrodes. Although this technique has not been thoroughly tested, it is expected to increase the life to greater than 10^8 pulses.

Many factors affect the performance and mass of spark gaps. After analyzing the available data, we determined that the mass of the spark gaps is primarily a function of the total charge transferred. With this approach, we account for the peak current, pulse width, and life of the spark gap. The resulting mass model is presented in Figure 33 and is written as:

$$m = 0.0525 C^{0.4477} \quad (83)$$

where m is the mass in kg and C is the total charge transferred in coulombs.

4.2.3 Velocity Increment

The optimum propulsion system mass was proportional to the velocity increment for stationkeeping missions (Figure 41). We assumed that the velocity increment for orbit transfer missions is constant.

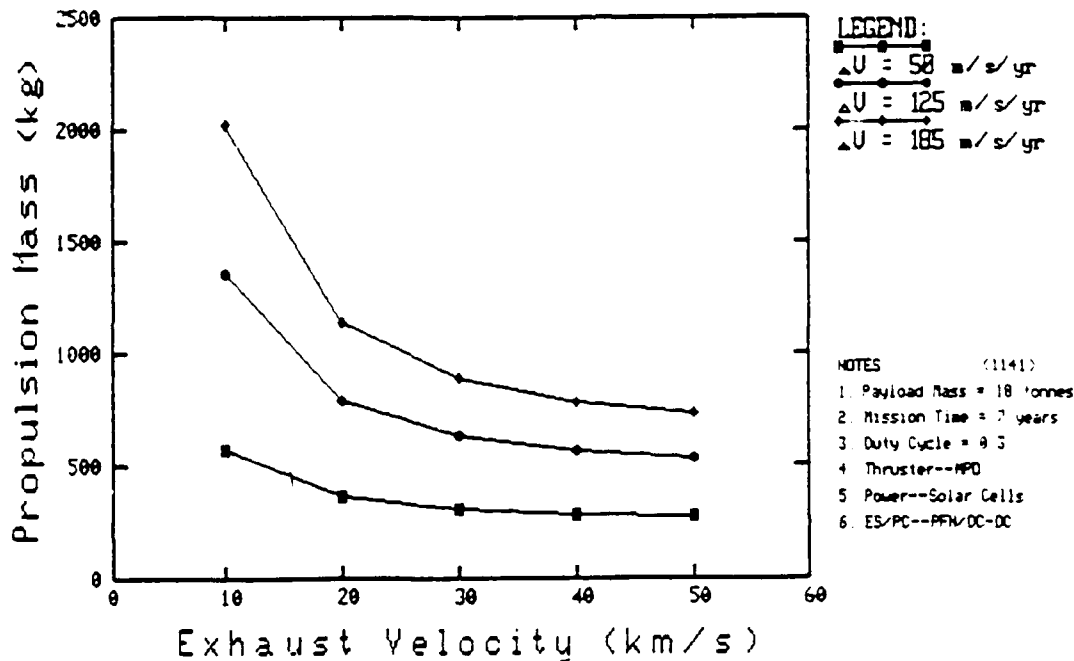


Figure 41. Velocity Increment Effects on Optimum Propulsion System Mass.

4.2.4 Primary Power Options

Photovoltaic power sources resulted in the lowest mass of optimum propulsion system for stationkeeping systems. This is illustrated in Figure 42.

Nuclear-based primary power sources become competitive with photovoltaic for orbit transfer missions. A typical example is illustrated in Figure 43.

4.2.5 ES/PC Options

The capacitive-based ES/PC options resulted in the lowest-mass optimum propulsion systems for stationkeeping missions. The normal inductive-based ES/PC options resulted in comparable optimum propulsion system mass. The

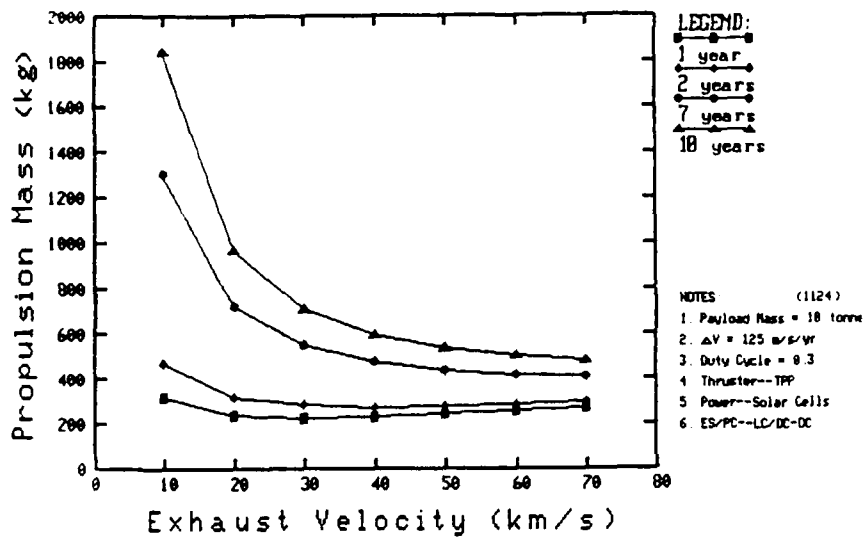


Figure 39. Optimum Propulsion System Mass for Different Mission Duration for Stationkeeping Missions.

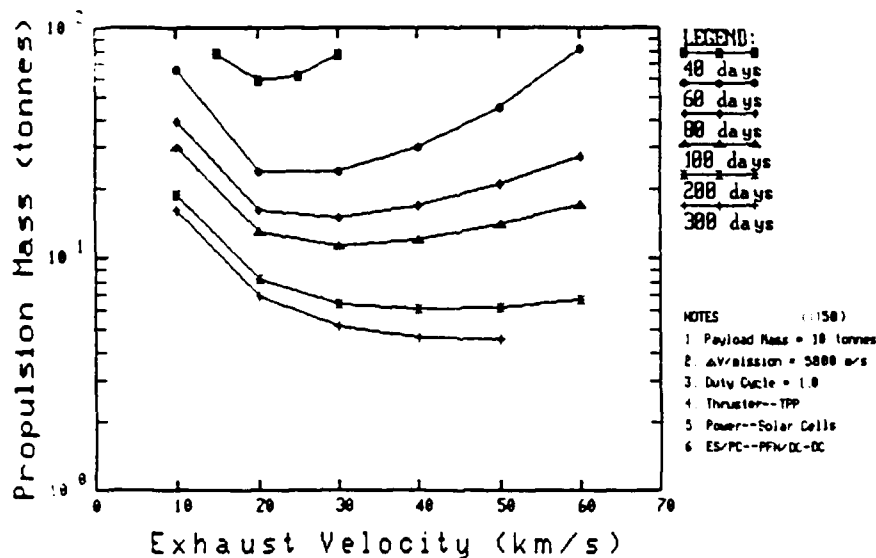


Figure 40. Optimum Propulsion System Mass for Different Mission Durations for Orbit Transfer Missions.

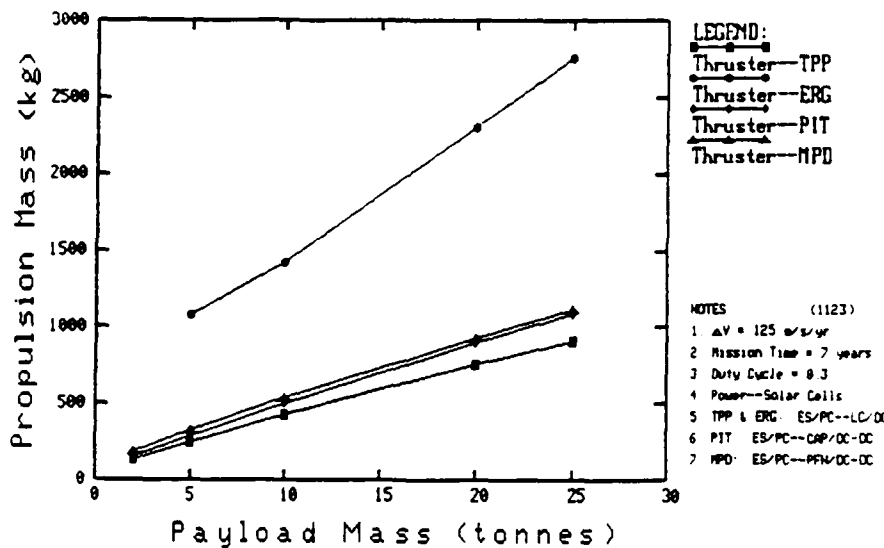


Figure 37. Optimum Propulsion System Mass for Different Payload Mass for Stationkeeping Missions.

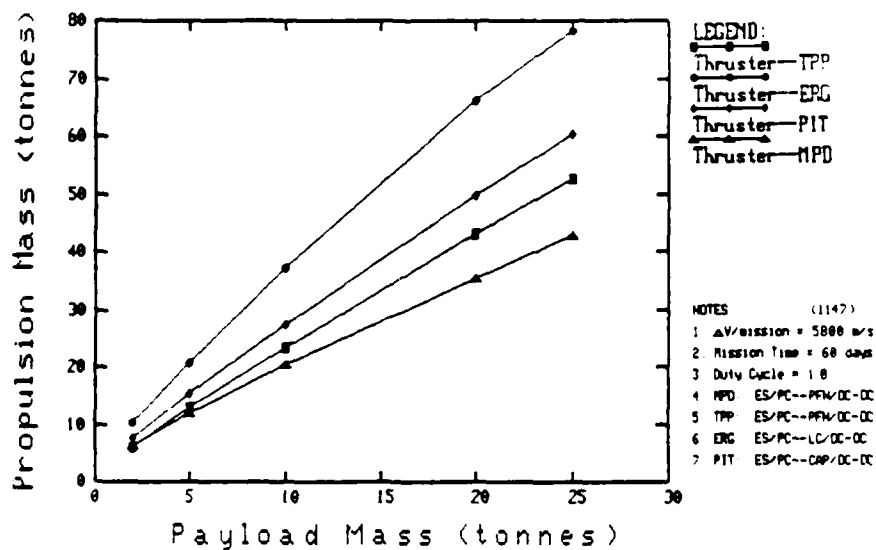


Figure 38. Optimum Propulsion System Mass for Different Payloads Mass for Orbit Transfer Missions.

In Table 12 we are presenting two propulsion systems designed by EPSDES. The first has an Isp of 1600 s, similar to the Martin Marietta system, and the second has an Isp of 3100 s. The propulsion system designed by EPSDES to operate at an Isp of 1600 s has the same mass as the Martin Marietta system. We cannot compare other characteristics of the system because of lack of information on Martin Marietta's system. But, we believe that the EPSDES-selected system operates with lower pulse mass and higher frequency than Martin Marietta's. The second system presented in Table 12 is the optimum system selected by EPSDES. The optimum system has 30% less mass than the Martin Marietta system and operates at an Isp of 3100 s. We believe that the optimum system has a higher frequency and lower pulse mass than Martin Marietta's system.

4.2 SENSITIVITY ANALYSIS

We analyzed the sensitivity of optimum propulsion system mass to variations in mission parameters, primary power options and ES/PC options for stationkeeping and orbit transfer missions. This was done by exercising EPSDES over the entire range of interest.

4.2.1 Payload Mass

The optimum propulsion system mass was proportional to payload mass for both stationkeeping and orbit transfer missions. This is illustrated in Figures 37 and 38 respectively. The mass of the propulsion systems for stationkeeping missions ranged from 5 to 15% of the payload mass depending on the thruster used. The ERG had the highest propulsion system mass and the other thrusters had similar masses. The mass of the propulsion systems for orbit transfer missions ranged from 2.5 to 3.5 times the payload mass. The ERG had the highest propulsion system mass.

4.2.2 Mission Duration

The optimum propulsion system mass was proportional to mission duration for stationkeeping missions (Figure 39), and increased exponentially with decreasing mission duration for orbit transfer missions (Figure 40). The optimum exhaust velocity decreased with decreasing mission durations for orbit transfer missions.

TABLE 11
ORBIT TRANSFER PERFORMANCE COMPARISON

Parameter	IAP MPD System (OPTIMUM)	IAP MPD System	MM18 MPD System	Chemical Systems	
				Advanced	Centaur
Payload Mass, kg	5000.	5000.	5000.	5000.	5000.
ΔV , m/s	5881.	5881.	5881.	5881.	5881.
Mission Time, days	408.	408.	408.	0.25	0.25
Thrust Eff., %	50.4	33.5	40.		
Total Eff., %	42.7	27.6	36.		
Average Power, kw	63.*	47.3*	50.*		
Isp, s	3700.	1600.	1600.	482.	443.
Power Mass, kg	859.6	655.5			
OTV Dry Mass, kg	1709.	1745	2958.	2295.	2590.
Propellant Mass, kg	1141.	2985	3582.	12145.	14120.
Propulsion Mass, kg	2850.	4730.	6540.	14440.	16710.

*BOL

TABLE 12
ORBIT TRANSFER PERFORMANCE COMPARISON
(The specific energy of capacitors was assumed to be 1.7 J/kg.)

Parameter	IAP MPD System (OPTIMUM)	IAP MPD System	MM18 MPD System	Chemical Systems	
				Advanced	Centaur
Payload Mass, kg	5000.	5000.	5000.	5000.	5000.
ΔV , m/s	5881.	5881.	5881.	5881.	5881.
Mission Time, days	408.	408.	408.	0.25	0.25
Thrust Eff., %	26.6	18.3	40.		
Total Eff., %	23.1	15.9	36.		
Average Power, kw	119.*	98.6*	50.*		
Isp, s	3100.	1600.	1600.	482.	443.
Power Mass, kg	1550.	1290.			
OTV Dry Mass, kg	2973.	3055.	2958.	2295.	2590.
Propellant Mass, kg	1666.	3575.	3582.	12145.	14120.
Propulsion Mass, kg	4640.	6630.	6540.	14440.	16710.

*BOL

TABLE 10

STATIONKEEPING PERFORMANCE COMPARISON
(The specific energy of capacitors was assumed to be 1.7 J/kg)

Parameter	IAP MPD System N-S Module	IAP MPD System E-W Module	IAP MPD System	MM ¹⁸ MPD System	Chemical System
Payload Mass, kg	20978.	20978.	19878	19878	19878
ΔV , m/s/yr	30.5	19.5	100.	100.	100.
Mission Time, yr	5.	5.	5.	5.	5.
Thruster No.	1	1	4	19	
Average Power, kw	6.39	7.2	27.2	4.9	
Thruster Eff., %	11.28	11.35	11.3	54.	
Total Eff., %	9.79	9.73	9.76	43.	
Isp, s	4000.	3500.	3700.	5000.	285.
Frequency, hz	80.6	73.7	77.1	2.7	
Pulse Energy, J	69.	83.7		625.	
Pulse Time, ms	0.1	0.11		1.	
ES/PC Mass, kg	102.	114.	432.	1476.	
Primary Power, kg	121.	132.	506.		
Dry Mass, kg	239.	258.	994.	2579.	1142.
Propellant Mass, kg	81.	59.	280.	233.	3984.
Propulsion Mass, kg	320.	317.	1274	2812.	5126.

The EPSDES selected a propulsion system that has a mass less than 1/2 the Martin Marietta system. The selected system has an Isp of 3700 s which is twice the Isp of the Martin Marietta system. This led to higher system efficiency and lower mass.

We suspect that the higher Isp was selected because of a difference in the specific energy of the energy store (capacitor). Therefore, we reran EPSDES with a specific energy of 1.7 J/kg which we believe that Martin Marietta used in their analysis. The results of the new run of EPSDES and Martin Marietta results are presented in Table 12.

TABLE 9
STATIONKEEPING PERFORMANCE COMPARISON

Parameter	IAP MPD System N-S Module	IAP MPD System E-W Module	IAP MPD System	MM ¹⁸ MPD System	Chemical System
Payload Mass, kg	20478.	20478.	19878	19878	19878
ΔV , m/s/yr	30.5	19.5	100.	100.	100.
Mission Time, yr	5.	5.	5.	5.	5.
Thruster No.	1	1	4	19	
Average Power, kw	3.52	4.09	15.22	4.9	
Thruster Eff., %	26.2	28.72	27.5	54.	
Total Eff., %	21.59	23.7	22.6	43.	
Isp, s	5000.	5000.	5000.	5000.	285.
Frequency, Hz	6.	5.21	5.6	2.7	
Pulse Energy, J	484.	650.		625.	
Pulse Time, ms	0.21	0.25		1.	
ES/PC Mass, kg	73.2	81.5	309.5	1476.	
Power Mass, kg	86.4	93.8	360.4		
Dry Mass, kg	171.	181.75	705.5	2579.	1142.
Propellant Mass, kg	63.	40.25	206.5	233.	3984.
Propulsion Mass, kg	234.	222.	912	2812.	5126.

4.1.3.2 The Orbit Transfer System

The orbit transfer mission specifications were:

Payload Mass = 5000 kg
 ΔV = 5881 m/s
Mission time = 408 days

Using the EPSDES computer code, we sized the optimum propulsion system for this mission. The EPSDES and Martin Marietta results are presented in Table 11.

4.1.3.1 The Stationkeeping System

The stationkeeping mission specifications were:

Payload mass	=	19878 kg
Mission time	=	5 years
ΔV	=	500 m/s

Martin Marietta assumed four thrusting modules. Three modules had five thrusters and one module had four thrusters. Each module had one ES/PC system. N-S stationkeeping required a ΔV of 61 m/s/yr and a duty cycle of 0.666. E-W stationkeeping required a ΔV of 39 m/s/yr and a duty cycle of 0.333. For EPSDES modeling purposes, we assumed that two modules were used for N-S and two for E-W stationkeeping, that each module had one thruster, and that each thruster was required to deliver half the required ΔV . The payload mass was also increased by a mass equivalent to 3 thrusting modules. Using EPSDES computer code, both E-W and N-S MPD propulsion systems were sized. The EPSDES and Martin Marietta results are presented in Table 9.

The system selected by the EPSDES has a propulsion system mass of less than 1/3 of the Martin Marietta system. The main difference between EPSDES and the Martin Marietta results was the mass of the ES/PC. EPSDES predicted an ES/PC which was one-fifth the mass of the ES/PC predicted by Martin Marietta. This was caused by the conservative specific energy of capacitors used by Martin Marietta, which was 1.7 J/kg. As a result of this comparison, we reran EPSDES for the same mission but we assumed that the capacitors had the same specific energy used by Martin Marietta. The EPSDES results of the new run and Martin Marietta results are presented in Table 10.

The new system selected by the EPSDES has a propulsion system mass of less than a half of the Martin Marietta system. EPSDES selected a propulsion system that delivers small pulses one-eighth the size of Martin Marietta's at a lot higher frequency than Martin Marietta (25 times). This is to be expected since a high price must be paid to store energy. In summary, the system selected by EPSDES uses the ES/PC more efficiently which leads to a saving of half the propulsion system mass.

4.1.2 Optimum Propulsion Systems

We used EPSDES to examine the general characteristics of optimized propulsion systems for both stationkeeping and orbit transfer. The mass of the optimum propulsion system for stationkeeping missions ranges from 5% to 15% of the payload mass depending on the thruster used. The ERG had the highest propulsion system mass. The minimum allowable pulse mass of the ERG is 0.1 g, 3 orders of magnitude higher than that for the other thrusters. This results in high stored energy and a corresponding high ES/PC mass. The largest mass component of the propulsion system for stationkeeping was the propellant at about 50%. The optimization tradeoff for stationkeeping is primarily between energy storage mass in the ES/PC and primary power mass. As expected the ES/PC and primary power have about equal mass in optimized systems.

The mass of the optimum propulsion system for orbit transfer missions ranges from 2.5 to 3.5 times the payload mass, with the ERG being the heaviest. The ES/PC mass was the least massive component at about 15% of propulsion system mass. In orbit transfer missions the optimization tradeoff is primarily between propellant and primary power. As expected these two components had about equal mass in optimized orbit transfer systems.

Within the ES/PC system, the major components of optimized stationkeeping systems had approximately equal mass. The ERG was an exception. The major mass component of the ES/PC for the ERG was the energy store at about 80% of the ES/PC mass. The major mass component of the ES/PC for orbit transfer missions was the radiator at about 45%. The energy store was 30%, the input conditioner 15%, and the output conditioner 10% of ES/PC mass.

4.1.3 Comparison of EPSDES with Martin Marietta Results

Martin Marietta¹⁸ conducted two propulsion system point designs in their 'MPD Definition Study Program'. The first point design was for a stationkeeping mission and the second was an orbit transfer mission. We exercised EPSDES for the same missions. Both designs were MPD thruster-based. Our objective was to compare the EPSDES approach to system sizing with the more traditional approach used by Martin Marietta.

¹⁸ 'MPD Thruster Definition Study,' Martin Marietta, 1983.

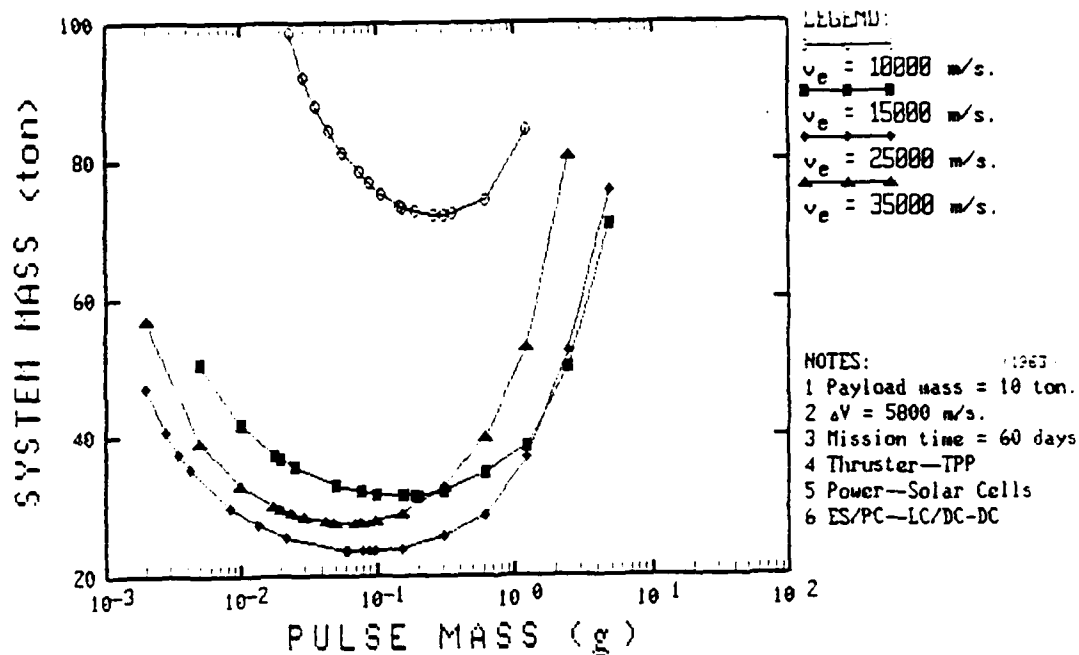


Figure 35. Propulsion System Optimization (Orbit Transfer, TPP).

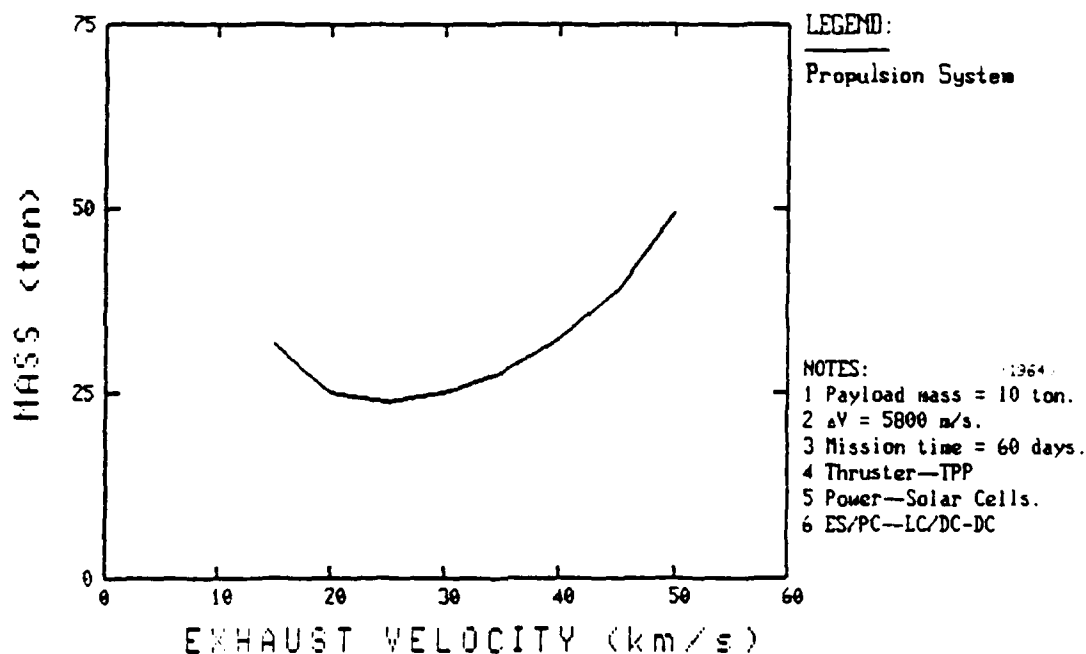


Figure 36. Optimum Propulsion System Mass (Orbit Transfer, TPP)

SECTION 4

RESULTS

We exercised the EPSDES program extensively. The first series of computations were designed to examine the performance of the program, to establish the validity of the solutions which it finds, and to determine the general characteristics of optimally sized propulsion systems. We then used EPSDES to conduct a sensitivity analysis. We examined the sensitivity of propulsion system size to variations in mission parameters over the entire range of mission parameters defined in Section 2.

4.1 EPSDES VALIDATION

4.1.1 EPSDES Optimization

The basic assumption underlying the development of EPSDES was that for each mission and thruster combination, there is one set of propulsion system output parameters (m_p , v_e and f) which minimizes the propulsion system mass. The first task was to verify this assumption.

We selected an orbit transfer mission and a TPP-based propulsion system to check the validity of EPSDES. EPSDES was run with a fixed exhaust velocity and the pulse mass (and frequency) was varied. The results at several exhaust velocities are shown in Figure 35. Each point on the graph represents an integrated TPP-based propulsion system which will be capable of doing the required mission. There is a clear minimum in propulsion system mass at each exhaust velocity. We conclude that for each exhaust velocity, there is an optimum pulse mass which minimizes the propulsion system mass.

Figure 35 also shows that selection of the exhaust velocity has a pronounced effect on propulsion system mass. The locus of the minima of the curves in Figure 35 are plotted in Figure 36. There is a combination of exhaust velocity and pulse mass (and frequency) which results in minimum propulsion system mass. This combination results in the 'optimized' propulsion system. We ran EPSDES for a wide range of missions and an optimum propulsion system was always found.

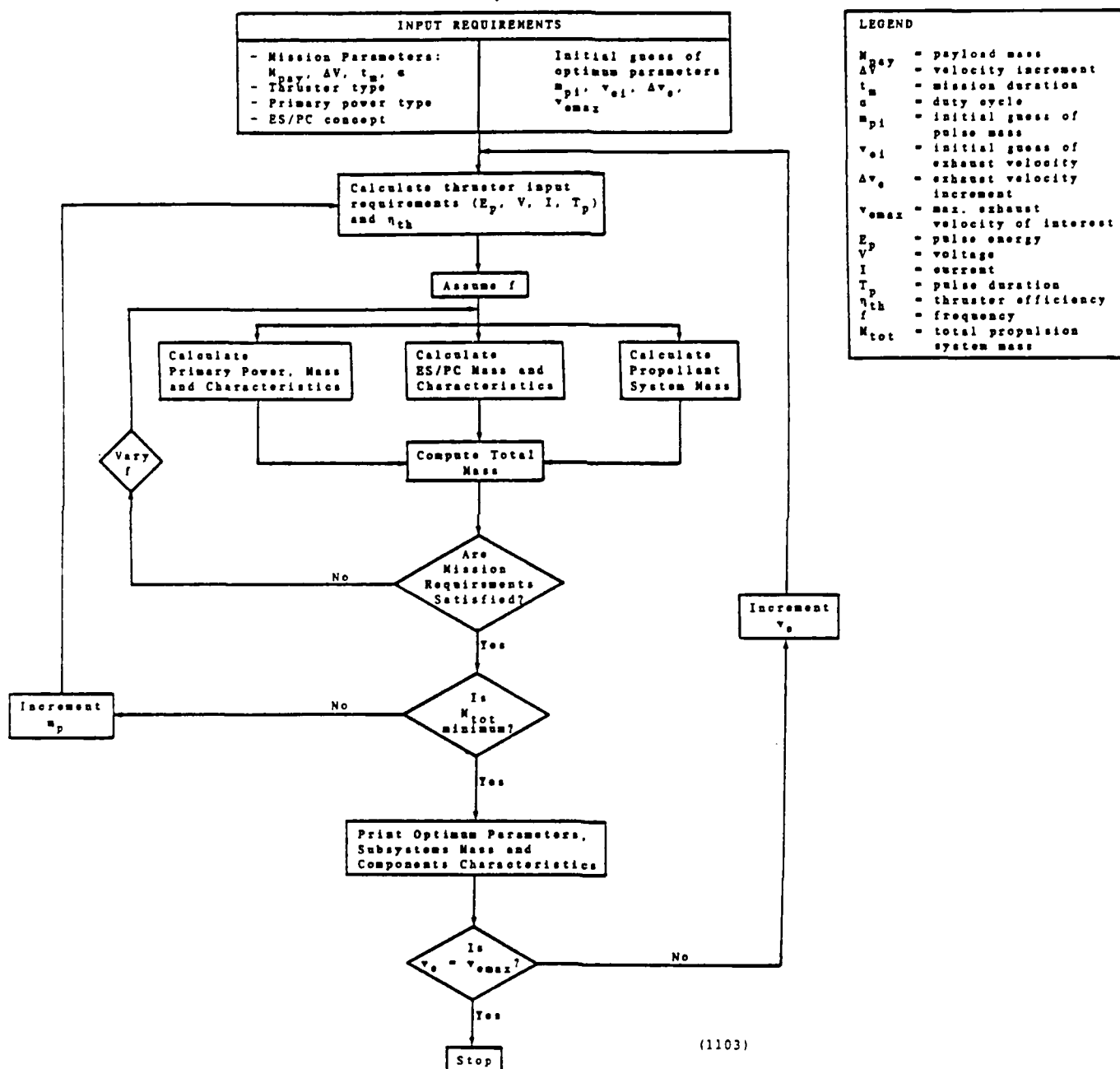


Figure 34. Flowchart of the Electric Propulsion System DESIGN (EPSDES) Computer Program.

3.5 SYSTEM INTEGRATION

To assess the propulsion system as an integrated system, the subsystems and components characteristics and performance models must be incorporated into a system level description of an electromagnetic propulsion system. The system integration can be best accomplished by using numerical techniques because of the complexity of the models and the large number of options.

We developed an Electromagnetic Propulsion System Design (EPSDES) computer program to assist in selecting and sizing the optimum propulsion system for a specific mission. EPSDES is written in FORTRAN. EPSDES calculates the combination of m_p , v_e , and f which minimizes the propulsion system mass and satisfies the mission requirements. A simplified flow chart is presented in Figure 34.

EPSDES is an interactive program which prompts the user for the required input data. The input data are: (1) the mission parameters M_{pay} , ΔV , t_m , and α , (2) the thruster type, (3) the primary power type, (4) the ES/PC type, (5) the exhaust velocity range and increment, and (6) an initial guess for the pulse mass. The output data are the optimum subsystem masses and component characteristics at each exhaust velocity within the range specified.

The validation of EPSDES as a propulsion system optimization program is presented in Section 4. Also, we are presenting in Section 4 a comparison between EPSDES results and known point designs, and the results of sensitivity analyses of the optimum propulsion system size to variations in mission parameters.

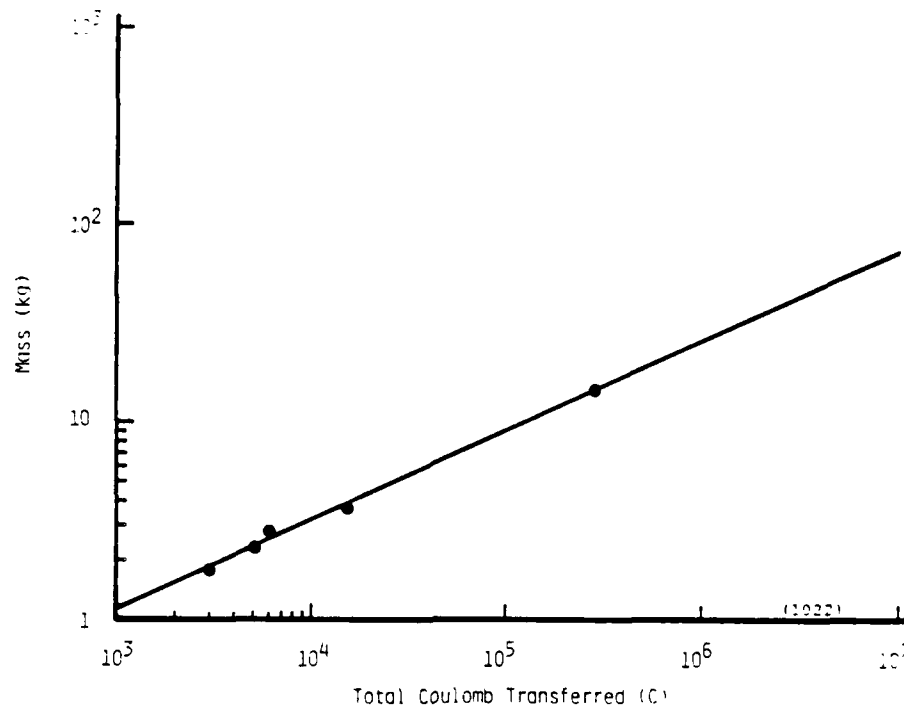


Figure 33. Spark Gap Mass.

This model assumes that the mass is independent of the spark gap type and that the total charge transfer is equal to the product of the number of pulses and the charge transfer per pulse. The efficiency of spark gaps was estimated to be 90%.

3.4.6 Heat Rejection System Model

The ES/PC system produces heat which must be rejected to maintain the operation and/or to keep temperatures within acceptable limits. We assumed that the heat is rejected through a low temperature radiator.

In a previous contract to the Air Force², we modelled the specific mass of a low temperature radiator for space applications. The specific mass is given by:

$$w = 7.24 \times 10^7 T^{-4} \quad (84)$$

where w is in kg/W and T is the temperature of the radiator in °K. Equation 84 is valid for temperatures ranging from 250°K to 500°K.

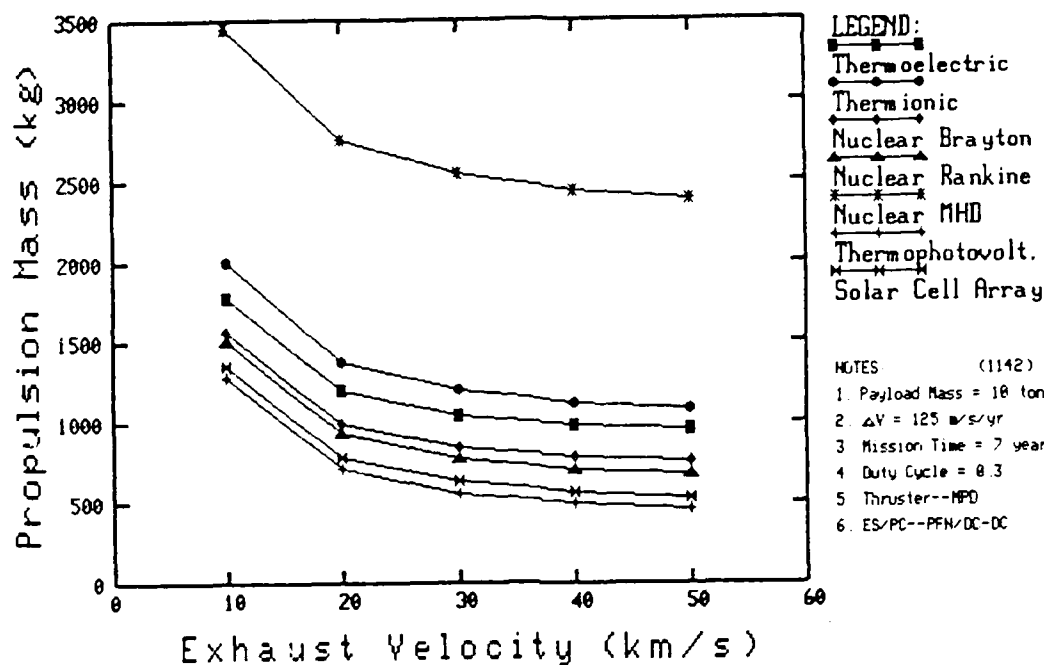


Figure 42. Effects of Primary Power Options on Optimum Propulsion System Mass for Stationkeeping Missions.

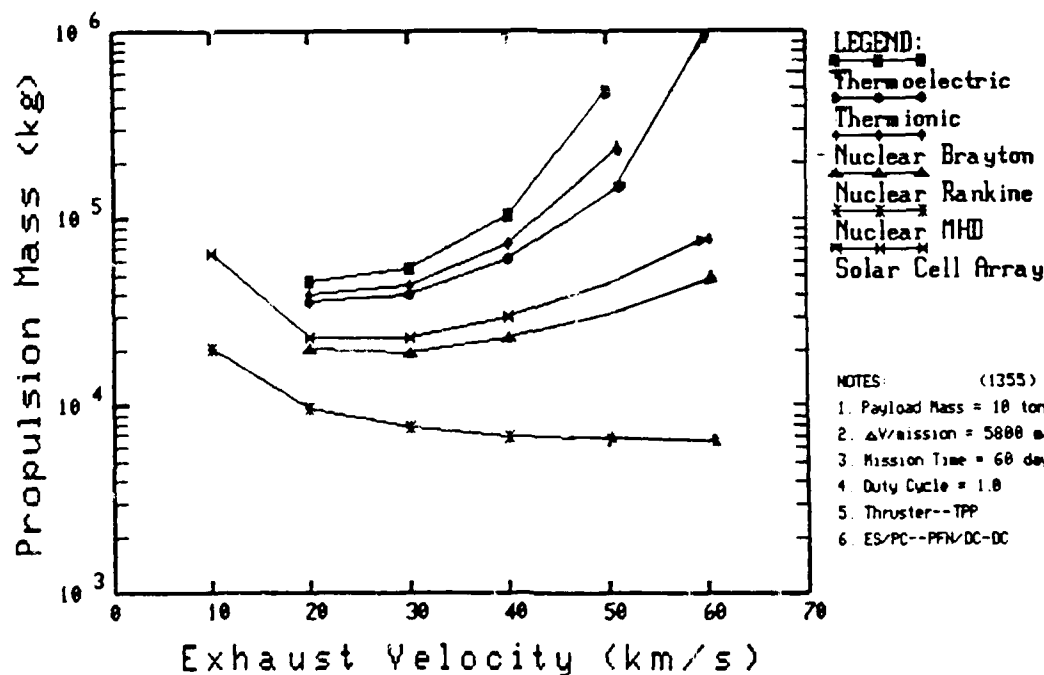
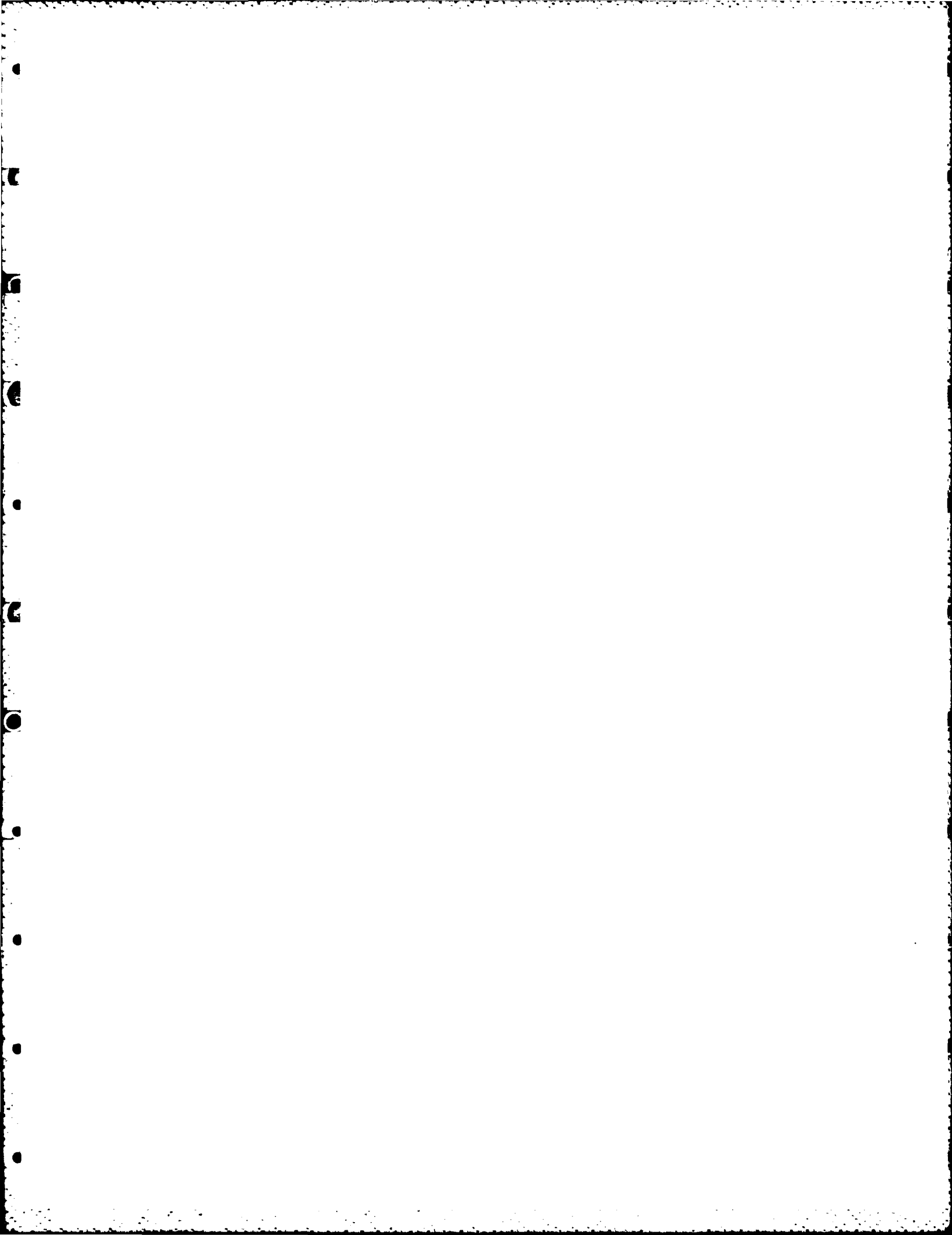


Figure 43. Effects of Primary Power Options on Optimum Propulsion System Mass for Orbit Transfer Missions.



superconductor inductive ES/PC resulted in a much heavier optimum propulsion system. The inertial energy stores were not feasible for the PIT and TPP thrusters because of the short pulse duration required. A typical example of the effects of ES/PC options on propulsion mass is presented in Figure 44.

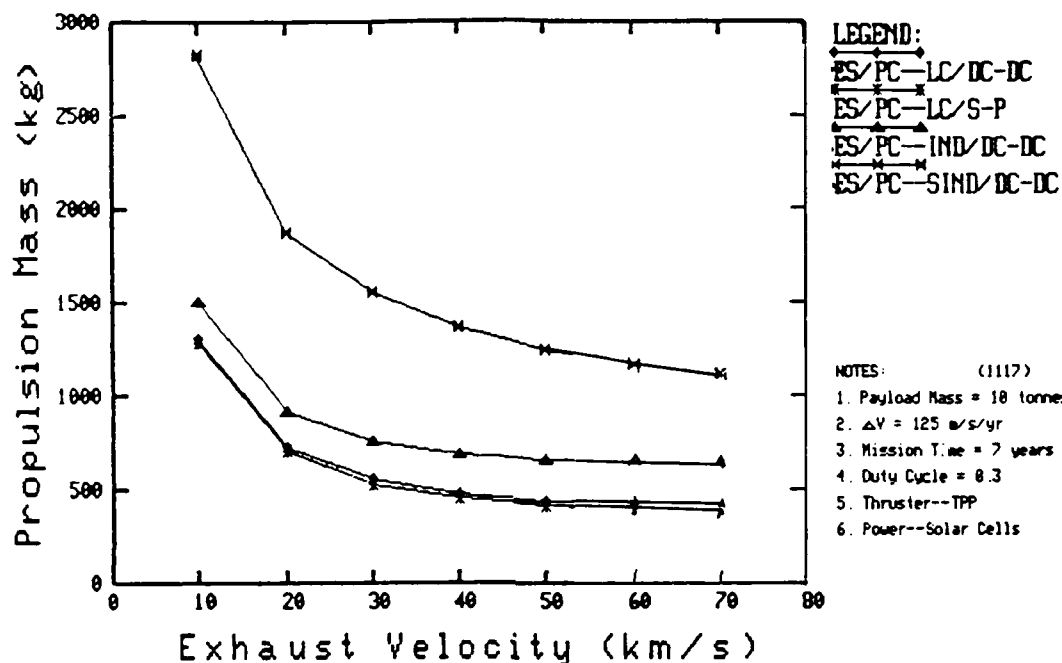


Figure 44. Propulsion System Mass for Different ES/PC Options for Stationkeeping Missions.

For orbit transfer missions, the capacitive-based ES/PC options resulted in the least massive optimum propulsion system. The inductive-based ES/PC options (both normal and superconductor) resulted in comparable results. The inertial energy stores resulted in much more massive propulsion systems. The propulsion system masses for various ES/PC options are presented in Figure 45.

4.3 POINT DESIGNS

To demonstrate the methodology developed in this program, we conducted two point designs, one was for a stationkeeping mission and one for an orbit transfer mission. The missions specifications and the results of the point designs are discussed below.

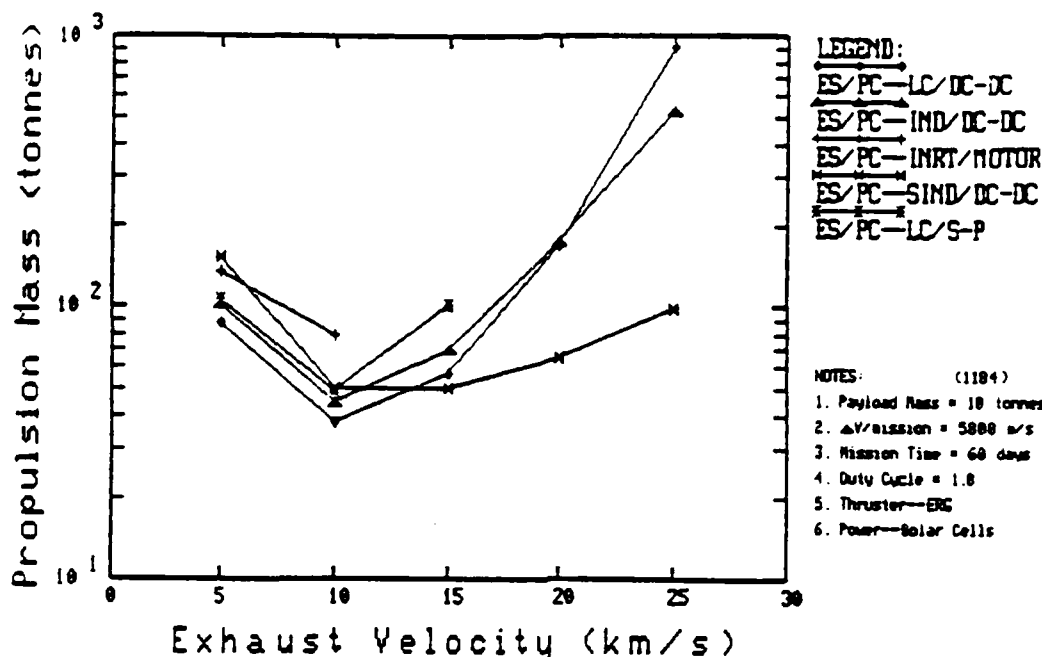


Figure 45. Propulsion System Mass for Orbit Transfer Missions Using Different ES/PC Options.

4.3.1 Stationkeeping Mission

The stationkeeping mission specifications were:

Thruster:	MPD
Primary power source:	Solar cell arrays
Payload mass:	20,000 kg.
ΔV :	875 m/s
Mission duration:	7 years

To analyze this mission we assumed that:

- (1) Four thrusters are required. Two for E-W stationkeeping and two for N-S.
- (2) The two thrusters for each function are identical.
- (3) Each thruster has an independent ES/PC.
- (4) The mission ΔV was divided equally among the four thrusters.
- (5) E-W stationkeeping was done continuously, i.e., duty cycle = 1.
- (6) N-S stationkeeping was done with a duty cycle = 0.3.

The optimum propulsion system for each thruster was then determined from the Propulsion System Optimization Computer Code. The optimum

propulsion system is presented in Table 13, the size and characteristics of the thrusters in Table 14, and the size and characteristics of the ES/PC components in Table 15.

The optimum propulsion system output parameters are: a pulse mass of 0.3 mg, an exhaust velocity of 50,000 m/s, and a frequency of 7 Hz. These output parameters resulted in a propulsion system which has a mass of 1200 kg, which is 6% of the payload mass, and a system efficiency of 22%. The average power level required to power the system is 19 kW.

The low system efficiency is caused by the low efficiency of the thrusters which is about 27%. The thrusters have a low efficiency because of the low pulse duration which is on the order of few hundred microseconds.

The optimum ES/PC mass is 350 kg which is 30% of the propulsion system mass. As expected, the major mass components of the ES/PC have equal weights.

TABLE 13

STATIONKEEPING OPTIMUM PROPULSION SYSTEM FOR A POINT DESIGN

Parameter	MPD System N-S Module	MPD System E-W Module	Propulsion System
Payload Mass, kg	21000.*	21000.*	20000.
ΔV , m/s/yr	31.25	31.25	125.
Mission Time, yr	7.	7.	7.
Thrust/Engine, N	0.07	0.021	0.045
Average Power, kw	6.27	2.80	18.14
Thrust Eff., %	30.90	23.06	26.98
Total Eff., %	25.52	19.00	22.25
Isp, s	4500.	5000.	4750.
Frequency, Hz	5.40	6.97	6.18
Pulse Energy, J	958.	331.	644.5
Pulse Time, ms	0.31	0.18	0.24
ES/PC Mass, kg	110.	62.7	345.4
Dry Mass, kg	250.7	157.5	816.4
Propellant Mass,kg	103.3	92.5	391.6
Propulsion Mass,kg	354.	250.	1208.

- * The payload mass was increased by an amount equivalent to the mass of 3 thrusting modules.

TABLE 14

THRUSTER SIZE AND CHARACTERISTICS FOR STATIONKEEPING POINT DESIGN

Parameter	MPD for N-S	MPD for E-W
Outer radius, cm	2.8	1.9
Length, cm	11.0	5.9
Efficiency, %	30.9	23.
Mass flow rate, g/s	0.95	0.33
Isp, s	4500.	5000.
Frequency, Hz	5.4	6.97
Pulse duration, ms	0.31	0.18
Pulse energy, J	957.	330.7
Average Voltage, V	196.5	183.
Average current, A	15810.	9889.

4.3.2 Orbit Transfer Mission

Two thrusters were assumed for this mission. The required ΔV was divided equally among the two.

The optimum propulsion system for the orbit transfer mission is presented in Table 16, the size and characteristics of the thruster in Table 17, and the ES/PC system in Table 18.

The selected ES/PC system was a DC-DC converter, a capacitor and a hydrogen thyatron closing switch.

The optimum propulsion system output parameters are: a pulse mass of 35 mg, an exhaust velocity of 26000 m/s and a frequency of 10.5 Hz. The propulsion system mass is 20,400 kg which is twice the payload mass. The system efficiency is 55%. The average power level required to power this mission is 450 kW.

The mass breakdown of the major components of the propulsion system is as follows: the primary power source mass is 10,000 kg, the propellant and containers mass are 7660 kg, and the ES/PC mass is 2600 kg. The primary power mass is the heaviest because of the relatively short mission time.

The heaviest component of the ES/PC was the radiator with a mass of 865 kg (35% of the ES/PC mass). The energy store mass was about 30% of the ES/PC mass, and the input and output conditioners have about equal mass (15% of the ES/PC mass).

TABLE 15

ES/PC SIZE AND CHARACTERISTICS FOR STATIONKEEPING POINT DESIGN

Component	Parameter	ES/PC for N-S*	ES/PC for E-W*
Capacitor**	Efficiency, %	98.	98.
	Mass, kg	5.62	2.76
	Volume, m ³	3.12E-3	1.53E-3
	Dimension, m	0.15	0.12
	Capacitance, F	2.48E-3	9.87E-4
	Voltage, V	393.1	366.
	Energy stored, J	191.4	66.1
	Number of cycles	3.58E8	1.54E9
	Specific energy, J/kg	34.	23.9
Inductor**	Efficiency, %	92.5	92.3
	Mass, kg	1.75	0.78
	Inductance, H	0.38E-6	0.34E-6
	Mean radius, cm	6.5	5.
	Length, cm	26.1	19.9
	No. of turns	2.8	3.
	Thickness, cm	0.67	0.51
	Resistance, ohm	5.05E-5	7.67E-5
SCR	Efficiency, %	99.	99.
	Mass, kg	21.5	13.5
	Volume, m ³	29.8E-3	19.9E-3
	Dimension, m	0.31	0.27
	No. of SCR's	6	4
	No. in parallel	6	4
	No. in series	1	1
DC-DC Converter	Efficiency, %	92.	92.
	Mass, kg	25.	18.7
	Average power, W	6259.	2797.
	Volume, m ³	9.25E-3	6.92E-3
Radiator	Dimension, m	0.21	0.19
	Temperature, Deg. K	300.	300.
	Mass, kg	19.4	8.7
	Surface area, m ²	6.	2.7
	Ave. power rejected, W	1092.	492.

* For one thruster module.

** For one stage of the PFN.

TABLE 16

ORBIT TRANSFER PROPULSION SYSTEM

Parameter	Propulsion System for 1 PIT	Total Propulsion System
=====	=====	=====
Payload Mass, kg	20000.*	10000.
ΔV , m/s	2900.	5880.
Mission Time, days	100.	100.
Thrust/Engine, N	9.60	9.60
Average Power, kW	225.	450.
Thrust Eff., %	62.3	62.3
Total Eff., %	55.5	55.5
Isp, s	2600.	2600.
Frequency, Hz	10.5	10.5
Pulse Energy, kJ	19.	19.
Pulse Time, μ s	16.5	16.5
ES/PC Mass, kg	1300.	2600.
Dry Mass, kg	7010.	14020.
Propellant Mass, kg	3190.	6380.
Propulsion Mass, kg	10200.	20400.

- * The payload mass was increased by an amount equivalent to the mass of one thrusting module.

TABLE 17

THRUSTER SIZE AND CHARACTERISTICS FOR ORBIT TRANSFER MISSION

Parameter	PIT
=====	=====
Diameter, m	2.18
Efficiency, %	62.3
Isp, s	2600.
Frequency, hz	10.5
Pulse duration, μ s	16.5
Pulse energy, kJ	19.
Average Voltage, kV	24.6
Average current, kA	126.6

TABLE 18

ES/PC SIZE AND CHARACTERISTICS FOR ORBIT TRANSFER MISSION

Component	Parameter	ES/PC System for 1 PIT
Capacitor	Efficiency, %	98.
	Mass, kg	402.4
	Volume, m ³	0.22
	Dimension, m	0.61
	Capacitance, μ F	62.7
	Voltage, kV	24.6
	Energy stored, kJ	19.
	Number of cycles	9.1E7
	Specific energy, J/kg	47.3
Thyratron	Efficiency, %	98.9
	Mass, kg	174.8
	Peak power, W	1.16E9
	Pulse Duration, μ s	16.5
	Current, kA	126.6
DC-DC Converter	Efficiency, %	92.
	Mass, kg	204.
	Average power, kW	225.
	Volume, m ³	7.5E-3
	Dimension, m	0.42
Radiator	Temperature, Deg. K	300.
	Mass, kg	432.5
	Surface area, m ²	134.1
	Avg. power rejected, kW	24.3

SECTION 5

CONCLUSIONS AND RECOMMENDATIONS

5.1 CONCLUSIONS

A number of specific conclusions can be drawn from this study.

- (1) Optimization of integrated propulsion systems requires that the primary power sources, the ES/PC, and the thruster performance be related to the primary propulsion system outputs (pulse mass, exhaust velocity, frequency, and total thrusting time).
- (2) Models which meet these requirements were successfully developed for all the systems of interest.
- (3) Most of the models developed were based on an understanding of the physical principles of operation and a number of assumptions concerning the performance of optimized systems. The rest of the models were developed by curve-fitting available performance data, either from manufacturer's literature or from point design studies.
- (4) The excellent qualitative and quantitative agreements between model prediction and observed performance lend considerable credence to the models.
- (5) The models are extremely versatile, permitting rapid evaluation of proposed alternatives for specific missions.
- (6) The models can easily be updated when new data becomes available.

Using these models to analyze optimized propulsion systems for stationkeeping and orbit transfer missions, we can conclude:

- (1) There exists one set of propulsion system outputs that minimizes the mass of the system.
- (2) The optimum propulsion system outputs are within the capabilities of the state-of-the-art thrusters.
- (3) The propulsion system mass is about 10 percent of the payload for stationkeeping and ranges from 2.5 to 3.5 times the payload mass for orbit transfer missions.
- (4) Photovoltaic power sources are the least massive for stationkeeping missions and nuclear-based power sources become competitive for orbit transfer missions.
- (5) Average power levels range from 2 to 35 kW for stationkeeping and from 200 kW to 2 MW for orbit transfer missions.
- (6) Capacitive based ES/PC systems are the least massive, inductive based systems are comparable, and inertial systems are much heavier.

- (7) ES/PC components have equal weights for stationkeeping systems, and the radiator is the largest component in the system for orbit transfer missions (45%).

5.2 RECOMMENDATIONS

The thruster performance plays an important role in sizing the ES/PC and the primary power source. It is necessary to validate the performance models of the thrusters over the wide range m_p and v_e of interest. There are two major areas of uncertainty in the thruster models developed. The first problem arises from the nature of the thrusters for which data was available. It is not clear that the experimental thruster performance data available to us was generated with optimum thrusters (that is, the thruster was optimized for every m_p and v_e for which data was reported). The performance data must be evaluated more carefully to answer this question. The second problem arises from the limited amount of data available. The missions considered in this study require the thruster models apply at operating conditions (m_p and v_e) which could be orders different from the conditions for which we have data. Therefore, we recommend that performance data for optimum thrusters be generated over a much more extensive range of m_p (or \dot{m}_p) and v_e .

The effects of the component life (number of cycles) on most of the components forming the ES/PC are not well understood. The performance of the components was degraded to account for the component life effects. We recommend that a more extensive analysis be conducted to evaluate the life effects on the components performance of the most promising ES/PC. This can be done by first selecting the most promising ES/PC. Our analysis show that the capacitive-based ES/PC is the most promising. Then each component in the ES/PC should be tested individually to study the life effects on the performance of the component. After testing the components individually, they should be integrated and tested as a system to insure that no compounded effect is available.

References

1. Smith, W. W. and Clark, J. P., 'Study of Electrical and Chemical Propulsion Systems for Auxiliary Propulsion of large Space Systems,' NASA CR-165502, 1981.
2. Bauer, David P., Barber, John P., Swift, Hallock F., Vahlberg, C. Julian, 'Electric Rail Gun Propulsion Study (Advanced Electric Propulsion Technology—High Thrust),' AFRPL-TR-81-02, 1981.
3. Bauer, D. P., Barber, J. P. and Vahlberg, C. J., 'The Electric Rail Gun for Space Propulsion,' NASA-CR-165312, Final Report, February 1981.
4. Lovberg, R. H. and Dailey, C. L., 'Large Inductive Thruster Performance Measurement,' AIAA-81-0708R, 1981.
5. Huberman, M. N. and Zafran, S., 'Pulsed Plasma Propulsion System/Spacecraft Design Guide,' AFRPL-TR-80-38, Final Report, September 1980, ADA091006.
6. Personal Communication - Dominic Palumbo - Fairchild Industries, Inc.
7. Personal Communication - Kenn Clark - Princeton University.
8. Sargent, W. J., 'Energy Storage Capacitors,' Los Alamos National Scientific Laboratory.
9. Dailey, C. L., White, C. W., 'Capacitors for Aircraft High Power,' AFAPL-TR-74-79.
10. Kunhardt, E. E., 'Electric and Magnetic Properties of Materials,' Texas Tech University.
11. Maxwell, Data Sheets - Series M Capacitors
12. Personal Communication - A. S. Gilmour, SUNYAB, April 1983.
13. Personal Communication - Howard Mauldin, Sandia National Laboratory, August 1983.
14. Weldon, W. F., Bird, W. I., Driga, M. D., Tolk, K. M., Rylander, H. G., and Woodson, H. H., 'Fundamental limitations and Design Considerations for Compensated Pulsed Alternators,' CEM University of Texas at Austin.
15. Ijichi, K. and Billerbeck, W. J., 'Capacitor Bank Charging by Series-Parallel Switching of Solar Arrays,' 16th International Electric Propulsion Conference, 1982, AIAA-82-1879.
16. Westinghouse Power Semiconductor User's Manual and Data Book.
17. EG and G Ceramic Metal Grounded Grid Thyratrons Data Sheet, H5003-1.
18. 'MPD Thruster Definition Study,' Martin Marietta, 1983.

APPENDIX A

PRIMARY POWER FOR ELECTROMAGNETIC PROPULSION

Table of Contents

A.1	SOLAR CELL ARRAYS	A-1
A.2	SOLAR THERMOPHOTOVOLTAIC	A-4
A.3	NUCLEAR THERMOELECTRIC	A-7
A.4	NUCLEAR-THERMIONIC	A-10
A.5	NUCLEAR BRAYTON/RANKINE	A-12
A.6	NUCLEAR MHD	A-13

AD-A152 244

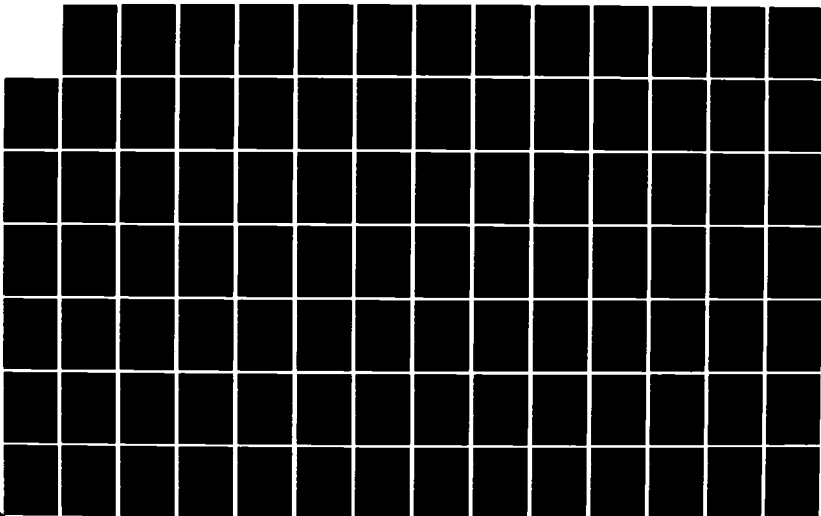
ADVANCED ENERGY STORAGE SYSTEMS(U) IAP RESEARCH INC
DAYTON OH A CHALLITA ET AL JAN 85 IAP-TR-83-7
AFRPL-TR-84-099 F04611-82-C-0029

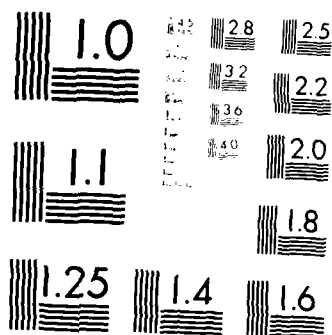
2/3

UNCLASSIFIED

F/G 21/3

NL





MICROCOPY RESOLUTION TEST CHART
NATIONAL BUREAU OF STANDARDS-1963-A

List of Figures

Figure		Page
A-1	Paschen Characteristics For Some Molecular Gases	A-2
A-2	Specific Mass of Solar Cell Array Systems	A-5
A-3	Energy Balance of a Solar Thermophotovoltaic System	A-6
A-4	Specific Mass Versus Concentrator Radius of Thermophoto- voltaic Systems	A-6
A-5	Specific Mass of TPV Systems	A-8
A-6	Specific Mass of Nuclear Thermoelectric Power Systems	A-10
A-7	Specific Mass of Nuclear Thermionic Power Systems	A-11
A-8	Specific Mass of Nuclear Brayton Cycle Power Systems	A-13
A-9	Specific Mass of Nuclear Rankine Cycle Power Systems	A-14
A-10	Specific Mass of Nuclear MHD Power System	A-15

List of Symbols

m_{sp}	specific mass, kg/w
P_{pp}	power level, w, average

APPENDIX A

PRIMARY POWER FOR ELECTROMAGNETIC PROPULSION

Primary power source performance and mass models are required to select, size, and design an integrated electromagnetic propulsion system. A primary power source delivers electrical output at a relatively low average level to an Energy Storage/Power Conditioning system (ES/PC) which conditions the power and delivers high-power pulses to the electrical thruster. The primary power source is defined as the 'raw' power source and all the components (radiator, generator, converter, etc.) required to deliver electrical power to the ES/PC.

The performance characteristics and mass models for the primary power sources were determined by conducting a literature survey to gather the necessary data, contacting technical experts to confirm the results and making refinements where needed. The literature contains considerable point design data but very little parametric or limit data.

A wide range of primary power options were considered including: solar cell arrays, solar thermophotovoltaic, nuclear thermionic, nuclear thermoelectric, nuclear Rankine cycle, nuclear Brayton cycle, and nuclear MHD. Parametric performance models were developed for power levels ranging from a few kilowatts to 10 MW.

A.1 SOLAR CELL ARRAYS

Solar cell arrays are designed in collapsible sections and are optimized to minimize power transmission losses. Transmission losses are ohmic losses and are minimized by power transmission at the highest possible voltage. Ohmic losses are directly proportional to the current squared for a fixed bus bar cross-sectional area.¹

The performance of the solar cell arrays is affected by: (1) plasma arcing, (2) voltage breakdown, (3) voltage transients and Van Allen Belts.

¹Bauer, David P., Barber, John P., Swift, Hallock F., Vahlberg, C. Julian, 'Electric Rail Gun Propulsion Study (Advanced Electric Technology--High Thrust)', AFRPL-TR-81-02, 1981.

Plasma arcing is a function of environment plasma density (altitude) and the voltage of the array. Gilmour² listed some of the laboratory arcing data obtained by Stevens at NASA-Lewis. The data show that arcing can be expected in GEO with array voltage around 1000 V, and can be expected in LEO at around 300 V. Voltage breakdown of gases may occur if the operating voltage is higher than the Paschen minimum. Gilmour presented Paschen characteristics for some molecular gases (see Figure A-1). This figure shows that for low pressure (high vacuum) 1000 V may be feasible. Voltage transients are experienced immediately after eclipse. When the cold solar array is suddenly exposed to sunlight, the voltage (for a given current) is 2 to 2.5 times higher than the warm array voltage. These voltage transients can be overcome if provisions are made in the design. Some of the suggestions to overcome this problem are: (1) to connect the solar array to the power system only after it warms up, or (2) to clamp the solar array voltage to a battery voltage and make provisions to accommodate the current pulse from the cold array.

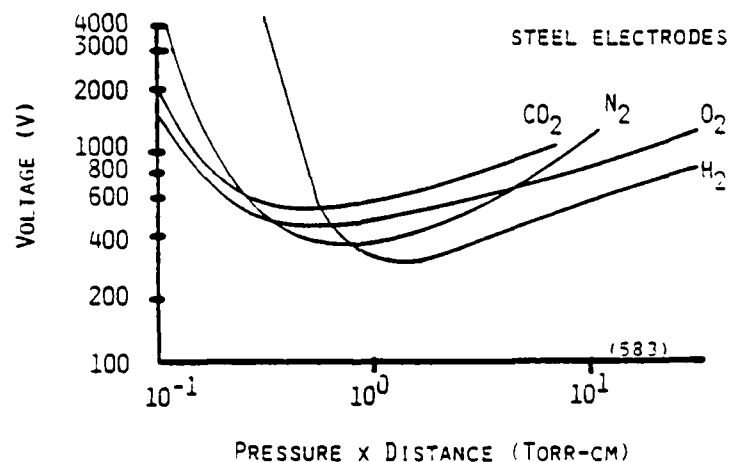


Figure A-1. Paschen Characteristics For Some Molecular Gases.²

²Gilmour, A. S. Jr., 'Investigation of Power Processing Technology for Spacecraft Applications,' AFWAL-TR-82-2054, June 1982.

Solar cell arrays degrade when passing through the Van Allen belts. Degradation of up to 40% is reported.³ Provisions must be made for this degradation if solar cell arrays are to be used in orbit transfer missions.

Solar cell arrays can be designed to deliver any power level required since they are composed of solar cells connected in series and parallel. Solar cell arrays capable of providing power levels up to 10 kW have been deployed in space (used on Skylab). Arrays capable of multi-hundred kilowatt have been designed and analyzed.

Operating voltages ranging from 28 V to 900 V have been reported. References 4, 5, 6, 7, and 8 report the performance of arrays delivering multi-hundred watts with operating voltage ranging from 28 to 42 VDC. References 7 and 9 report analyses of solar power systems ranging from 100 to 300 V. References 10 and 11 reported tradeoff analyses for power management and transmission of multi-hundred kilowatt and multi-megawatt systems. The multi-hundred kilowatt system had an operating voltage of 750 for the DC transmission and an operating voltage of 440 for an AC/DC transmission.

³Taussig, R., et al., 'Overview Study of Space Power Technologies for the Advanced Energetics Program,' NASA CR-165269, 1981.

⁴Brooks, G. R., 'Orbiting Solar Observatory (OSO-8) Solar Panel Design and in Orbit Performance,' Intersociety Energy Conversion Engineering Conference (IECEC), 789321, 1978.

⁵Thronton, 'ATM Solar Array In-Flight Performance Analysis,' IECEC, 1974.

⁶Goldhammer, L. J., 'Design and Flight Performance of the Pioneer Venus Multiprobe and Orbiter Solar Arrays,' IECEC, 809076, 1980.

⁷Lukens, F. E., 'Advanced Development of a Programmable Power Processor,' IECEC, 809076, 1980.

⁸McKinney, H. N., Briggs, D. C., 'Electrical Power Subsystem for the Intelsat V Satellite,' IECEC, 789084, 1978.

⁹Glass, M. C., 'A Six Kilowatt Transformer-Coupled Converter for Space Shuttle Solar Power Systems,' IECEC, 809146, 1980.

¹⁰Mildice, J. W., 'Study of Power Management Technology for Orbital Multi-100 kW Applications,' NASA CR159834, July 1980.

¹¹Peterson, D. M. and Pleasant, R. L., 'Study of Multimegawatt Technology Needs for Photovoltaic Space Power Systems,' GDC-AST-81-019, August 1981.

The multi-megawatt system had an operating voltage of 900 for AC and DC. The multi-transmission megawatt system will require multiple shuttle launches and construction in space.

System mass data gathered from references 1 - 18 are presented in Figure A-2. Figure A-2 shows that the specific mass is about 50 kg/kW for one kilowatt arrays and decreases asymptotically to 10 kg/kW for 100 kW and above. This data was curve-fitted to generate a mass model:

$$m_{sp} = 0.013 + 40.61/P_{pp} \quad (A-1)$$

where m_{sp} is the specific mass in kg/W and P_{pp} is the average power level in watts. Equation A-1 is true for power levels above 1000 W. For power levels lower than 1000 W, the mass of the system is assumed to be 54 kg independent of power level. An overall degradation of 20% in the performance of the arrays was assumed for orbit transfer mission.

A.2 SOLAR THERMOPHOTOVOLTAIC

The thermophotovoltaic (TPV) concept offers a viable alternative to conventional solar cell arrays. It offers a high efficiency (50%),¹⁹ thus

¹²Briggs, D. C., Pollard, H. E., 'Intelsat V Solar Array Design and Development Summary,' IECEC, 789322, 1978.

¹³Kelly, F. G., Luft, W., Kurland, R. M., 'Design Features of the TRDSS Solar Array,' IECEC, 789323, 1978.

¹⁴Borduas, H. F., et al., 'Medium Power Deployable Hybrid Solar Arrays,' IECEC, 780328, 1978.

¹⁵Peterson, D. G., 'INSAT-1 Solar Array Design and Development Summary,' IECEC, 1980.

¹⁶Souza, C. J., 'Large Area Flexible Solar Array Design for Space Shuttle Application,' IECEC, 809485, 1980.

¹⁷Woodcock, W. G. III, 'Multi-Hundred Kilowatt Solar Arrays for Space,' IECEC, 809271, 1980.

¹⁸Trumble, T. M., 'Space Application for Gallium Arsenide Solar Cells,' IECEC, 829269, 1982.

¹⁹Horne, W. E., et al., 'Solar Thermophotovoltaic Space Power System,' IECEC, 809072, 1980.

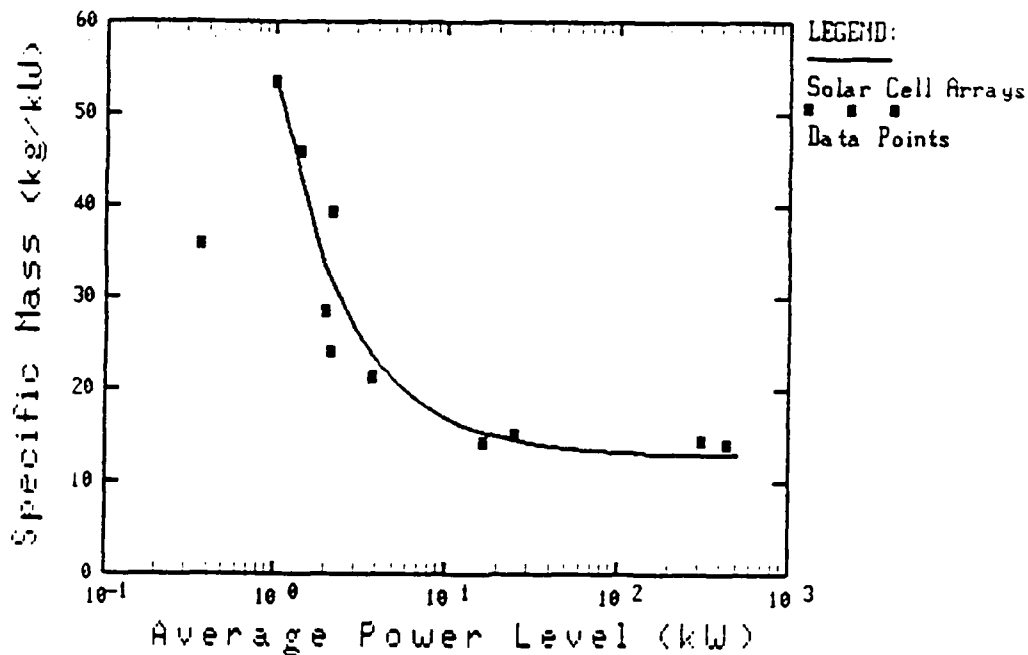


Figure A-2. Specific Mass of Solar Cell Array Systems.

a reduction in photovoltaic cell area and a possible reduction in weight. The photovoltaic cells are shielded from the external environment and do not suffer radiation degradation to the extent that conventional panels do.

TPV power systems can be designed to deliver any power level required and the same limiting factors which apply to solar cell arrays (voltage levels, breakdown, and transients) apply to TPV systems.

TPV systems are still in their infancy and many parameters which affect performance are still not well understood. Design criteria and methods have not been developed. A literature survey revealed that feasibility and sensitivity studies have been conducted.^{19,20,21} Very little specific mass data was located. Reference 19 reported some specific mass data, which we used in conjunction with a system energy balance model (Figure A-3).

²⁰Swanson, R. M., et al., 'Silicon Photovoltaic Cells in Thermophotovoltaic Conversion,' EPI-ER-478 Progress Report, Stanford Electronics Lab., February 1977.

²¹Horne, W. E., et al., 'Improved Thermophotovoltaic Power Systems,' IECEC, 829018, 1982.

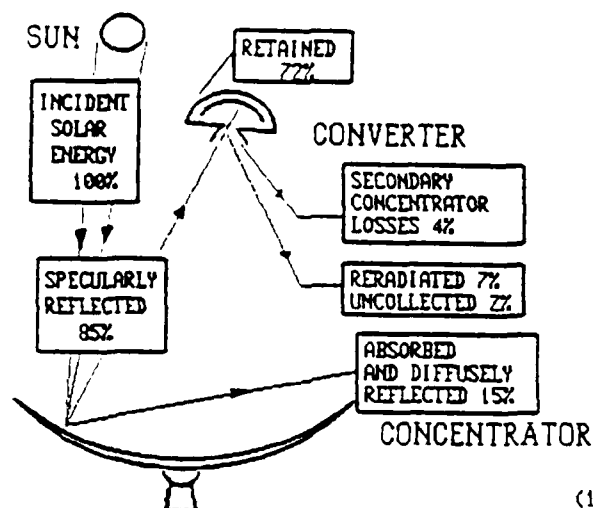


Figure A-3. Energy Balance Of A Solar Thermophotovoltaic System.²⁰

reported in reference 20, to develop a specific mass model. The specific mass for a single unit is presented in Figure A-4. Figure A-4 indicates that a panel made with clusters of small TPV converters would be lighter than a single large concentrator due to the increased performance of the heat pipes (in the converter) as heat pipe length is decreased.

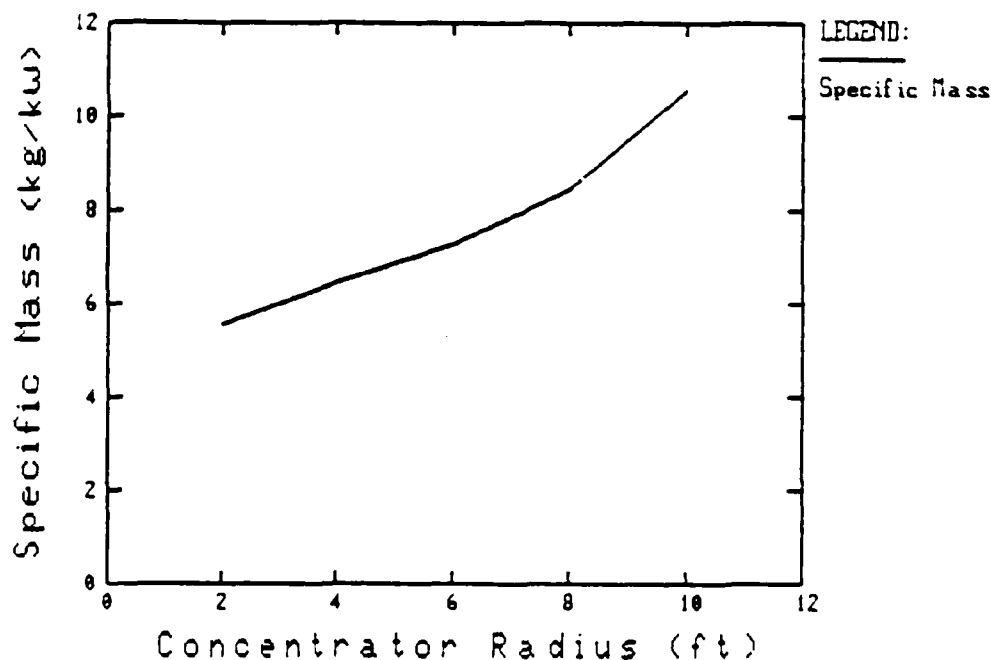


Figure A-4. Specific Mass Versus Concentrator Radius Of Thermophotovoltaic Systems.

The assumptions made in order to model the specific mass for large arrays were:

- (1) 72% of the incident solar energy is retained in the TPV converter.
- (2) The efficiency of the photovoltaic cells is 40%.
- (3) One concentrator is used if the required power level can be achieved with a concentrator radius less than 3m. (limitations of the available data), and multi-3m. radius concentrators are used for higher power levels. i.e., the specific mass is constant for power levels requiring more than 3m. radius concentrators.

We assumed that large TPV panels will be formed with large concentrators, even though smaller concentrators have a lower specific mass, because we felt that their advantages outweigh the possible savings in mass of the TPV system. The advantages of the large concentrators are: they minimize the number of concentrators required to achieve a power level (leads to less complex system), they reduce manufacturing slope errors of concentrator surfaces, and they simplify the sun-TPV alignment requirement.

The specific mass model for power levels ranges from 1 kW to 11 kW is:

$$m_{sp} = 0.005 + 4.6 \times 10^{-7} P_{pp} \quad (A-2)$$

where m_{sp} is in kg/W and P_{pp} is the average power level in watts. For higher power levels the specific mass was assumed constant and equal to 10.1 kg/kw. The complete model is illustrated in Figure A-5.

A.3 NUCLEAR THERMOELECTRIC

Nuclear primary power for electromagnetic propulsion requires thermal-to-electrical converters capable of operating for long periods of time at high temperatures. Thermoelectric converters are in a unique position to meet these requirements. They are a direct energy conversion system. Static conversion and modularity are attractive characteristics. A large number of parallel converters provide a system with high redundancy and reliability. Modular design permits flexibility in design and operation.

Mission studies have shown that a 400 kW nuclear thermoelectric power system can be deployed in a single shuttle launch with the largest payload of interest to this study. Thermoelectric power systems capable of 120 kW have been analyzed by JPL and LASL with the 400 kW being their ultimate

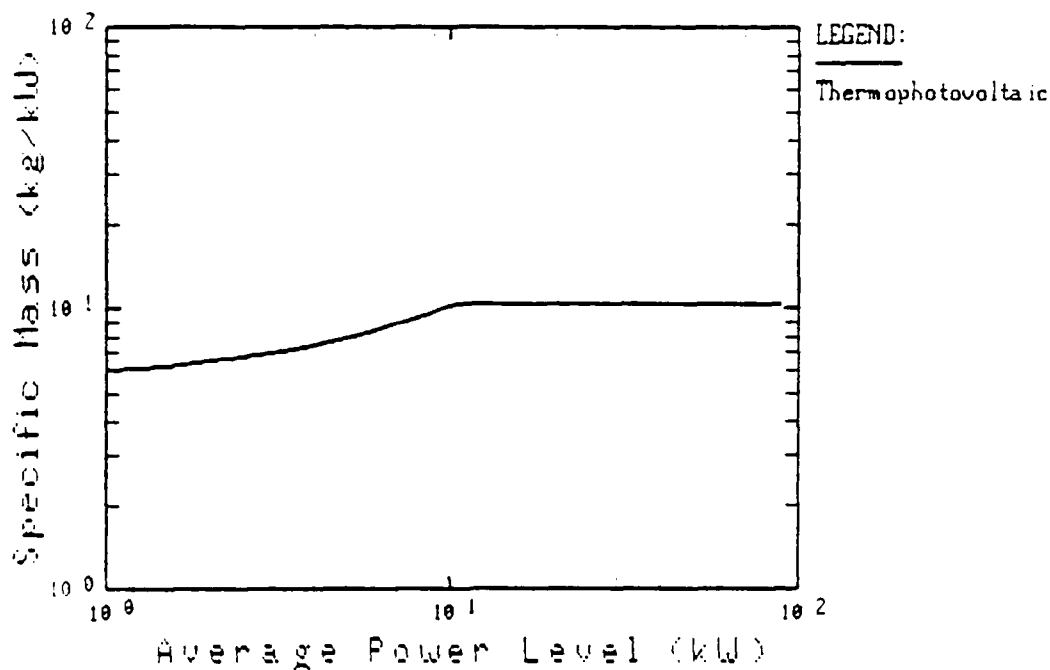


Figure A-5. Specific Mass Of TPV Systems.

range. Power systems for higher power levels can be designed but will require multiple shuttle launches.

Output voltage levels of up to 150 volts have been proposed for 120 kW thermoelectric power systems.^{22,23} The voltage level is limited by the electrical insulating material. The high operating temperature degrades the insulating material. Bauer in reference 1 reported a personal communication with Dr. Ranken (LASL) who projected that developments in insulating materials will permit three times the presently projected voltage within a decade.

²² Mondt, J. F., et al., 'Nuclear Power Source for Electric Propulsion,' 14th International Electric Propulsion Conference, 1979.

²³ Ranken, W. A., 'Experimental Results for Space Nuclear Power Plant Design,' IECEC, 809142, 1980.

A specific mass model was generated from data in references 22 thru 32. The referenced data was for different reactors, radiators, and operating strategies. The type of reactor and radiator has a strong impact on the mass of the system. The specific mass model was generated by curve-fitting the conservative data. The specific mass, for power levels ranging from 1 kW to 150 kW (limitation of the available data) can be expressed as:

$$m_{sp} = 0.021 + 370.3/P_{pp} \quad (A-3)$$

where m_{sp} is in kg/W and p_{pp} in W. We will assume that the specific mass model (Equation A-3) is valid for power levels above the range of the available data. Equation A-3 and the referenced data points are presented in Figure A-6.

²⁴Kelly, C. E., Ambrose, G. R., 'Testing of the GPHS Electrically Heated Thermoelectric Converter,' IECEC, 829234, 1982.

²⁵Eisner, N. B., 'Development of An Advanced RTG Using Segmented Thermoelectrics,' IECEC, 1980.

²⁶Koeing, D. R., 'Heat Pipe Reactors for Space Power Applications,' AIAA-77-491, 1977.

²⁷Ewell, R. C., Stapfer, G., 'Thermoelectric Conversion for Space Nuclear Power Systems,' IECEC, 829238, 1982.

²⁸Rockey, D. E., et al., 'Comparison of Evolving Photovoltaic and Nuclear Power Systems,' IECEC, 829011, 1982.

²⁹Mahefkey, T., 'Future Space Power--The D.O.D. Perspective,' IECEC, 809016, 1980.

³⁰Ranken, W. A., 'Experimental Results for Space Nuclear Power Plant Design,' IECEC, 809142, 1980.

³¹Buden, D., 'Space Nuclear Reactor Power Plants,' Los Alamos, LA8823-MS, 1980.

³²Buden, D., 'Reactor Technology for Space Electrical Power (10 - 100 kW_e),' LA6891-MS, 1977.

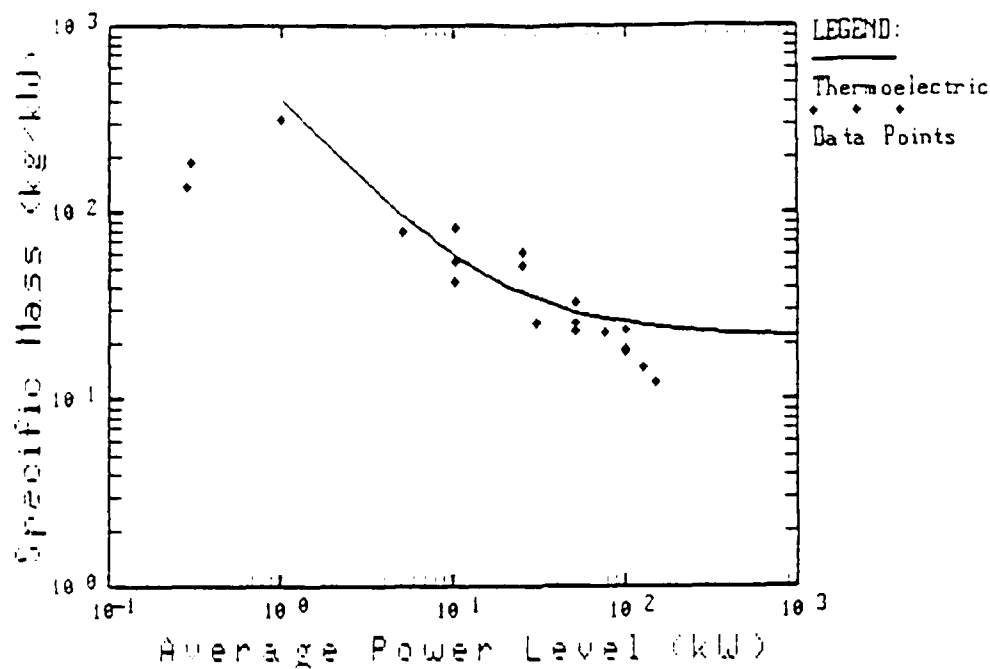


Figure A-6. Specific Mass Of Nuclear Thermoelectric Power Systems.

A.4 NUCLEAR-THERMIONIC

Thermionic converters are also good candidates to meet the nuclear electromagnetic propulsion needs. They are also direct energy conversion systems and are modular.

Thermionic power systems can be designed for the power level range of interest. Power systems above 400 kW will require multiple shuttle launches. Thermionic converters offer high current density (10 A/cm^2) and low module voltage. The maximum system voltage which has been projected is 50 V.³³ The voltage is limited by the strength of the high temperature electrical insulation.

Data from references 26, 29, 32, 34, 35, and 36 were used to model the

³³Phillips, W., (JPL), Personal Communication, July 1982.

³⁴Dick, R. S. Jr., 'Collector Temperature Effects on the Performance of Advanced Thermionic Converters and Nuclear Electric Propulsion Systems,' IECEC, 809359, 1980.

³⁵Phillips, W. M., 'Nuclear Electric Power System for Solar System Exploration,' ALAA 79 13374.

List of Symbols (concluded)

α	duty cycle
η	efficiency
μ_0	permeability of free space
ξ	plasma resistivity
ρ	density

List of Symbols

d	plasma/thruster dimensions
e_i	'specific ionization' constant
h	height
m_p	pulse mass
\dot{m}_p	propellant mass flow rate
r_i	inner electrode radius
r_o	outer electrode radius
t/t_p	fraction of pulse duration in which ionization takes place
t_p	pulse duration
v_e	exhaust velocity
w	width
A	cross-sectional area
D	coil diameter
E_{dis}	dissipation energy
E_{ion}	'ionization' energy
E_{kin}	kinetic energy
E_p	pulse energy
J	current
J_{avg}	average current
J_{max}	maximum current
L'	axial inductance gradient
R	resistance
V	voltage
V_{acc}	voltage required for acceleration
V_{avg}	average voltage
V_{bdn}	breakdown voltage
V_{dis}	voltage characteristic of energy dissipated
V_f	'electrode fall voltage'
V_{ion}	ionization voltage
ℓ	acceleration length
ℓ	effective plasma length

List of Tables

Table		Page
B-1	Parameters Affecting Rail Gun Efficiency	B-2
B-2	Pulse Energy Coefficients	B-10

List of Figures

Figure		Page
B-1	Efficiency Data and Model Results for the PIT	B-11
B-2	Efficiency Data and Model Results for the TPP	B-11
B-3	Efficiency Data and Model Results for the MPD	B-12
B-4	Pulse Time for the PIT	B-14
B-5	Average Current for the PIT	B-15
B-6	Peak Current for the PIT	B-16
B-7	Maximum Current for the TPP	B-17
B-8	Pulse Time for the TPP	B-18
B-9	Current for the MPD	B-20
B-10	Average Voltage for the PIT	B-22
B-11	Voltage Components for the PIT	B-23
B-12	Breakdown Voltage for the PIT	B-24
B-13	Average Voltage for the TPP	B-24
B-14	Voltage Components for the TPP	B-25
B-15	Average Voltage for the MPD	B-26
B-16	Voltage Components for the MPD	B-27

Table of Contents

B.1	INTRODUCTION	B-1
B.2	PULSE ENERGY	B-3
B.3	CURRENT/PULSE TIME	B-12
B.3.1	The PIT	B-13
B.3.2	The TPP	B-16
B.3.3	The MPD	B-19
B.4	VOLTAGE	B-19
B.4.1	The PIT	B-21
B.4.2	The TPP	B-23
B.4.3	The MPD	B-26
B.5	CONCLUSIONS	B-27
B.6	RECOMMENDATIONS	B-28

APPENDIX B

ELECTROMAGNETIC THRUSTER MODELS

References (concluded)

34. Dick, R. S. Jr., 'Collector Temperature Effects on the Performance of Advanced Thermionic Converters and Nuclear Electric Propulsion Systems,' IECEC, 809359, 1980.
35. Phillips, W. M., 'Nuclear Electric Power System for Solar System Exploration,' AIAA 79 13374.
36. Phillips, W. M., Koenig, D. R., 'Reactor Design and Integration into a Nuclear Electric Spacecraft,' IECEC, 789564, 1978.
37. Preston, J., 'Reactor/Brayton Power Systems for Nuclear Electric Spacecraft,' Princeton.
38. Layton, J. P., 'Reactor/Brayton Power Systems for Nuclear Electric Spacecraft,' IECEC, 809140, 1980.
39. Gable, R. D., McCormick, J. E., 'Brayton Isotope Power System --The Versatile Dynamic Power Converter,' IECEC, 789383, 1978.
40. Thompson, R. E., 'Gas Cooled Reactors for Space Power Plants,' AIAA-77-490, 1977.
41. T. Botts, et al., 'A Compact High Performance Electrical Power Source Based Upon the Rotating Bed Nuclear Reactor,' Brookhaven National Laboratory, January 1980.
42. Rosa, R. J., 'MHD Applied to Aerospace and Deep Space Propulsion,' AIAA 82-1212, June 1982.
43. Botts, T. E., et al., 'Nuclear Reactors Using Fine Particulate Fuel for Primary Power in Space,' Brookhaven National Laboratory, August 1982.

References (continued)

17. Woodcock, W. G. III, 'Multi-Hundred Kilowatt Solar Arrays for Space,' IECEC, 809271, 1980.
18. Trumble, T. M., 'Space Application for Gallium Arsenide Solar Cells,' IECEC, 829269, 1982.
19. Horne, W. E., et al., 'Solar Thermophotovoltaic Space Power System,' IECEC, 809072, 1980.
20. Swanson, R. M., et al., 'Silicon Photovoltaic Cells in Thermophotovoltaic Conversion,' EPI-ER-478 Progress Report, Stanford Electronics Lab., February 1977.
21. Horne, W. E., et al., 'Improved Thermophotovoltaic Power Systems,' IECEC, 829018, 1982.
22. Mondt, J. F., et al., 'Nuclear Power Source for Electric Propulsion,' 14th International Electric Propulsion Conference, 1979.
23. Ranken, W. A., 'Experimental Results for Space Nuclear Power Plant Design,' IECEC, 809142, 1980.
24. Kelly, C. E., Ambrose, G. R., 'Testing of the GPHS Electrically Heated Thermoelectric Converter,' IECEC, 829234, 1982.
25. Eisner, N. B., 'Development of an Advanced RTG Using Segmented Thermoelectrics,' IECEC, 1980.
26. Koeing, D. R., 'Heat Pipe Reactors for Space Power Applications,' AIAA-77-491, 1977.
27. Ewell, R. C., Stapfer, G., 'Thermoelectric Conversion for Space Nuclear Power Systems,' IECEC, 829238, 1982.
28. Rockey, D. E., et al., 'Comparison of Evolving Photovoltaic and Nuclear Power Systems,' IECEC, 829011, 1982.
29. Mahefkey, T., 'Future Space Power--The D.O.D. Perspective,' IECEC, 809016, 1980.
30. Ranken, W. A., 'Experimental Results for Space Nuclear Power Plant Design,' IECEC, 809142, 1980.
31. Buden, D., 'Space Nuclear Reactor Power Plants,' Los Alamos, LA8823-MS, 1980.
32. Buden, D., 'Reactor Technology for Space Electrical Power (10 - 100 kW_e),' LA6891-MS, 1977.
33. Phillips, W., (JPL), Personal Communication, July 1982.

References

1. Bauer, David P., Barber, John P., Swift, Hallock F., Vahlberg, C. Julian, 'Electric Rail Gun Propulsion Study (Advanced Electric Technology—High Thrust),' AFRPL-TR-81-02, 1981.
2. Gilmour, A. S. Jr., 'Investigation of Power Processing Technology for Spacecraft Applications,' AFWAL-TR-82-2054, June 1982.
3. Taussig, R., et al., 'Overview Study of Space Power Technologies for the Advanced Energetics Program,' NASA CR-165269, 1981.
4. Brooks, G. R., 'Orbiting Solar Observatory (OSO-8) Solar Panel Design and in Orbit Performance,' Intersociety Energy Conversion Engineering Conference (IECEC), 789321, 1978.
5. Thronton, 'ATM Solar Array In-Flight Performance Analysis,' IECEC, 1974.
6. Goldhammer, L. J., 'Design and Flight Performance of the Pioneer Venus Multiprobe and Orbiter Solar Arrays,' IECEC, 809076, 1980.
7. Lukens, F. E., 'Advanced Development of a Programmable Power Processor,' IECEC, 809076, 1980.
8. McKinney, H. N., Briggs, D. C., 'Electrical Power Subsystem for the Intelsat V Satellite,' IECEC, 789084, 1978.
9. Glass, M. C., 'A Six Kilowatt Transformer-Coupled Converter for Space Shuttle Solar Power Systems,' IECEC, 809146, 1980.
10. Mildice, J. W., 'Study of Power Management Technology for Orbital Multi-100 kW Applications,' NASA CR159834, July 1980.
11. Peterson, D. M. and Pleasant, R. L., 'Study of Multimegawatt Technology Needs for Photovoltaic Space Power System,' GDC-AST-81-019, August 1981.
12. Briggs, D. C., Pollard, H. E., 'Intelsat V Solar Array Design and Development Summary,' IECEC, 789322, 1978.
13. Kelly, F. G., Luft, W., Kurland, R. M., 'Design Features of the TRDSS Solar Array,' IECEC, 789323, 1978.
14. Bordaas, H. F., et al., 'Medium Power Deployable Hybrid Solar Arrays,' IECEC, 780328, 1978.
15. Peterson, D. G., 'INSAT-1 Solar Array Design and Development Summary,' IECEC, 1980.
16. Souza, C. J., 'Large Area Flexible Solar Array Design for Space Shuttle Application,' IECEC, 809485, 1980.

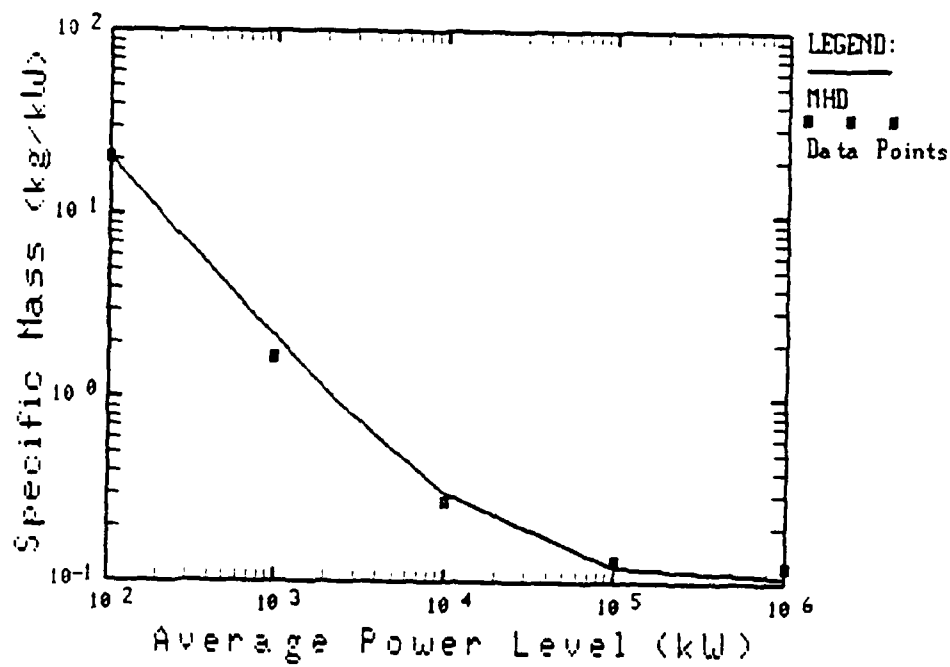


Figure A-10. Specific Mass of Nuclear MHD Power System.

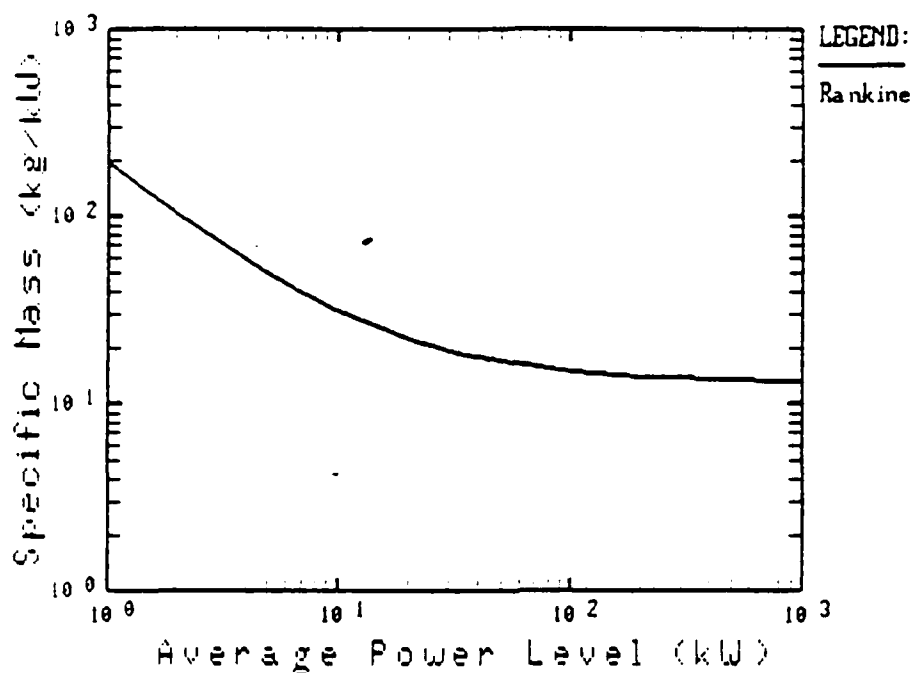


Figure A-9. Specific Mass Of Nuclear Rankine Cycle Power Systems.

the magnetic field gives rise to an electromotive force and causes a transverse current to flow in the moving gas. The current is collected by the electrodes and carried to the external load. References 41 and 42 discuss MHD generation at power levels (10 - 200 MW) orders of magnitude higher than that required for propulsion. The only pertinent data (at the upper level of the power range of interest) was found in reference 43. This data was used to model the specific mass. The specific mass for power levels above 100 kW is:

$$m_{sp} = 10^{-4} + 1990.1/P_{pp} \quad (A-8)$$

where m_{sp} is in kg/W and P_{pp} in W. The results are shown in Figure A-10.

⁴¹T. Botts, et al., 'A Compact High Performance Electrical Power Source Based Upon the Rotating Bed Nuclear Reactor,' Brookhaven National Laboratory, January 1980.

⁴²Rosa, R. J., 'MHD Applied to Aerospace and Deep Space Propulsion,' AIAA 82-1212, June 1982.

⁴³Botts, T. E., et al., 'Nuclear Reactors Using Fine Particulate Fuel for Primary Power in Space,' Brookhaven National Laboratory, August 1982.

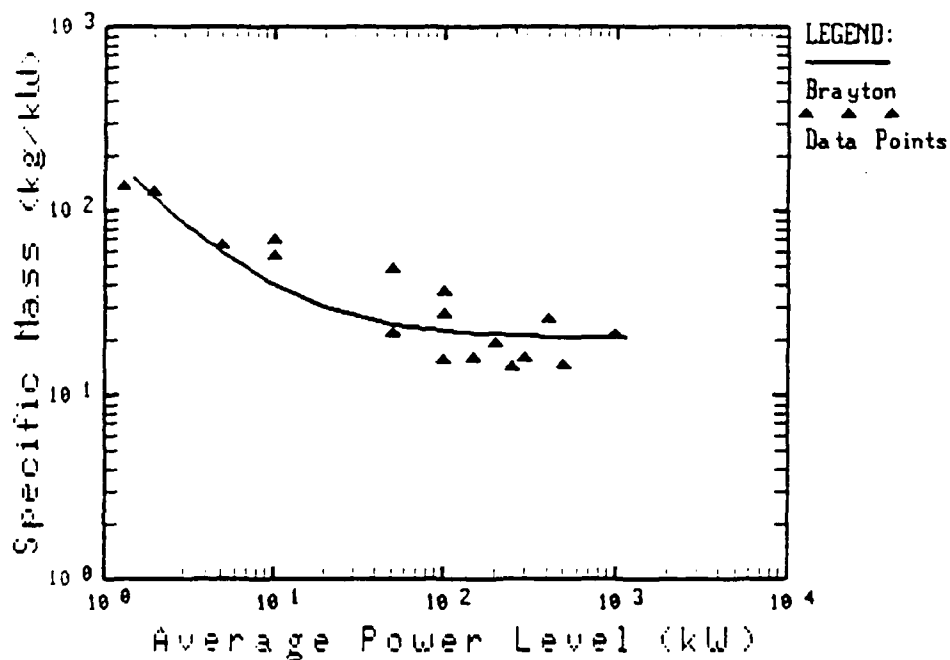


Figure A-8. Specific Mass of Nuclear Brayton Cycle Power Systems.

No quantitative specific mass data of the nuclear Rankine system was found in the literature. The mass of a nuclear Rankine system should be similar to the mass of the Brayton system. The Rankine cycle operates at higher temperature than Brayton cycle but there are no other significant differences. We assumed that the lower bound of the data for Brayton system is the mean for Rankine system.

The specific mass is then expressed as:

$$m_{sp} = 0.013 + 178.6/P_{pp} \quad (A-7)$$

and is illustrated in Figure A-9.

A.6 NUCLEAR MHD

An MHD energy converter consists of a gas dynamic nozzle (expander) followed by a duct. The duct is surrounded by a coil which produces a magnetic field in the duct. Electrodes are placed at the top and bottom of the duct. Ionized gas is expanded in the nozzle and converts some of its pressure and internal energy into directed motion. The gas motion through

A.5 NUCLEAR BRAYTON/RANKINE

The Brayton and Rankine cycles used in turbo-generators have low specific mass. They are designed as modular units and are connected in parallel for redundancy and increased system reliability. Each unit is usually designed to deliver a fraction of the total power required with the capability of delivering much longer power in case of module failure. The input pressure level to either cycle is approximately proportional to the output power level required.

Mission studies requiring power levels ranging from 25 to 600 kW have been conducted with the nuclear Brayton cycle.^{37,38,39,40} The power was delivered at 120 VDC or at 67 VAC, three phase, 1733 Hz. Reference 37 is a study of a Brayton cycle delivering 400 kW, 500 V, single phase, 3000 Hz. The voltage in all cases is limited by the alternator. As alternator technology improves, higher voltages and frequencies may be feasible.

Data for the nuclear Brayton power system from references 32, 35, 37, 38, 39, and 40 was used to model the specific mass. The specific mass model is:

$$m_{sp} = 0.019 + 190.6/P_{pp} \quad (A-6)$$

for power levels above 1.5 kW and is presented in Figure A-8.

³⁷Preston, J., 'Reactor/Brayton Power Systems for Nuclear Electric Spacecraft,' Princeton.

³⁸Layton, J. P., 'Reactor/Brayton Power Systems for Nuclear Electric Spacecraft,' IECEC, 809140, 1980.

³⁹Gable, R. D., McCormick, J. E., 'Brayton Isotope Power System --The Versatile Dynamic Power Converter,' IECEC, 789383, 1978.

⁴⁰Thompson, R. E., 'Gas Cooled Reactors for Space Power Plants,' AIAA-77-490, 1977.

specific mass. The specific mass is expressed as:

$$m_{sp} = 0.018 + 514/P_{pp} \quad (A-5)$$

for power levels above 10 kW (the lower limit of the available data). We will assume that this model is valid beyond the range of the available data. This model and the data are presented in Figure A-7. The data presented in Figure A-7 include system design and analysis results for different reactors (heat pipe, heat pipe solid core, solid core fluidized bed) and for different radiators (conventional, advanced, and open loop). The type of reactor and radiator selected has a considerable effect on the mass. The model presented in Figure A-7 and Equation A-5 represents an average of all the data.

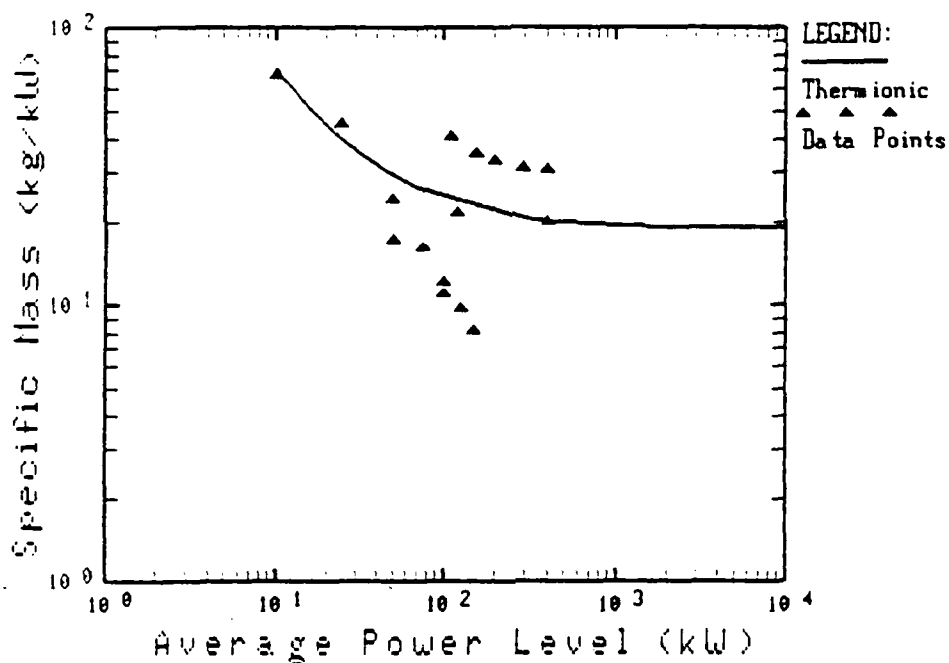


Figure A-7. Specific Mass Of Nuclear Thermionic Power Systems.

³⁶Phillips, W. M., Koenig, D. R., 'Reactor Design and Integration into a Nuclear Electric Spacecraft,' IECEC, 789564, 1978.

APPENDIX B

PERFORMANCE MODELING APPROACH

B.1 INTRODUCTION

The thruster input pulse parameters are (1) pulse energy, E_p , (2) current, J , (3) voltage, V , and (4) pulse duration, t_p . These input parameters are related to the thruster output parameters and many other thruster characteristics. The thruster output parameters which affect the input requirements are pulse mass and exhaust velocity. The other output parameters, pulse frequency and thruster lifetime, do not directly affect thruster input pulse requirements. Other thruster characteristics (such as size, electrode geometry and material, propellant material, etc.) clearly affect thruster performance and therefore must be considered. These other characteristics cannot be selected arbitrarily since they do affect thruster performance (i.e., thruster input requirements). In principle, they would be determined by optimizing the design of the thruster.

The efficiency of the thruster has a direct effect on the power and energy requirements, and therefore the size of the primary power supply and the ES/PC system. Therefore, the optimization criterion for the thruster is the maximization of efficiency. Thruster characteristics must be chosen to maximize efficiency. Assuming this can be accomplished, the input pulse parameters for optimum thrusters are functions of only the pulse mass and exhaust velocity. (That is, for each combination of pulse mass and exhaust velocity there is only one thruster configuration which has maximum efficiency and it is this one which is of interest here.)

Let us assume that a large body of data existed (either experimental or analytical) for optimized thrusters and that this data contained values for the thruster input pulse parameters over wide ranges of m_p and v_e . A simple, multi-variate curve fitting technique could then be employed to develop the required relationships for E_p , J , V , and t_p as functions of m_p and v_e . This is the approach which was used for modeling the electric rail gun.¹ Table B-1 lists the thruster characteristics which were chosen optimally, leaving only m_p and v_e as independent thruster output parameters.

¹Bauer, D. P., Barber, J. P., Vahlberg, C. J., 'The Electric Rail Gun for Space Propulsion,' NASA-CR-165312, Final Report, February 1981.

TABLE B-1. PARAMETERS AFFECTING RAIL GUN EFFICIENCY

PARAMETER	INCREASING EFFICIENCY RESULTS FROM INCREASING/DECREASING MAGNITUDE OF PARAMETER	OPTIMIZING VALUE OR PHYSICALLY IMPOSED CONSTRAINT	PHYSICAL IMPLICATIONS	VALUE OF PARAMETERS USED OR DERIVED
RAIL GUN INDUCTANCE PER UNIT LENGTH	INCREASING	OPTIMUM	RAIL GUNS WITH SQUARE BORE ARE OPTIMAL.*	$L' = 0.63 \mu\text{H}/\text{m}$
RAIL GUN LENGTH	INCREASING	OPTIMUM	PRACTICAL OPTIMUM LENGTH, x , IS A FUNCTION OF BORE SIZE AND EXHAUST VELOCITY FOR GIVEN VALUES OF OTHER PARAMETERS.	$x = 45.6 \times 10^{-6} \text{m}^2$
RAIL TEMPERATURE	DECREASING	CONSTRAINED	TRADEOFFS REQUIRED, TO OBTAIN PRACTICAL WASTE HEAT RADIATOR SIZE AND ADEQUATE STRENGTH RAILS WITH ACCEPTABLE RESISTIVITY.	$T = 450^\circ\text{K}$
RAIL GUN BORE SIZE	INCREASING	CONSTRAINED	SPECIFIED BY MISSION REQUIREMENTS.	$0.1 \text{ cm} < m < 1.0 \text{ cm}$
PELLET EXHAUST VELOCITY	DECREASING	CONSTRAINED	SPECIFIED BY MISSION REQUIREMENTS. BOUNDS WERE IMPOSED.	$5 \text{ km/s} < v < 20 \text{ km/s}$
PELLET ACCELERATING STRESS	INCREASING	CONSTRAINED	ACCELERATING STRESS LIMITED TO MAXIMUM ALLOWABLE STRESS IN PELLET.	$\sigma_0 = 200 \text{ MN}/\text{m}^2$
PELLET AREAL DENSITY	DECREASING	CONSTRAINED	BOTH PELLET DENSITY, ρ , AND PELLET LENGTH, D , SHOULD BE MINIMIZED. PRACTICAL PELLET DENSITY CHOSEN. PELLET LENGTH IN DIRECTION OF TRAVEL MUST BE LONGER THAN ONE-HALF THE BORE SIZE, TO PREVENT IN-BORE PELLET TUMBLING.*	$\rho = 3000 \text{ kg}/\text{m}^3$ $D = m/2$

*THE COMBINATION OF A SQUARE BORE AND PELLET LENGTH EQUAL TO ONE-HALF THE BORE SIZE ALLOWS THE PELLET MASS TO BE RELATED DIRECTLY TO BORE SIZE (I.E., $m = \rho h^3/2 = 1500h^3$). GIVEN THE PELLET DENSITY, PELLET MASS AND BORE SIZE MAY BE USED INTERCHANGEABLY.

**A PRACTICAL OPTIMUM CHARACTERISTIC PELLET ACCELERATION TIME IS THEREFORE IMPLIED AND WAS FOUND TO CORRELATE TO RAIL HEIGHT AND EXHAUST VELOCITY AS, $\tau_A = 51 \times 10^{-6} \text{m}^2$.

***THE COMBINATION OF A DEFINED OPTIMAL RAIL INDUCTANCE, L' , AND A DEFINED ALLOWABLE STRESS, σ_0 , DEFINES THE PEAK RAIL GUN CURRENT, J_0 , AS GIVEN BY, $J_0 = (2\sigma_0/L')^{1/2} h = 2.52 \times 10^7 \text{A}$.

(1593)

A rail gun simulation computer program (containing these optimum characteristics) was used to generate a large data base of thruster input pulse requirements over wide ranges of m_p and v_e . The data was then reduced using regression techniques to produce a set of parametric equations describing optimum ERG performance. The equations are:

$$\eta = 13.67 m_p^{0.104} v_e^{-0.299} \quad (B-1)$$

$$J = 2.2 \times 10^6 m_p^{1/3} \quad (B-2)$$

$$t_p = 4.45 \times 10^{-6} m_p^{1/3} v_e \quad (B-3)$$

This simple data-based approach cannot be applied to the other three thruster types (PIT, TPP, MPD) because not enough performance data (either experimental or analytical) is available over a wide enough range of m_p and v_e . In addition, it is not always clear that existing data represents optimum thruster performance. For example, data over considerable ranges of m_p and v_e is usually generated experimentally with one thruster configuration. Intuitively, one would expect that the configuration of an optimum thruster would be different at these wide extremes. The task of generating a more complete body of performance data (either experimentally or analytically) is considerable and is beyond the scope of this report. Methods of performance extrapolation based on a sound physical understanding of basic thruster operation must therefore be employed.

In the following paragraphs we will examine each of the thruster input parameters and develop methods of extrapolating thruster performance based on existing performance data and physically reasonable assumptions concerning thruster operation.

B.2 PULSE ENERGY

The purpose of this section is to relate the pulse energy to the independent output parameters of exhaust velocity and pulse mass. We begin with an assumption concerning the components of pulse energy.

Assumption No. 1 - The pulse energy is the sum of 3 components: (1) kinetic energy, (2) 'ionization' energy and (3) dissipation energy and may be expressed as:

$$E_p = E_{kin} + E_{ion} + E_{dis} \quad (B-4)$$

The first term in the pulse energy equation, the kinetic energy, is the useful energy imparted to the pulse mass during the pulse and is given by:

$$E_{kin} = m_p v_e^2 / 2 \quad (B-5)$$

The second term, the 'ionization' energy, includes all energy that is 'frozen' into the propellant and is characteristic of the state of the exhausted gas. The term is not strictly ionization but includes depolymerization (where applicable), ionization, and heating of the gas. This term cannot be easily evaluated without a further assumption.

Assumption No. 2 - The state of the plasma exiting the thruster is independent of exhaust velocity and thruster size (pulse mass).

With this assumption, the term can be written as:

$$E_{ion} = m_p e_i \quad (B-6)$$

where e_i is a 'specific ionization energy' characteristic of the state of the plasma at the thruster exit and has units of energy/mass. Caution should be exercised in interpreting this term physically. The specific energy, e_i , is just a parameter and its value will be determined from experimental performance data.

The third term in the pulse energy equation is a dissipative energy loss term. It includes all the energy required to maintain the plasma at temperature. For both the PIT and TPP, the energy loss mechanism was characterized as a resistance. The term contains all dissipative energy losses in the thruster, including electrode losses and radiative losses from the plasma. The dissipative loss term for the PIT and TPP can be written as:

$$E_{dis} = \int RJ^2 dt \quad (B-7)$$

where R is the apparent 'resistance' of the thruster and J is the pulse current.

For the MPD thruster, the dissipative energy loss term was broken into two components; a resistive loss term and an 'electrode fall' loss term. The complete dissipative loss term can be written as:

$$E_{dis} = \int RJ^2 dt + \int V_f J dt \quad (B-8)$$

where V_f is the 'electrode fall voltage'. The first component is identical to the energy loss mechanism for the TPP and PIT. The second component is an energy loss attributed to 'electrode fall.' The voltage drop, V_f , is the voltage penalty that must be paid to remove current from the electrodes and is assumed to be constant.

Thruster performance data strongly indicates that the predominant resistive element in the circuit is the plasma. We conclude that:

Assumption No. 3 - The resistive dissipation in the thruster is primarily due to plasma resistance.

We further note that ionization must occur early in the acceleration (neutrals are accelerated only poorly at best). This implies that the final state of the plasma is reached in a small fraction of the pulse time and that:

Assumption No. 4 - The apparent dissipative resistance remains constant during acceleration.

Equation B-7 can then be rewritten as:

$$E_{dis} = R \int J^2 dt \quad (B-9)$$

(It should be noted that even if assumption no. 4 is not strictly obeyed, but the variation of resistance scales similarly with time as thruster output is varied, then Equation B-9 will still be valid.)

Equation B-8 can also be rewritten as:

$$E_{dis} = R \int J^2 dt + V_f \int J dt \quad (B-10)$$

Experimental thruster performance measurements indicate that for exhaust velocities of interest ($>10,000$ m/s), the thrust due to electrothermal effects is very small and:

Assumption No. 5 - The acceleration of the plasma is primarily magnetic.

The electromagnetic impulse can then be written:

$$m_p v_e = (L'/2) \int J^2 dt \quad (B-11)$$

where L' is the axial inductance gradient for the device. The inductance gradient is a constant which depends on device geometry but does not vary with time.

The dissipative energy loss term for the TPP and PIT can be rewritten by combining equations B-9 and B-11 thus producing:

$$E_{dis} = (2R/L') m_p v_e \quad (B-12)$$

For the MPD, the resulting equation is:

$$E_{dis} = (2R/L') m_p v_e + V_f (2\dot{m}_p v_e / L')^{1/2} t_p \quad (B-13)$$

These equations imply the very interesting result that the dissipated energy depends on the impulse bit, $m_p v_e$.

We must now examine how R and L' vary with pulse mass and exhaust velocity. The plasma resistance should be independent of exhaust velocity according to assumptions 2 and 3 and will depend on plasma geometry and size. The resistance can be expressed as:

$$R = \xi \ell / A \quad (B-14)$$

where ξ is the plasma resistivity, ℓ is the effective plasma length, and A is the cross-sectional area of the plasma perpendicular to the path of current flow.

The pulse mass for the PIT and TPP is related to the plasma dimensions and plasma density by:

$$m_p = \rho \ell A \quad (B-15)$$

where ℓ is the plasma length and A is the plasma cross-sectional area. Obviously, the plasma resistance, R , is related to the plasma mass, m_p , through the geometry of the plasma and the material properties ξ and ρ .

We do not know, a priori, very much about the plasma geometry; however, it appears to be reasonable to assume that:

Assumption No. 6 - The plasma body will scale geometrically with pulse mass (i.e., ratios of dimensions remain fixed as the thruster size and pulse mass are varied).

Assumptions 2 and 4 imply that both plasma resistivity and plasma density are constant and independent of pulse mass and exhaust velocity. From Equation B-15, we therefore conclude that plasma (and thruster) dimensions, d , scale as:

$$d \propto m_p^{1/3} \quad (B-16)$$

and from Equation B-14 plasma resistance scales as:

$$R \propto m_p^{-1/3} \quad (B-17)$$

which may be rewritten as:

$$R = k m_p^{-1/3} \quad (B-18)$$

where k is a constant to be determined from experimental measurements.

Plasma dimensions and resistance scale somewhat differently for the MPD which operates in a quasi-steady rather than a pulsed mode. The MPD channel is completely filled with plasma. The density and current have a stable distribution during the entire pulse. The current flows radially in the plasma. From assumptions 2, 3 and 4 we can write the plasma resistance in an MPD device in terms of an effective (constant) resistivity as:

$$R = \xi \int_{r_i}^{r_o} dr / (2\pi r \ell) \quad (B-19)$$

where ℓ = the length of the MPD channel

r_i = inner electrode radius

r_o = outer electrode radius

The integration may be completed to yield:

$$R = \xi \ln(r_o/r_i) / 2\pi \ell \quad (B-20)$$

From assumption no. 6 we see that r_o/r_i remains constant as the thruster is scaled and we conclude that:

$$R \propto 1/\ell \quad (B-21)$$

From the data available on MPD thrusters we find that the mass flow rate scales as the annular area of the device:

$$\dot{m}_p \propto r_o^2 (1 - (r_i/r_o)^2) \quad (B-22)$$

From assumption 6 we can therefore infer that:

$$\ell \propto r_o \propto r_i \propto \dot{m}_p^{1/2} \quad (B-23)$$

which may be combined with Equation (B-21) to yield:

$$R = k \dot{m}_p^{-1/2} \quad (B-24)$$

where k is a constant to be determined from MPD performance data.

The scaling relation for the inductance gradient, L' , is the remaining unknown. The inductance gradient is a function of the geometry of the thruster electrodes. Parallel plate devices (such as the PIT) have a gradient given approximately by:

$$L' = \mu_0 w / h \quad (B-25)$$

where μ_0 = permeability of free space

w = separation of plates

h = height of plates

The gradient for coaxial devices (such as the MPD) is:

$$L' = (\mu_0 / 2\pi) \ln(r_o / r_i) \quad (B-26)$$

where r_o = radius of outer electrode

r_i = radius of inner electrode

From assumption no. 6, L' is independent of pulse mass (thruster size) and exhaust velocity.

Combining the inductance and resistance results for the PIT and TPP and collecting all of the constants together we obtain, (Equations B-12, B-18):

$$E_{dis} = km_p^{2/3} v_e \quad (B-27)$$

where k is a constant which will be determined from performance data. For the MPD device we obtain a slightly different result, (Equations B-13, B-24):

$$E_{dis} = k_1 \dot{m}_p^{1/2} v_e t_p + k_2 (\dot{m}_p v_e)^{1/2} t_p \quad (B-28)$$

where k_1 and k_2 are constants to be determined from performance data.

The pulse energy equation can now be rewritten for the PIT and TPP as:

$$E_p = m_p v_e^2 / 2 + m_p e_i + km_p^{2/3} v_e \quad (B-29)$$

and the efficiency as:

$$\eta = 1/[1 + 2e_i/v_e^2 + 2k/(\dot{m}_p^{1/3} v_e)] \quad (B-30)$$

For the MPD, the equivalent expressions are:

$$E_p = \dot{m}_p v_e^2 t_p / 2 + \dot{m}_p t_p e_i + k_1 \dot{m}_p^{1/2} t_p v_e + k_2 (\dot{m}_p v_e)^{1/2} t_p \quad (B-31)$$

and

$$\eta = 1/[1 + 2e_i/v_e^2 + 2k_1/(\dot{m}_p^{1/2} v_e) + 2k_2/(\dot{m}_p^{1/2} v_e^{3/2})] \quad (B-32)$$

All of the available data on efficiency for varying pulse mass and exhaust velocity was collected for each device. The values for e_i and k (k_1 and k_2 for the MPD) which best fit the data were then determined and are shown in Table B-2. Also shown in Table B-2 is the specific energy required to reach the first ionization level for argon and Teflon (argon is the propellant used in the PIT and MPD and Teflon in the TPP). The parameter e_i is just a parameter, however, if the physical model is good, then its value should be comparable to that of the actual ionization energy. The results shown in Table B-2 support the model. The differences between e_i and the ionization potential indicate the model is not exact.

TABLE B-2. PULSE ENERGY COEFFICIENTS

	e_i (MJ/kg)	CONSTANTS	1st IONIZATION POTENTIAL (MJ/kg)
PIT	88.8	$k = 145$	Ar 40
TPP	120.0	$k = 140$	Teflon 90
MPD	28.0	$k_1 = 1206$ $k_2 = 68,600$	Ar 40

(158)

The efficiency data and model predictions are illustrated in Figures B-1, B-2, and B-3. Inspection of these figures indicates a good fit to the available data. Closer examination of Equations B-30 and B-32 shows excellent qualitative agreement with observed trends:

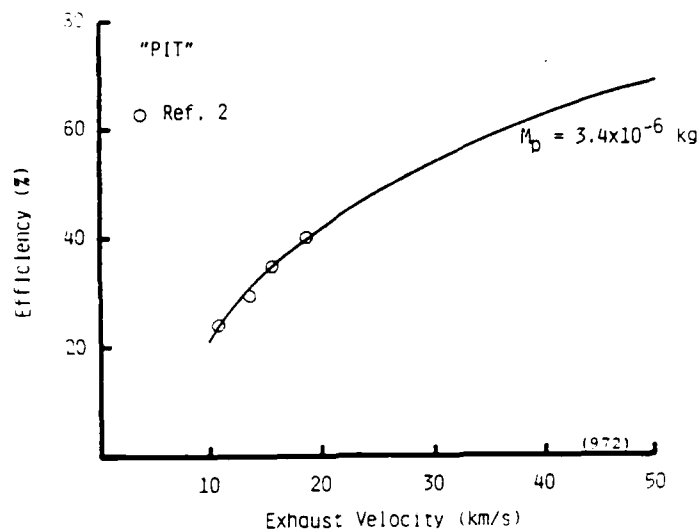


Figure B-1. Efficiency Data and Model Results for the PIT.²

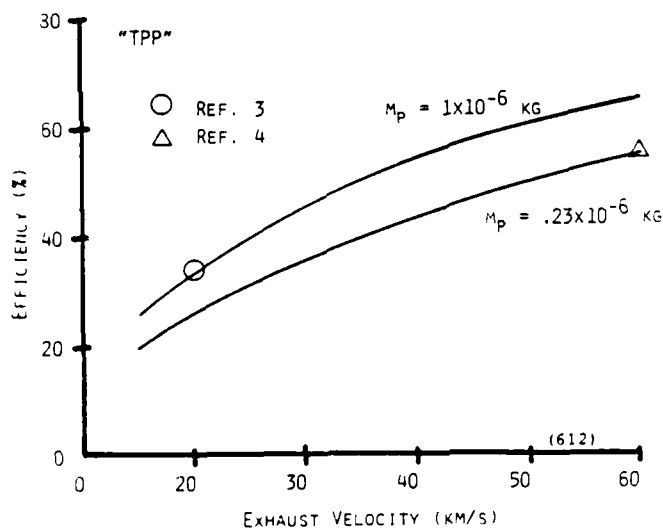


Figure B-2. Efficiency Data and Model Results for the TPP.^{3,4}

²Lowberg, R. H. and Dailey, C. L., 'Large Inductive Thruster Performance Measurement,' AIAA-81-0708R, 1981.

³Huberman, M. N. and Zafran, S., 'Pulsed Plasma Propulsion System/Spacecraft Design Guide,' AFRPL-TR-80-38, Final Report, September 1980, ADA091006.

⁴ Personal Communication - Dominic Palumbo - Fairchild Industries, Inc.

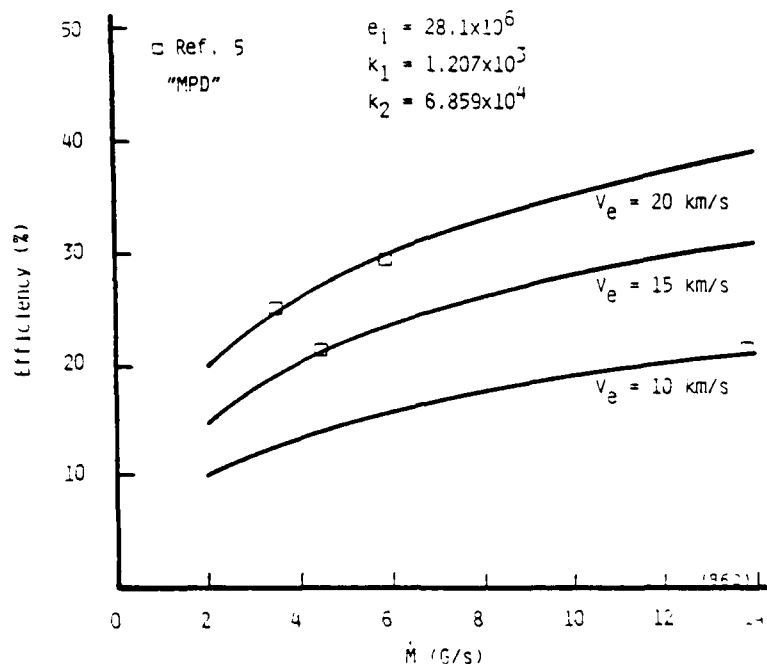


Figure B-3. Efficiency Data and Model Results for the MPD.

- (1) Efficiency increases with exhaust velocity (but can never exceed 100%).
- (2) The increase of efficiency with exhaust velocity is most pronounced at low velocities (<10,000 m/s).
- (3) Efficiency increases with pulse mass (thruster size).
- (4) The effect of pulse mass is pronounced below a critical size where efficiency drops rapidly with decreasing pulse mass.
- (5) At pulse masses above the critical value, efficiency is insensitive to pulse mass.

B.3 CURRENT/PULSE TIME

An average current can be defined from:

$$J_{avg} = \left(\int_0^{t_p} J^2 dt / t_p \right)^{1/2} \quad (B-33)$$

⁵Personal Communication - Kenn Clark - Princeton University.

which can be further reduced by, substitution of Equation B-11, to:

$$J_{avg} = (2m_p v_e / L' t_p)^{1/2} \quad (B-34)$$

Equation B-34 embodies most of the desired model characteristics. The inductance gradient, L' , is independent of m_p and v_e . The average current therefore depends directly on the impulse bit. However, the average current and the pulse time are obviously interdependent. Assessment of current requirements must be preceded by an analysis of pulse time. Each of the thrusters (PIT, TPP and MPD) have different pulse time constraints and must be treated separately.

B.3.1 The PIT

The PIT accelerates a flat sheet of plasma by repulsion from a flat coil. As the separation between the plasma sheet and the coil increases, the mutual inductance (the PIT equivalent of L') decreases. The accelerating force then drops and the plasma becomes 'decoupled' (i.e., current flowing in the drive coil no longer accelerates the plasma). The data in the literature indicates relatively good (and constant) coupling up to a separation of about 1/10 of the coil diameter (the decoupling distance should scale directly with the coil diameter). Coil diameter will scale with pulse mass according to assumption no. 6 as expressed in Equation B-16. Correlating the available data⁶ we find that coil diameter, D , is:

$$D = 66.5 m_p^{1/3} \quad (B-35)$$

Therefore, the acceleration length, ℓ , is given by:

$$\ell = 6.5 m_p^{1/3} \quad (B-36)$$

The measured inductance gradient for the PIT is:

$$L' = 7 \mu H/m \quad (B-37)$$

⁶Personal Communication - Dailey, C.L., TRW Space and Technology Group.

If the current is constant at the average current value during the pulse, then the plasma acceleration will be constant and the acceleration time (which must correspond to the pulse time) is:

$$t_p = 2 / v_e \quad (B-38)$$

which may be combined with Equation B-36 to yield:

$$t_p = 13.0 m_p^{1/3} / v_e \quad (B-39)$$

This result is illustrated in Figure B-4. Substituting Equations B-36, B-37 and B-39 into Equation B-34 provides:

$$J_{avg} = 148.25 m_p^{1/3} v_e \quad (B-40)$$

which is illustrated in Figure B-5.

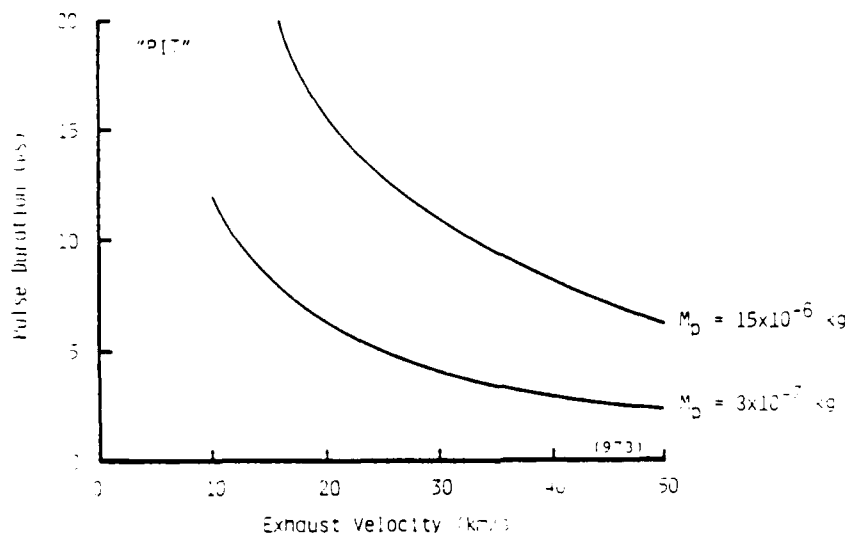


Figure B-4. Pulse Time for the PIT.

Very little experimental data is available in the literature on current and pulse times for the PIT. The data available was generated with current (and therefore the acceleration) which was not constant during a pulse. The

- (4) The models fit the available experimental data extremely well (considering the simplicity of the models and the paucity of data).
- (5) The excellent qualitative and quantitative agreement between model prediction and observed performance lend considerable credence to the models and the underlying assumptions.
- (6) The models are extremely versatile, permitting rapid evaluation of thruster input requirements over a wide range of output conditions. The models can easily be updated if and when new data becomes available.

B.6 RECOMMENDATIONS

There are two major areas of uncertainty in the thruster models developed. The first arises from the nature of the thrusters for which data was available. It is not clear that the experimental thruster performance data available to us was generated with 'optimum' thrusters (i.e., that the thruster was optimized for every \dot{m}_p and v_e for which data was reported). The performance data must be evaluated more carefully in order to answer this question. The second problem arises from the limited amount of data available. The missions considered in this study require that the thruster models apply at operating conditions (\dot{m}_p and v_e) which could be orders of magnitude different from the conditions for which we have data. We recommend that performance data for optimum thrusters be generated over an expanded range of \dot{m}_p (or \dot{m}_p) and v_e .

The acceleration voltage is derived from Equation B-56 and is:

$$V_{acc} = 2.07 \times 10^{-4} \dot{m}_p^{1/2} v_e^{3/2} \quad (B-70)$$

These voltage components are shown in Figure B-16.

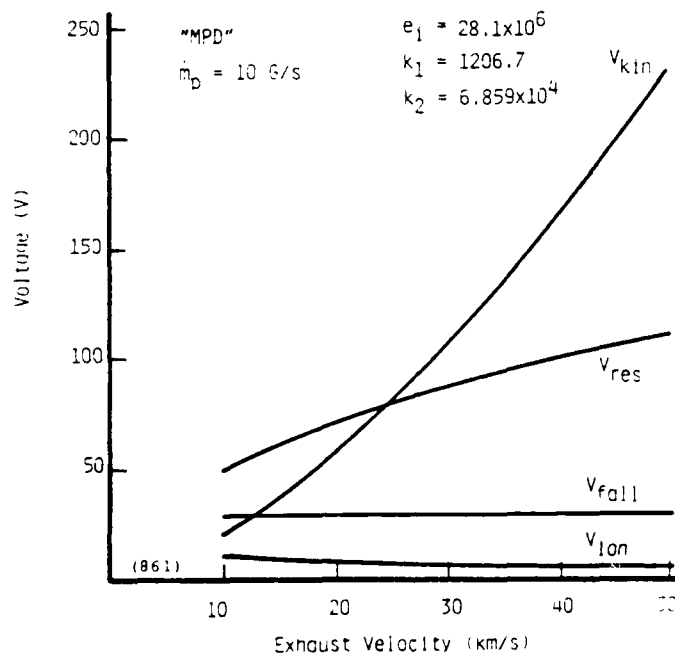


Figure B-16. Voltage Components for the MPD.

B.5 CONCLUSIONS

A number of specific conclusions can be drawn from this investigation of performance modeling for electromagnetic thrusters.

- (1) Thruster modeling for integrated propulsion system optimization requires that thruster input requirements (pulse energy, current, voltage, and time) be related to the primary propulsion system outputs (pulse mass, exhaust velocity, frequency, and total thrusting time).
- (2) Models which meet these requirements were successfully developed for all of the thrusters of interest.
- (3) The models developed for the thrusters (except for the ERG) were based on an understanding of the physical principles of operation and a number of assumptions concerning the performance of optimized thrusters.

B.4.3 The MPD

The average voltage can be found from Equation B-52 and is:

$$V_{avg} = 2.07 \times 10^{-4} \dot{m}_p^{1/2} v_e^{3/2} + 1.16 \times 10^4 \dot{m}_p^{1/2} v_e^{-1/2} + 0.498 v_e^{1/2} + 28.3 \quad (B-67)$$

which is shown in Figure B-15. Each of the voltage components was evaluated.

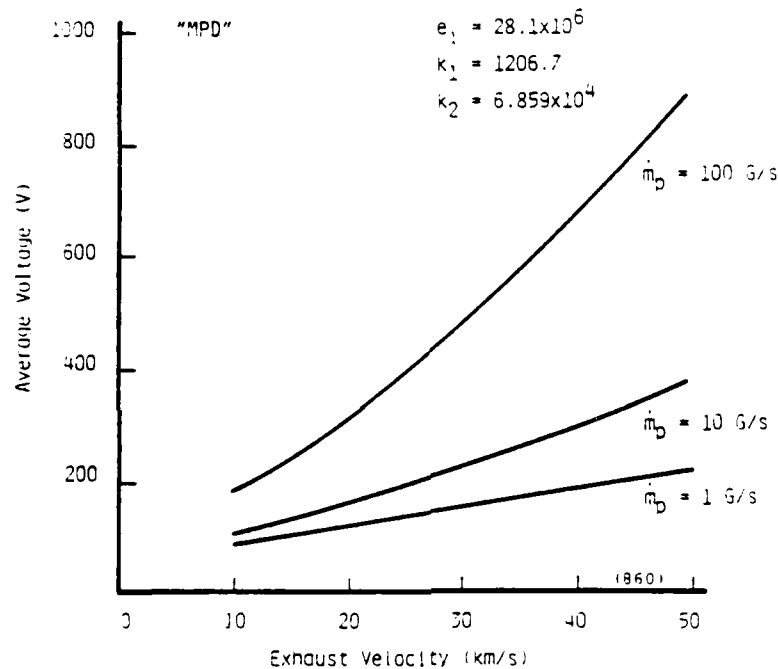


Figure B-15. Average Voltage for the MPD.

The ionization voltage for a quasi-steady MPD thruster is constant throughout the pulse and is given by Equation B-54. Evaluation of Equation B-54 yields:

$$V_{ion} = 1.16 \times 10^4 \dot{m}_p^{1/2} v_e^{-1/2} \quad (B-68)$$

The dissipation voltage is derived from Equation B-57 and is:

$$V_{dis} = 0.498 v_e^{1/2} + 28.3 \quad (B-69)$$

of the total pulse time. The ionization voltage can then be written from Equation B-53 as:

$$V_{ion} = 7.5 \times 10^8 m_p^{1/3} / v_e \quad (B-64)$$

The acceleration voltage is derived from Equation B-55 as:

$$V_{acc} = 0.311 m_p^{1/3} v_e \quad (B-65)$$

The dissipation voltage, computed from Equation B-57 is a constant:

$$V_{dis} = 87.2 \quad (B-66)$$

These voltage components are shown in Figure B-14. The TPP thruster does not require a 'breakdown voltage', since the breakdown across the electrodes is initiated by an external ignition circuit. There is a minimum allowable voltage for operation of the device. Lack of experimental data precluded developing a relationship for this parameter.

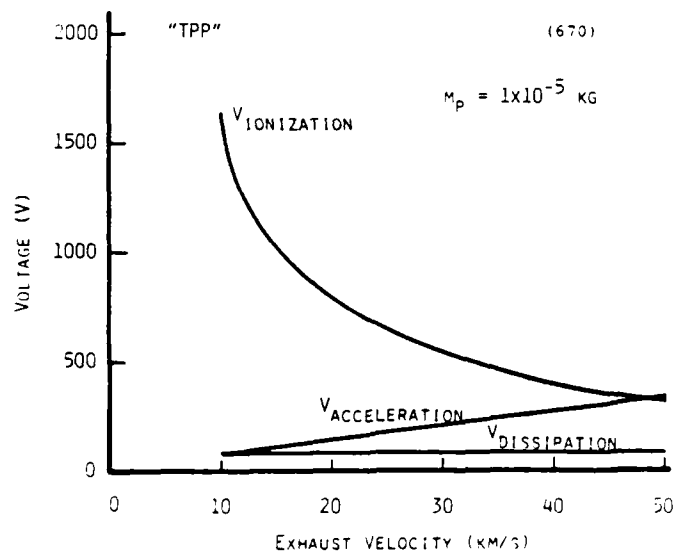


Figure B-14. Voltage Components for the TPP.

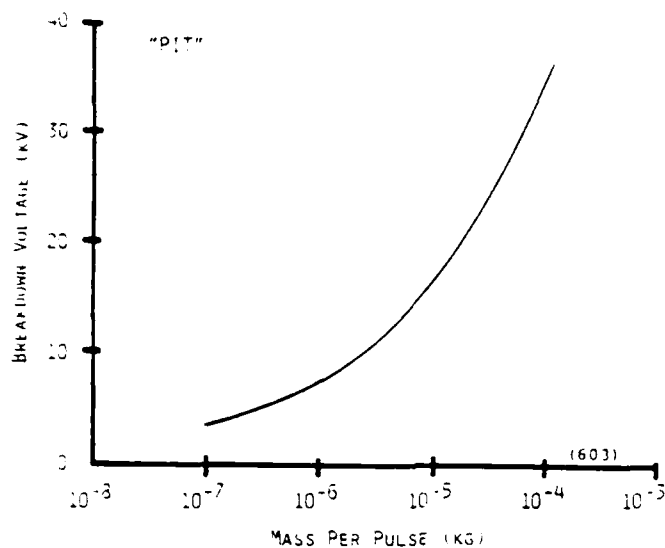


Figure B-12. Breakdown Voltage for the PIT.

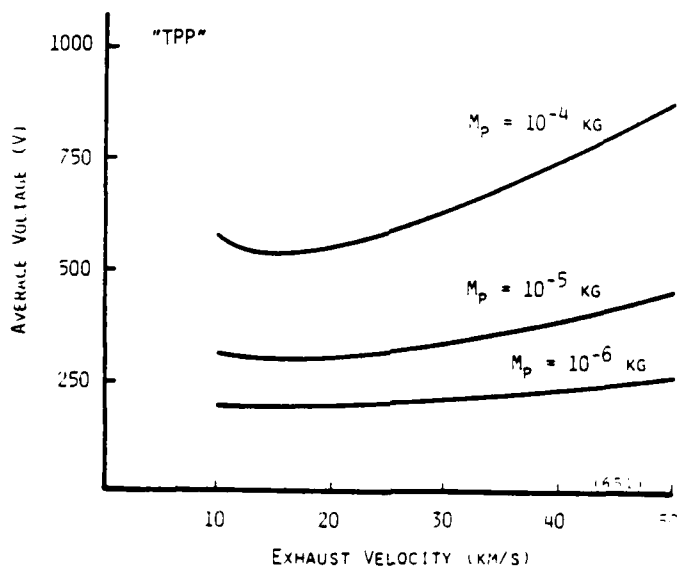


Figure B-13. Average Voltage for the TPP.

Each of the voltage components was examined separately. A relatively high voltage is required for Teflon ablation and plasma formation at the beginning of the pulse. The time for plasma formation was assumed to be 10%

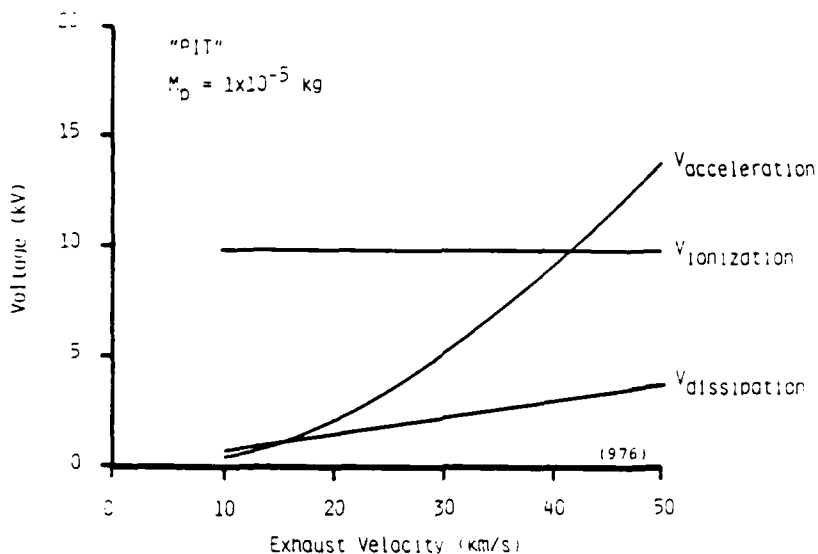


Figure B-11. Voltage Components for the PIT.

'ionization voltage' but reflects the practical requirement of achieving adequate electric field to ionize the gas. From the experimental data, Equation B-53 was reevaluated to yield:

$$V_{bdn} = 7.5 \times 10^5 m_p^{1/3} \quad (B-62)$$

which is plotted in Figure B-12. Comparison of Equation B-62 with Equation B-59 shows that the breakdown voltage is higher than our 'ionization voltage'. This indicates that ionization will be completed in less than 10% of the pulse time.

B.4.2 The TPP

The average voltage for the TPP thruster can be found from Equation B-52 and is:

$$V_{avg} = 0.311 m_p^{1/3} v_e + 7.5 \times 10^7 m_p^{1/3} / v_e + 87.2 \quad (B-63)$$

which is shown plotted in Figure B-13.

and is plotted in Figure B-10.

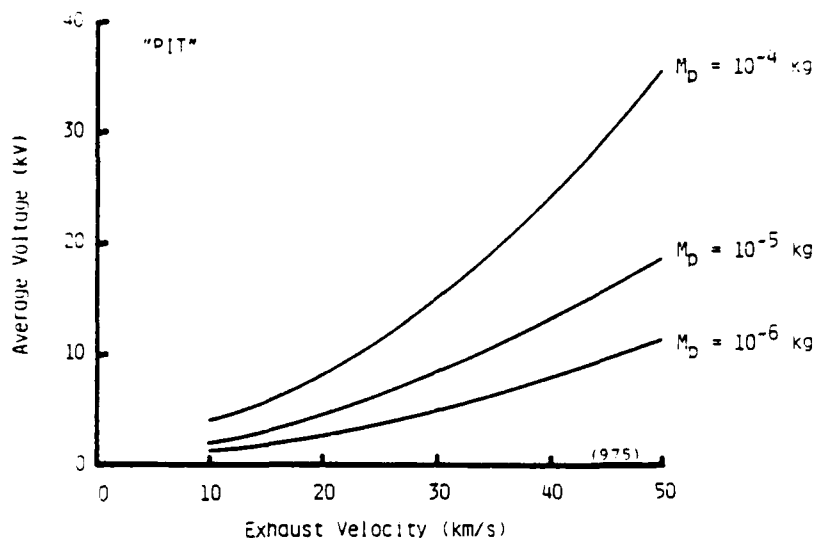


Figure B-10. Average Voltage for the PIT.

Each of the voltage components was examined separately. Assuming that the plasma is formed during the first 10% of the total pulse duration, the factor (t_p/t) is equal to 10. The ionization voltage can be written from Equation B-53 as:

$$V_{ion} = 4.61 \times 10^5 m_p^{1/3} \quad (B-59)$$

The acceleration voltage derived from Equation B-55 is:

$$V_{acc} = 2.59 \times 10^{-4} m_p^{1/3} v_e^2 \quad (B-60)$$

and the dissipation voltage derived from Equation B-57 is:

$$V_{dis} = 7.52 \times 10^{-2} v_e \quad (B-61)$$

The three voltage components are plotted in Figure B-11.

The PIT also has a minimum allowable voltage required for gas breakdown and plasma formation. This 'breakdown voltage' is identical to our

The ionization voltage, as defined here, should not be confused with the voltage required to ionize (the breakdown voltage). The factor, (t/t_p) , is the fraction of the pulse duration in which the ionization takes place. For example, the PIT and TPP require a very high voltage for plasma formation at the beginning of the pulse. Once the plasma has formed, this voltage is no longer required. On the other hand, the MPD thruster requires voltage for ionization of propellant throughout the pulse. For the MPD, $(t_p/t) = 1$ and the 'ionization' voltage is written as:

$$V_{ion} = \dot{m}_p v_e / J \quad (B-54)$$

The voltage required to deliver the acceleration power to the pulse mass is the acceleration (or useful) voltage. It is related to the kinetic energy, the average current, and pulse duration as:

$$V_{acc} = \dot{m}_p v_e^2 / (J t_p) \quad (B-55)$$

For the MPD the acceleration is quasi-steady and the acceleration voltage can be written as:

$$V_{acc} = \dot{m}_p v_e^2 / J \quad (B-56)$$

The voltage that is associated with the energy dissipated during the pulse is related to the dissipated energy, the average current, and pulse duration. The dissipative resistance of the thrusters was assumed to be a constant throughout the pulse. The dissipated voltage is given by:

$$V_{dis} = E_{dis} / (J t_p) \quad (B-57)$$

We now examine these voltages for each thruster.

B.4.1 The PIT

Since all of the factors in Equation B-52 are known, the PIT average voltage can be written as:

$$V_{avg} = 2.59 \times 10^{-4} \dot{m}_p^{1/3} v_e^2 + 4.61 \times 10^4 \dot{m}_p^{1/3} + 7.52 \times 10^{-2} v_e \quad (B-58)$$

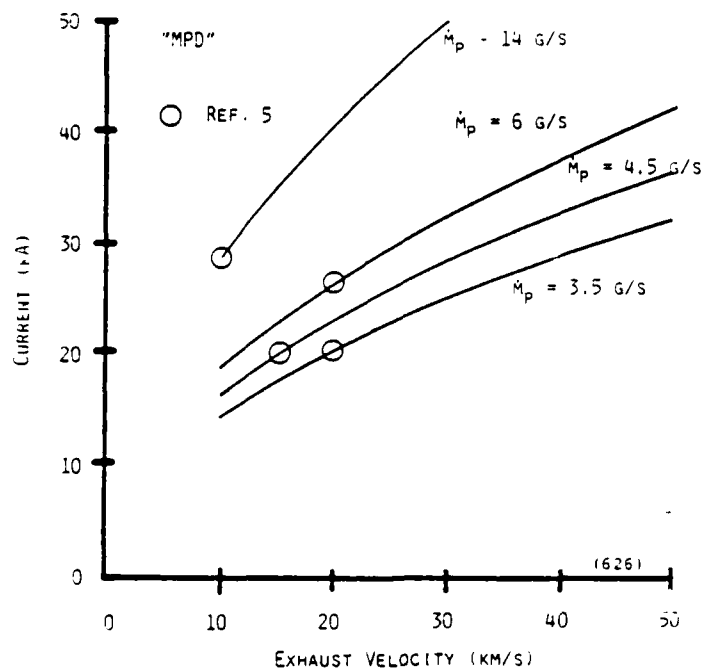


Figure B-9. Current for the MPD.

The average voltage is computed from the pulse energy, the pulse time and the average current as:

$$V_{avg} = E_p / (t_p J_{avg}) \quad (B-52)$$

The origin of the voltage can be better understood if it is written as the sum of voltage components related to the components of pulse energy. These voltage components are denoted by: V_{ion} - voltage required to heat and ionize the propellant, V_{acc} - voltage required to accelerate the propellant, and V_{dis} - the voltage characteristic of the energy dissipated. A minimum voltage required to initiate operation (breakdown voltage) has also been analyzed for some devices.

The 'ionization' voltage is computed from the ionization energy (Equation (B-6)) substituted into Equation (B-52) to yield:

$$V_{ion} = m_{pe_i} / (J t_p) \times (t_p / t) \quad (B-53)$$

B.3.3 The MPD

Since the MPD operates in a 'quasi-steady' mode, the pulse duration is an independent parameter. The current is therefore independent of the pulse time and is assumed constant during the pulse. The electromagnetic thrust for an MPD thruster can be written as:

$$F = \dot{m}_p v_e = L' J^2 / 2 \quad (B-48)$$

This can be generalized to form a relationship between the current and the independent pulse parameters:

$$J \propto (\dot{m}_p v_e)^{1/2} \quad (B-49)$$

or written in equation form as:

$$J = k(\dot{m}_p v_e)^{1/2} \quad (B-50)$$

where k is an experimentally determined constant. From the available data⁵ the constant was evaluated and Equation B-50 becomes:

$$J = 2.42 \times 10^3 (\dot{m}_p v_e)^{1/2} \quad (B-51)$$

which is illustrated in Figure B-9.

B.4 VOLTAGE

The thrusters treated are all electromagnetic and are 'current driven' (i.e., the acceleration force is related to current, not voltage). These devices do not, in general, require a high voltage to accelerate the pulse mass (although some require a relatively high voltage for the formation of the current-carrying plasma and to produce the required short pulses). The voltage is, therefore, a derived parameter in electromagnetic thrusters and is indicative of the impedance of the device. The primary function of the ES/PC system is to provide the required current.

The pulse time can be computed by rewriting Equation B-36 as:

$$t_p = 2m_p v_e / L' J_{avg}^2 \quad (B-45)$$

Unfortunately for the TPP, we don't know either L' or J_{avg} (or even the relationship of J_{avg} to J_{max}). If the acceleration pulse is similar in scaled devices then the ratio of J_{avg} to J_{max} will be constant and Equations B-44 and B-45 can be combined to yield:

$$t_p = k m_p^{1/3} v_e \quad (B-46)$$

where k is a constant to be determined from performance data. Available data^{10,11} was used to obtain:

$$t_p = 150 \times 10^{-9} m_p^{1/3} v_e \quad (B-47)$$

which is illustrated in Figure B-8.

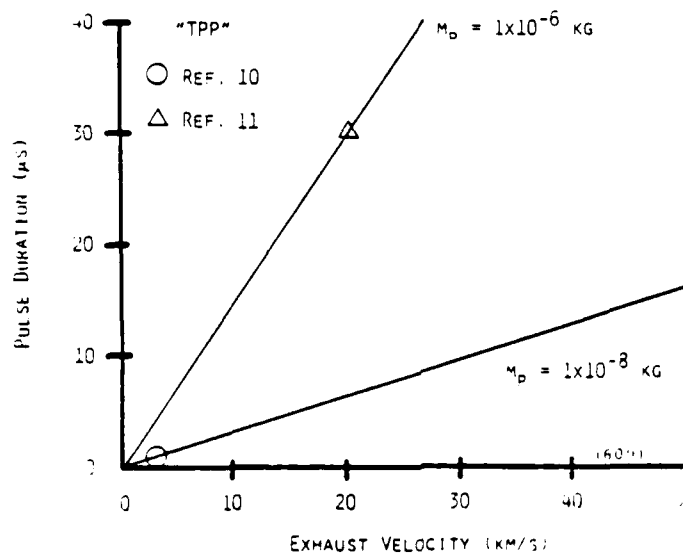


Figure B-8. Pulse Time for the TPP.

¹⁰Vondra, R. J., Thomassen, K., Solbes, A., 'Analysis of Solid Teflon Pulsed Plasma Thrusters,' Journal of Spacecraft and Rockets, Vol. 7, No. 12.

¹¹Poeschel, R. L., 'A Comparison of Electric Propulsion Technologies,' AIAA-82-1243, Presented at the 18th Joint Propulsion Conference (Cleveland, OH).

Assumption No. 7 - For TPP thrusters, the magnetic pressure is maximized and is independent of thruster size and exhaust velocity.

The maximum current scales directly with thruster size according to Equation B-42. From assumption no. 6 and Equation B-16, thruster size scales with pulse mass. Combining Equations B-16 and B-42 we obtain:

$$J_{\max} = km_p^{1/3} \quad (B-43)$$

where k = a constant to be determined from data. The available data⁹ were used to evaluate the constant and the result is:

$$J_{\max} = 1.07 \times 10^7 m_p^{1/3} \quad (B-44)$$

which is illustrated in Figure B-7.

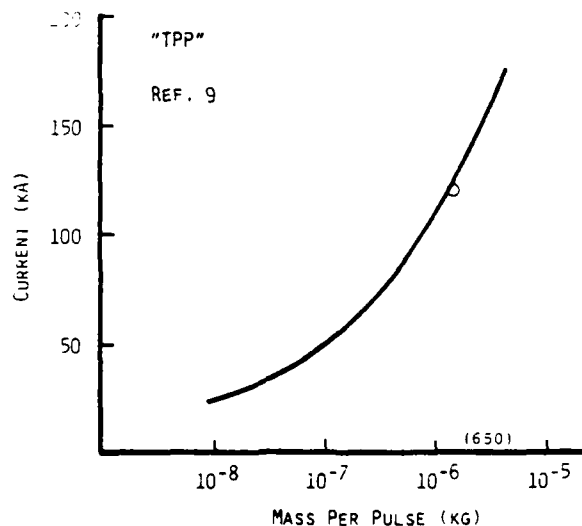


Figure B-7. Maximum Current for the TPP.

⁹Personal Communication - Dominic Palumbo - Fairchild Industries, Inc.

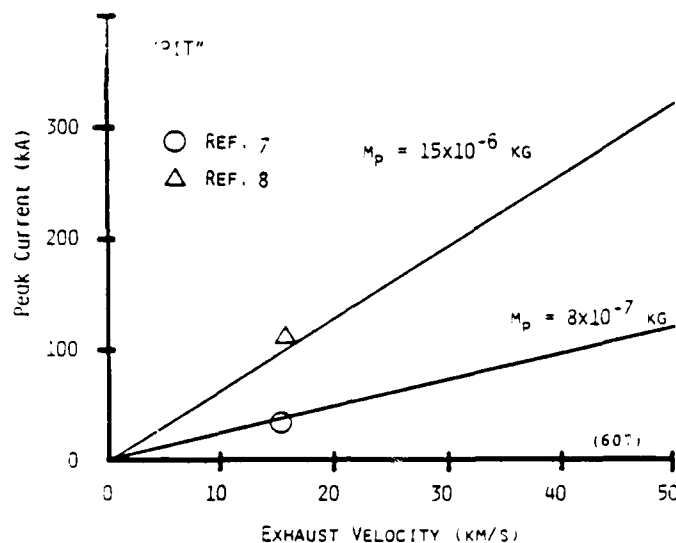


Figure B-6. Peak Current for the PIT.

B.3.2 The TPP

The TPP is a parallel plate electrode device and the electrodes can, presumably, be made as long as necessary to reach the desired velocity. The pulse time is therefore, not constrained, and we must search for other constraints on the current.

The TPP operates in a very similar manner to the ERG. The primary difference between the two is the presence of a solid 'pellet' in the ERG. Optimum TPP design should be similar to optimum ERG design. The optimization strategies for ERG design are summarized in Table B-1. One of the primary optimization strategies is to maximize the magnetic (accelerating) stress. The stress is related to current and electrode dimensions by:

$$\sigma \propto (J/h)^2 \quad (B-42)$$

where h = the electrode height. The maximum stress will be constrained by thruster strength, electrode erosion (from the resultant current density) or some other factor. For scaled TPP thrusters designed for optimum efficiency we would expect that:

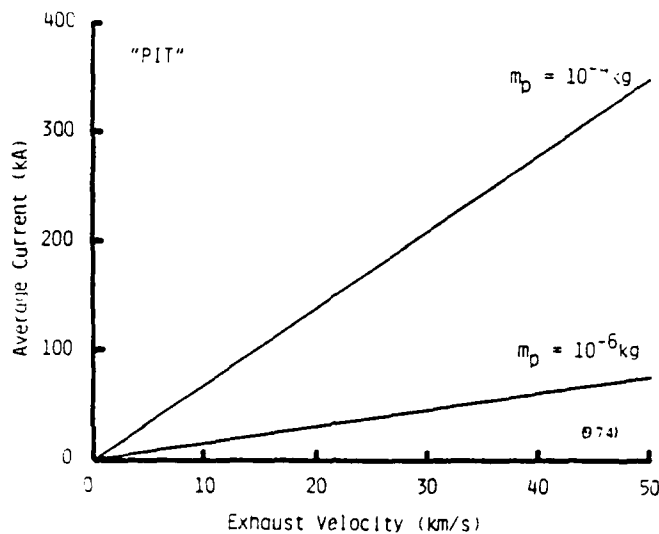


Figure B-5. Average Current for the PIT.

measured pulse times are, as expected, longer than Equation B-39 predicts, but only by about 15%. There are a few measurements of peak current reported and, as expected, they correlate with pulse mass and exhaust velocity as predicted by Equation B-41. The data^{7,8} for peak current yields:

$$J_{\max} = 261 m_p^{1/3} v_e \quad (\text{B-41})$$

which is illustrated in Figure B-6.

Comparison of Equations B-40 and B-41 indicate that, for the particular ES/PC system used in the experiments, the peak-to-average current ratio was approximately 1.75.

⁷Dailey, C.L., 'Large Diameter Inductive Plasma Thrusters,' AIAA-79-2093, Presented at the 14th International Electric Propulsion Conference (Princeton, NJ).

⁸Dailey, C. L., 'Large Diameter Inductive Plasma Thruster,' AIAA-79-2093, presented at the 14th International Electric Propulsion Conference (Princeton, NJ).

REFERENCES

1. Bauer, D.P., Barber, J.P., Vahlberg, C.J., 'The Electric Rail Gun for Space Propulsion,' NASA-CR-165312, Final Report, February 1981.
2. Lovberg, R.H. and Dailey, C.L., 'Large Inductive Thruster Performance Measurement,' AIAA-81-0708R.
3. Huberman, M.N. and Zafran, S., 'Pulsed Plasma Propulsion System/Spacecraft Design Guide,' AFRPL-TR-80-38, Final Report, September 1980, ADA091006.
4. Personal Communication - Dominic Palumbo - Fairchild Industries, Inc.
5. Personal Communication - Kenn Clark - Princeton University.
6. Personal Communication - C.L. Dailey - TRW Space and Technology Group.
7. Dailey, C.L., 'Large Diameter Inductive Plasma Thrusters,' AIAA-79-2093, Presented at the 14th International Electric Propulsion Conference (Princeton, NJ).
8. Dailey, C.L. and Lovberg, R.H., 'Pulsed Inductive Thruster Development (Advanced Electric Propulsion Technology--High Thrust),' AFRPL-TR-80-67, Final Report, January 1981.
9. Personal Communication - Dominic Palumbo - Fairchild Industries, Inc.
10. Vondra, R.J., Thomassen, K., Solbes, A., 'Analysis of Solid Teflon Pulsed Plasma Thrusters,' Journal of Spacecraft and Rockets, Vol. 7, No. 12.
11. Poeschel, R.L., 'A Comparison of Electric Propulsion Technologies,' AIAA-82-1243, Presented at the 18th Joint Propulsion Conference (Cleveland, OH).

APPENDIX C

INDUCTORS IN PULSE POWER SYSTEMS

By

John P. Barber

June, 1983

IAP-TR-83-2 (Revision 2)

Table of Contents

Section	Page
C.1 INTRODUCTION	C-1
C.2 CIRCUIT CHARACTERISTICS	C-2
C.3 INDUCTOR SIZING	C-5
C.3.1 THE INDUCTANCE	C-5
C.3.2 INDUCTOR MASS	C-7
C.3.3 CONDUCTOR CROSS-SECTIONAL AREA	C-7
C.3.3.1 Thermal Constraints	C-7
C.3.3.1.1 Thermal Inertia	C-8
C.3.3.1.2 Active Cooling	C-9
C.3.3.2 Stress Constraints	C-11
C.3.3.3 Geometrical Constraints	C-12
C.3.3.4 High Frequency Effects	C-13
C.3.3.4.1 Resistance	C-14
C.3.3.4.2 Inductance	C-14
C.3.4 INDUCTOR RESISTANCE	C-15
C.3.4.1 Minimum Mass Inductors	C-15
C.3.4.2 Resistance-Mass Scaling	C-15
C.3.5 COMPUTATIONAL TECHNIQUE	C-16
C.4 RESULTS	C-17
C.4.1 THE PARAMETERS	C-17
C.4.1.1 The Independent Parameters	C-17
C.4.1.2 The Material Properties	C-17
C.4.1.3 The Geometry	C-18
C.4.1.4 The Outputs	C-18
C.4.2 INDUCTOR GEOMETRY	C-18
C.4.3 CONDUCTOR TEMPERATURE	C-20
C.4.4 CURRENT	C-20
C.4.5 INDUCTANCE	C-21
C.4.6 CONDUCTION TIME	C-22

List of Figures

Figure		Page
C-1	Current Variation in Energy Storage	C-3
C-2	The Efficiency Factor, α	C-4
C-3	Inductor Efficiency	C-4
C-4	Solenoid Geometry	C-6
C-5	Inductance Factor for Solenoids	C-7
C-6	Action Constant for Aluminum	C-9
C-7	The Electrical Skin Depth for Aluminum	C-14
C-8	Specific Energy vs. Length to Radius Ratio	C-19
C-9	Specific Energy vs. Thickness to Radius Ratio	C-19
C-10	Specific Energy vs. Conductor Temperature for AL-1100-0 .	C-20
C-11	Specific Energy vs. Current	C-21
C-12	Specific Energy vs. Inductance	C-21
C-13	Specific Energy vs. Conduction Time	C-22

Tables

Table		Page
C-1	Material Properties AL-1100-0	C-17

List of Symbols

a	mean inductor radius
c	coil thickness, inductor thickness
c_s	skin depth
d	mean thickness of webs
g_1	action constant
k	inductance factor
k_0	constant
k_1	constant
k'	constant
m	mass
\dot{q}	heat transfer rate
\dot{q}_w	\dot{q} for water
\dot{q}_H	\dot{q} for hydrogen
\dot{q}_N	\dot{q} for liquid nitrogen
s	'wetted' perimeter
t	time of conduction
t_p	pulse time
z	length of conductor
A	cross-sectional area
A_g	geometrical cross-section
A_B	'solidity' ratio
B	magnetic flux density
E_{dis}	dissipated energy
E_{use}	useful energy
I	current
I_f	min. current
I_0	max. current
L	inductance
N	number of turns
P_m	magnetic pressure
R	resistance of inductor
T	inductor time constant
θ	efficiency factor

List of Symbols (concluded)

α	efficiency factor
η	efficiency
μ_0	permeability of free space
ξ	resistivity
ρ	density
σ	stress

SECTION C.1

INTRODUCTION

Inductors can be used either as energy stores or as pulse-forming components in pulse power systems. In the energy storage role inductors are attractive because they offer high stored energy at relatively low mass. In addition, they provide a low-impedance, constant-current source characteristic. This characteristic is very important for some applications such as electromagnetic launchers and electromagnetic thrusters. The disadvantages of inductors as energy stores is that they are lossy (i.e., have a low Q) and are therefore relatively inefficient. The losses can be eliminated and the efficiency improved by employing superconductors. Superconductors, however, are not tolerant to pulse discharge and pose serious thermal design problems in high current applications.

Inductors are also used as pulse-forming components to control the shape and duration of pulses delivered from capacitive energy stores. Inductors can be used in either a normal LC combination or in multi-staged pulse forming networks. In these applications, the inductors carry current for only a short time and the resistive losses inherent in inductors are not so important.

In many applications of interest for both inductive energy storage and inductive pulse forming, component mass must be minimized. The objective of this report is to develop methods of minimum mass selection and sizing of inductors for both energy storage and pulse forming duty.

SECTION C.2
CIRCUIT CHARACTERISTICS

The circuit performance of inductors plays an important role in inductor sizing and selection. The energy efficiency of the inductor in the circuit is of particular interest. We define the efficiency as:

$$\eta = E_{use} / (E_{dis} + E_{use}) \quad (C-1)$$

where E_{dis} = dissipated energy.

E_{use} = useful energy extracted.

The dissipated energy is:

$$E_{dis} = R \int I^2 dt \quad (C-2)$$

where R = resistance of the inductor.

The useful energy is:

$$E_{use} = L(I_0^2 - I_f^2)/2 \quad (C-3)$$

where I_0 = maximum current during period of interest

I_f = minimum current during period of interest

Substituting Equations 2 and 3 into Equation 1 provides:

$$\eta = 1 / (1 + 2\theta/\tau) \quad (C-4)$$

where $\theta = \int I^2 dt / (I_0^2 - I_f^2)$, the efficiency factor

$\tau = L/R$, the inductor time constant.

The factor, θ , depends on the details of the application and the characteristics of the circuit.

In pulse-forming duty, θ can be readily evaluated from the circuit performance characteristics and is approximately equal to the pulse duration. If the inductor time constant is long with respect to the pulse duration the efficiency will be high.

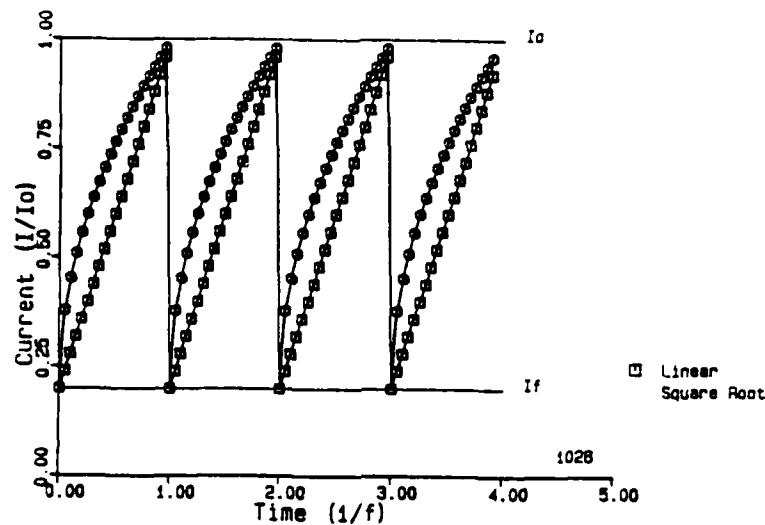


Figure C-1. Current Variation in Energy Storage.

In energy storage duty, ϕ is related to the frequency of pulsing and the depth of discharge. The basic current-time characteristic for energy storage duty is illustrated in Figure C-1. The discharge time is typically orders of magnitude shorter than the charging time. The efficiency of the inductor is therefore primarily determined by the charging process. Two different charging variations are illustrated, a linear current rise and a square root current rise (which more nearly approximates the desired constant power charging). The factor ϕ can be evaluated for both cases and is related to the frequency by:

$$\phi = \alpha / 2f \quad (C-5)$$

where α = an efficiency factor. The efficiency factor is a function of the current ratio, I_f/I_o , and is illustrated in Figure C-2. For reasonable current ratios (<0.5) the efficiency factor is independent of current ratio and is approximately equal to one.

The efficiency can be evaluated from Equation C-4. The results for inductors with various time constants are illustrated in Figure C-3. The inductor time constant and its dependence on inductor mass is of major importance.

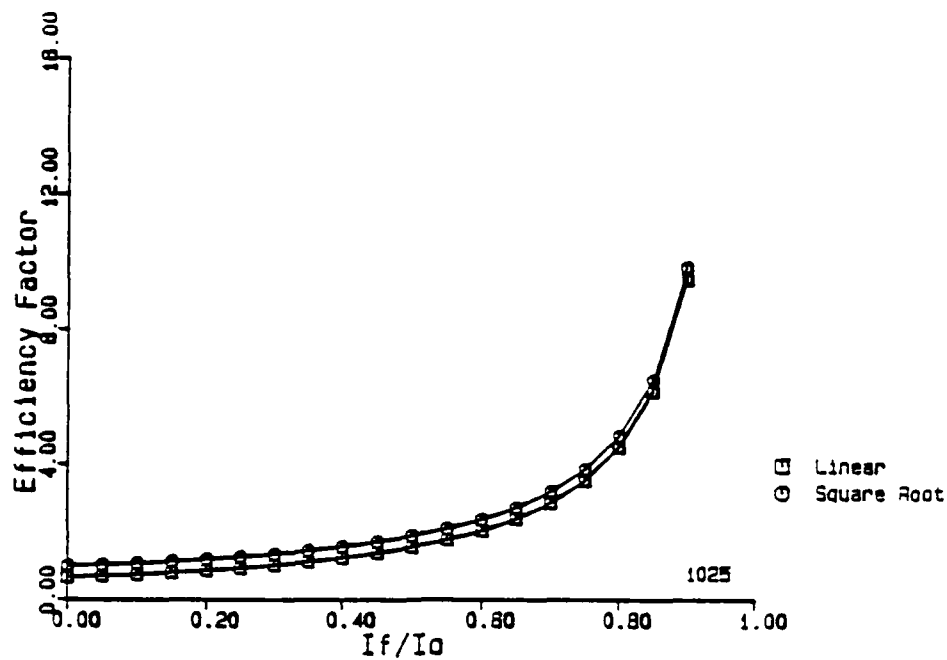


Figure C-2. The Efficiency Factor, α .

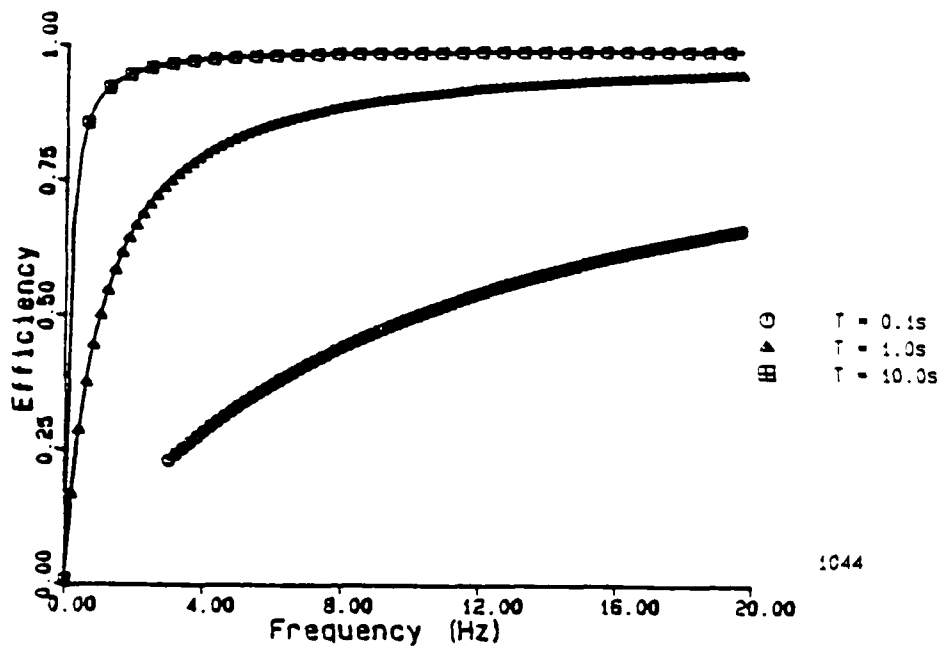


Figure C-3. Inductor Efficiency.

SECTION C.3

INDUCTOR SIZING

C.3.1 THE INDUCTANCE

From the point of view of inductor sizing and design, the inductance is not a design parameter. The designer is not free to choose the inductance in order to minimize mass. The inductance is usually fixed by the application and the designer's job is to size and design an inductor with the required inductance and minimum mass. From the designer's point of view, therefore, the inductance is an independent parameter.

The inductance of an inductor is dependent upon the configuration and the size of the inductor. The inductance may be conveniently expressed as:

$$L = kNz \quad (C-6)$$

where L = inductance
 k = inductance factor
 N = number of turns
 z = length of conductor.

The geometrical factor, k , depends on the choice of configuration (toroid, solenoid, etc.) and on the geometry of the inductor (length-to-radius ratio, etc.). The value of the inductance factor is independent of coil size. Values for the inductance factor can readily be calculated for all common configurations and geometries. In this report we concentrate on solenoids as they are simple and display the same basic scaling characteristics as other multi-turn concepts such as toroids.

The geometry of a solenoid is illustrated in Figure C-4. The inductance factor for solenoids can readily be evaluated from the formulas of Grover¹ and Wheeler.² The inductance factor is a function of the geometrical ratios c/a and b/a and is illustrated in Figure C-5. We note that for

¹Grover, F. W., 'Inductance Calculations,' D. Van Nostrand Co., New York, 1946.

²Wheeler, H. A., 'Inductance Formulas for Circular and Square Coils,' IEEE Proc., 70, pp 1449-1450, 1982.

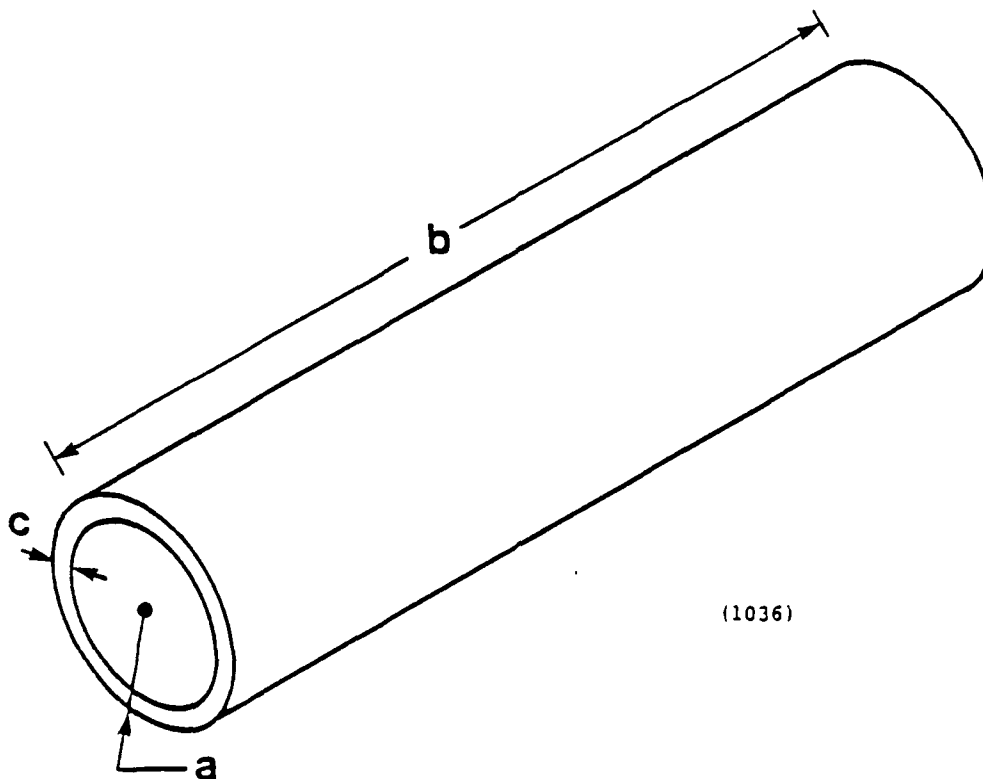


Figure C-4. Solenoid Geometry.

long coils ($b/a > 1$) the inductance factor is not a strong function of the thickness ratio (c/a). The parameters for a Brooks coil are also identified in Figure C-5. The Brooks coil is important as it is the solenoid configuration which has the highest inductance for a given length of conductor. It is sometimes thought of as a minimum mass configuration. However, it is only a minimum length configuration. As we shall see in the following sections, inductor mass depends on other factors as well as conductor length.

The inductance factor for solenoids can be expressed approximately as:

$$k = k_0 - k_1 \quad (C-7)$$

where $k_0 = 2 \times 10^{-7} [2.78 / ((b/a) + 1) + \ln(1 + 0.39(b/a))]$

$k_1 = 6.28 \times 10^{-7} (a/b)(c/a)k'$

$k' = (0.331 - 0.011/(b/a)) \exp[-(0.361 + 0.088/(b/a))(c/a)]$.

The approximation is very good over the range of geometries of interest.

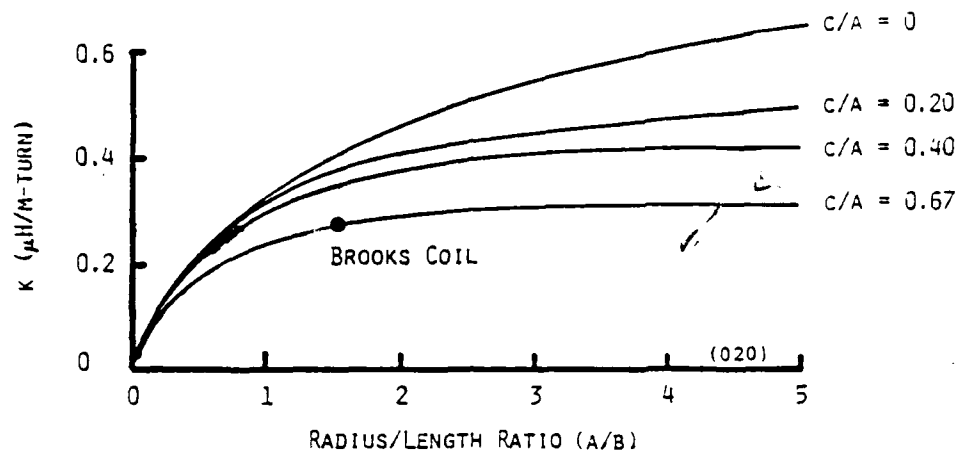


Figure C-5. Inductance Factor for Solenoids.

C.3.2 INDUCTOR MASS

The mass of a solenoid can be expressed as:

$$m = \rho Az \quad (C-8)$$

where m = inductor mass

ρ = mass density of the conductor

A = cross-sectional area.

Inductor mass is minimized by minimizing the product of z and A . Inspection of Equation C-6 shows that z will be minimized if N is maximized (for a fixed inductance) and that inductor mass will be directly related to the inductance. Equations C-6 and C-8 provide no information on the selection of conductor cross section, A . For a minimum mass inductor, A must be as small as possible.

C.3.3 CONDUCTOR CROSS-SECTIONAL AREA

The conductor cross-sectional area can in principle be reduced until the stress and/or the temperature (due to resistive dissipation) becomes unacceptable. Further reduction in cross section will result in coil failure.

C.3.3.1 Thermal Constraints

The thermal design of an inductor can proceed in either of two directions. In the first approach the inductor is not actively cooled, but is

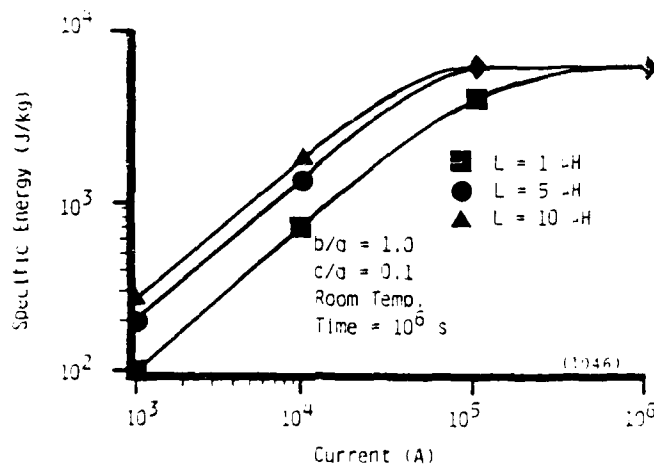


Figure C-11. Specific Energy vs. Current.

C.4.5 INDUCTANCE

The effect of inductance on specific energy is more clearly illustrated in Figure C-12. The specific energy increases with Figure C-11 inductance at low current levels and is independent of inductance at high current.

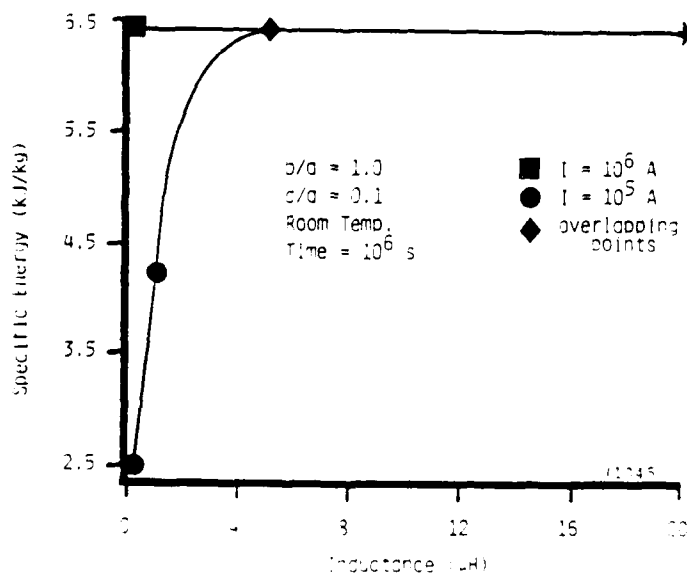


Figure C-12. Specific Energy vs. Inductance.

small c/a (<0.2). The effect of thickness-to-radius ratio is illustrated more clearly in Figure C-9.

C.4.3 CONDUCTOR TEMPERATURE

The conductor temperature primarily affects the resistivity but also has an effect on heat transfer. The variation of specific energy with temperature is illustrated in Figure C-10. The specific energy of the inductor is almost independent of temperature. The total mass of the system must include the cryogenic system and will not necessarily show the same effects as the inductor only.

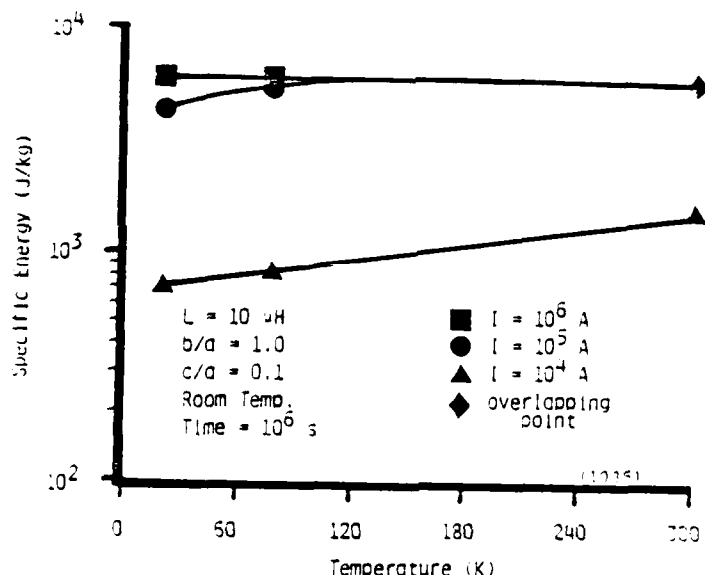


Figure C-10. Specific Energy vs. Conductor Temperature for Al-1100-0.

C.4.4 CURRENT

The effect of current on inductor specific energy is illustrated in Figure C-11. At low current, the specific energy is proportional to the current and has a slight dependence on the inductance. At high current, the energy density is independent of current and inductance.

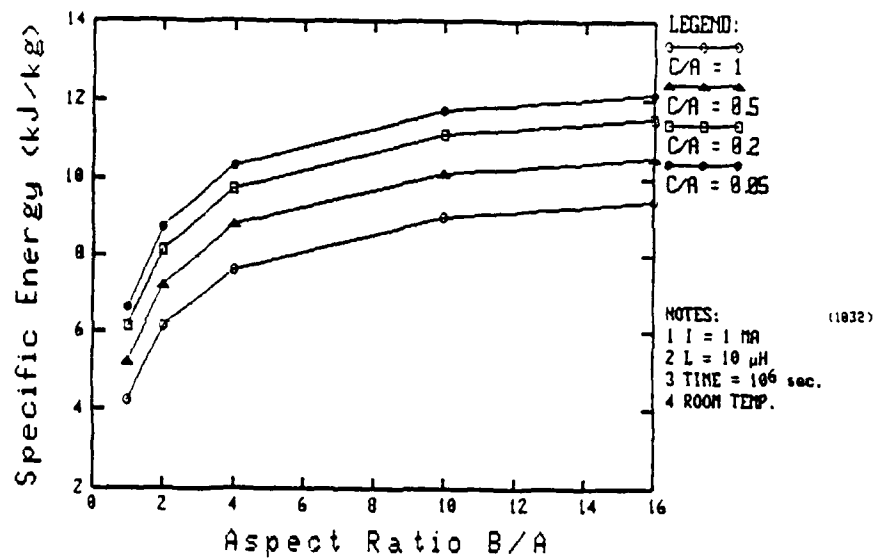


Figure C-8. Specific Energy vs. Length-to-Radius Ratio.

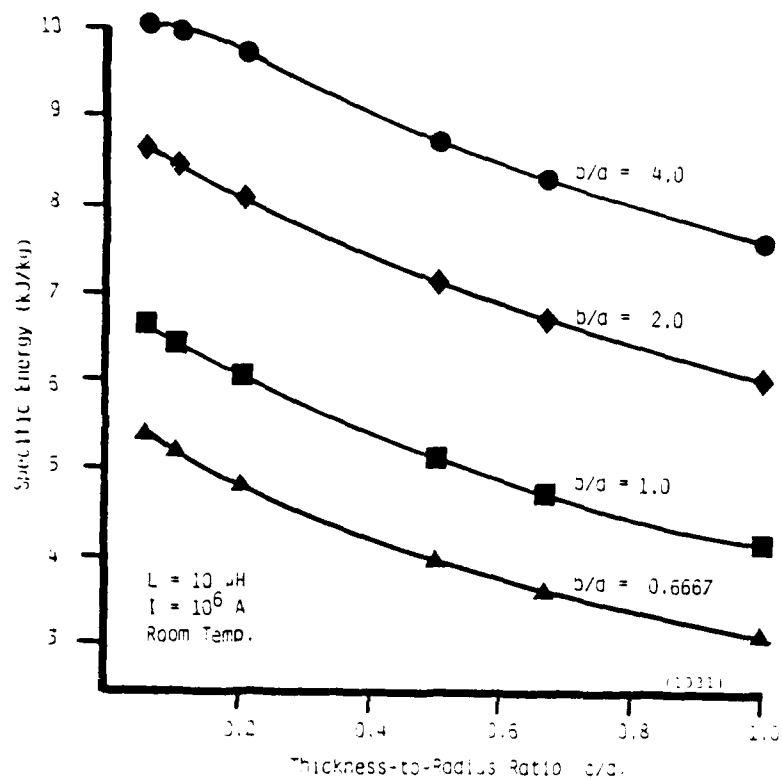


Figure C-9. Specific Energy vs. Thickness-to-Radius Ratio.

C.4.1.3 The Geometry

The geometry was varied to determine inductor mass sensitivity to these factors. The ranges examined were

$$0.05 < c/a < 1 \quad (C-32)$$

$$0.125 < b/a < 16 \quad (C-33)$$

$$s/A = 2500 \text{ m}^{-1} \quad (C-34)$$

C.4.1.4 The Outputs

The program calculates a number of inductor parameters. For the purposes of comparison the specific energy (stored energy per unit mass) was chosen as a figure of merit. The higher the specific energy the 'better' the inductor (i.e., a lower mass for a given stored energy). This parameter also permits rapid comparison of inductors with other types of energy storage for which specific energy is usually known. The specific energy was examined over the entire range of parameters described in the preceding paragraphs.

C.4.2 INDUCTOR GEOMETRY

The length-to-radius and the thickness-to-radius ratio both have an effect on the specific energy of inductors. A typical electromagnetic thruster case was chosen to examine the effect. The inductance was $10\mu\text{H}$, the current was 100kA , the conduction time was set at 10^6s (an energy storage case) and a temperature of 300°K was assumed. The results are shown in Figures C-8 and C-9.

Figure C-8 shows the effect of length to radius ratio at various thickness to radius ratios. For these conditions the specific energy is a few hundred joules per kilogram, an order of magnitude higher than dielectric capacitors. The specific energy for very long solenoids is approximately $1/2$ that of very short ones. Increasing the thickness-to-radius ratio improves the specific energy, however the results for very short ($b/a < 1$) solenoids are not accurate. The formula currently used to compute the inductance factor, k , is only accurate for either large b/a (>1) and/or

SECTION C.4

RESULTS

The computer program was exercised over a wide range of inductor parameters. The purpose was to examine the ability of the program to select realistic minimum mass inductors and to determine the characteristics of such inductors.

C.4.1 THE PARAMETERS

C.4.1.1 The Independent Parameters

The independent parameters are the inductance, L , the current, I , and the conduction time, t . The ranges investigated were derived from electromagnetic thruster considerations and were:

$$0.1\mu\text{H} < L < 25\mu\text{H} \quad (\text{C-29})$$

$$10^3\text{A} < I < 10^6\text{A} \quad (\text{C-30})$$

$$10^{-6}\text{s} < t < 10\text{yr} \quad (\text{C-31})$$

C.4.1.2 The Material Properties

The properties of Al-1100-0 aluminum were used. The performance at three temperatures, 21°K, 77°K and 300°K was examined. The properties used are summarized in TABLE 1.

TABLE 1. MATERIAL PROPERTIES, AL-1100-0

Temperature (°K)	Density (kg/m ²)	Stress (MN/m ³)	Resistivity (Ω-m)	Temperature Rise (°K)	Action Constant (A ² -s/m ⁴)	Heat Transfer (w/m ³)
21.00	2700.00	70.0	0.110E-8	50.0	0.130E17	0.100E5
77.00	2700.00	70.0	0.400E-8	50.0	0.110E17	0.500E5
300.00	2700.00	70.0	0.255E-7	50.0	0.300E16	0.100E7

C.3.5 COMPUTATIONAL TECHNIQUE

The minimum mass configuration is found by simultaneous solution of the equations developed in the previous sections. A closed form solution is not possible and a numerical approach must be used. A computer program was developed to find the solutions. The inductance, current, and conduction time were treated as the independent variables. The material properties of resistivity, density, action constant, and maximum stress must be chosen. The thermal transfer rate and perimeter-to-area ratio must also be selected. Finally, the geometrical factors c/a and b/a must be chosen. The program then finds the minimum mass inductor and determines the mass, resistance, number of turns, stress, and dimensions of the inductor. The choice between active and passive cooling is made based on minimizing mass. Reduced resistance configurations are found by incrementing the conductor cross sectional area and repeating the computation. The stress and thermal requirements are reduced in reduced-resistance inductors.

inductance during rapid discharge. During charging, current and magnetic field diffuse into the conductors. When the inductor is subsequently discharged, the magnetic field diffused into the conductors (and the energy associated with it) cannot be recovered. Only the field and energy stored in the 'open' area of the inductor and in the skin depth of the conductors can be recovered. The result is an apparent drop of inductance during discharge. The effect is most pronounced in thick coils, such as the Brooks configuration, where reductions of 20% or more can be expected. In addition, for multi-layer coils, internal circulating currents are induced which result in significantly increased resistive losses.

These high frequency effects can be controlled by minimizing inductor thickness, c , and by maximizing inductor thickness-to-radius ratio, c/a . If c/a is constrained to be less than about 0.1, the high frequency effects are modest.

C.3.4 INDUCTOR RESISTANCE

C.3.4.1 Minimum Mass Inductors

In the preceding paragraphs the conductor geometry for minimum mass inductors was developed. The resistance of these inductors can be readily calculated from

$$R = \xi z / A \quad (C-28)$$

The cross sectional area, A , is determined from thermal constraints and the conductor length, z , is determined from stress considerations. The minimum mass constraints result in maximum resistance. For some applications this resistance may be unacceptably high. The resistance can always be reduced but there is a mass penalty.

C.3.4.2 Resistance-Mass Scaling

In order to reduce the resistance the size of the inductor must be increased. The process begins by increasing the cross sectional area. The size and other characteristics of the inductor can then be recalculated using the previously developed formulas. There is no simple relationship between inductor mass and resistance.

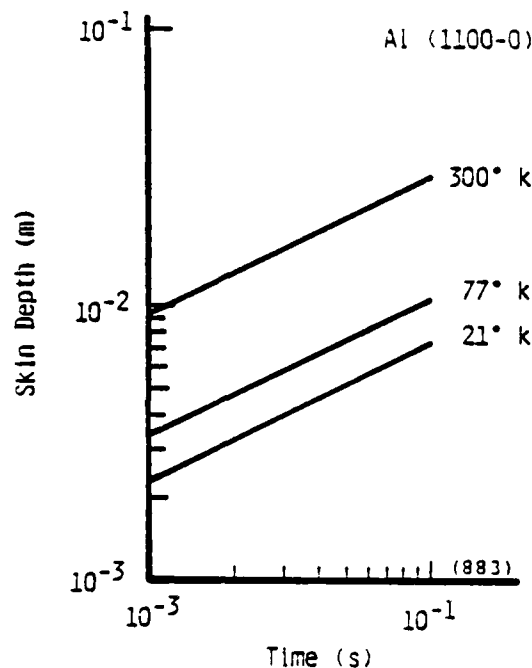


Figure C-7. The Electrical Skin Depth for Aluminum.

C3.3.4.1 Resistance

For pulses in which the skin depth is less than the conductor thickness, the resistance of the conductor increases above the DC resistance inversely with the skin depth. Therefore, an inductor can have a low DC resistance but yet have a high discharge resistance.

In energy storage applications the inductor must respond in two quite different time scales. Charging is a relatively slow process related to the frequency at which pulses are required. The discharge time, or pulse duration, is usually much shorter (typically by orders of magnitude) than the charging time. (Otherwise an energy store would not be required.) The skin effect resistance is not usually a problem during charging, but can be important during discharge. The thinner the conductors are, the less dependent the resistance is on pulse time. The high frequency resistance of an inductor can usually be designed to acceptably low values without seriously affecting inductor sizing or configuration.

C.3.3.4.2 Inductance

The other effect of diffusion limited skin depth is a reduction of inductance. This effect can result in a substantial reduction of apparent

forces the coil thickness, c , to increase (in order to retain the required conductor cross-sectional area). Under these circumstances, the required inductor thickness, c , can be considerably greater than the mean inductor radius, a . This of course is an impossible configuration. The stress (and therefore, the number of turns) must be reduced in order to achieve a geometrically possible inductor. The implication is that for certain application regimes a highly stressed inductor cannot physically be constructed. The geometrical constraint may be expressed as:

$$c/a < 1 \quad (C-26)$$

and must always be applied.

C.3.3.4 High Frequency Effects

Both energy-storage and pulse-forming inductors are subjected to high frequencies during pulsing. The effects of high frequencies on the resistance and the inductance of the coil can be important, particularly for high current designs where conductor size is large. When current is changed rapidly in a conductor, current diffusion effects confine the changing current to a thin surface layer or skin. The depth of this layer is related to the pulse duration by:

$$c_s = (\pi \xi t_p / \mu_0)^{1/2} \quad (C-27)$$

where c_s = skin depth
 t_p = pulse time.

The skin depth for aluminum at various temperatures is illustrated in Figure C-7. The skin depth for millisecond pulses (those of interest here) is less than 1 cm. If the skin depth is less than the conductor thickness then both the resistance and the inductance of the coil are affected.

$$\sigma = \mu_0 (NI)^2 a / 2\beta cb^2 \quad (C-22)$$

We note that:

$$NA_g = cb \quad (C-23)$$

and Equation C-23 can be reduced to:

$$\sigma = (\mu_0 I^2 / 2) (N/A_g) (a/b) / \beta \quad (C-24)$$

Equation C-24 can be rearranged to provide:

$$N = \beta (2\sigma A_g / \mu_0 I^2) (b/a) \quad (C-25)$$

The total number of turns in the solenoid is therefore determined by the allowable stress in the conductors.

Inspection of Equations C-6 and C-8 shows that coil mass is minimized by maximizing the number of turns in the inductor. From Equation C-25 we see that the number of turns is maximized by maximizing the allowable stress and by decreasing the allowable current. The effect of inductor aspect ratio (b/a) on the number of turns is not so clear because the aspect ratio also has a direct effect on the inductance factor, k. Increasing the geometrical cross section, A_g , increases the number of turns, but also directly increases inductor mass.

In summary, the conductor cross section is sized by thermal constraints while the number of turns is determined by allowable stress. Finally, there are two other constraints which also must be considered in inductor sizing. These constraints are geometry and high frequency affects.

C.3.3.3 Geometrical Constraints

Simultaneous application of the stress and thermal constraints described in the previous paragraphs can lead to impossible physical inductor dimensions. The problem is particularly severe for low current and/or long pulse duration inductors. In order to meet the stress design constraints (Eqn. C-19) the number of turns required becomes very large. This in turn

The presence of fins and/or cooling channels increases the geometrical cross section of the conductors. The geometrical cross section and the physical cross section are then related by:

$$A = \beta A_g \quad (C-18)$$

where A_g = geometrical cross section

β = 'solidity' ratio ≤ 1.0 .

The solidity ratio could be as low as 0.5 in order to achieve maximum cooling rates.

C.3.3.2 Stress Constraints

A solenoid acts as a magnetic pressure vessel. The magnetic field exerts a bursting pressure on the solenoid and this in turn induces stress in the windings. The stress in the conductors of a solenoid is related to the magnetic pressure by:

$$\sigma = P_m a / c \beta \quad (C-19)$$

where σ = conductor stress

P_m = magnetic pressure.

This equation is strictly true only if the stress is uniform throughout the conductors. The magnetic pressure is related to the magnetic flux density by:

$$P_m = B^2 / 2\mu_0 \quad (C-20)$$

where B = magnetic flux density

μ_0 = permeability of free space.

The magnetic flux density is related to inductor geometry and current through the Biot-Savart law by:

$$B = \mu_0 NI / b \quad (C-21)$$

Combining Equations C-19, C-20, and C-21 we obtain:

by increasing the heat transfer rate (i.e., forced convection/nuclear boiling), and by increasing the perimeter-to-area ratio (i.e., finning or channeling of the conductors).

Heat transfer rates vary from a few kW/m² for cryogenic cooling to a few MW/m² for boiling water cooling. The maximum achievable transfer rates depend strongly on the detailed design of the coolant channels and the velocity, pressure and Reynolds Number of the coolant flow. We shall assume the following heat transfer values for this study:

$$\dot{q}_H = 10^4 \text{ w/m}^2 \quad (\text{C-13})$$

for liquid hydrogen,

$$\dot{q}_N = 5 \times 10^4 \text{ w/m}^2 \quad (\text{C-14})$$

for liquid nitrogen, and

$$\dot{q}_W = 10^6 \text{ w/m}^2 \quad (\text{C-15})$$

for water.

The perimeter-to-area ratio, s/A , is maximized by finning and/or by providing many small channels for coolant flow in the conductor. In addition the surface of the fins or channels should be finely grooved to further increase the available cooling area. If this is done, the ratio is related only to the mean thickness of the conductor fins or webs by:

$$s/A = 4/d \quad (\text{C-16})$$

where d = mean thickness of the fins or webs. The perimeter to area ratio is maximized by minimizing the fin or web thickness. The minimum thickness is in practice probably related to the mean conductor thickness (i.e., c in Figure C-4). We shall assume that the minimum is given by:

$$d = 0.1c \quad (\text{C-17})$$

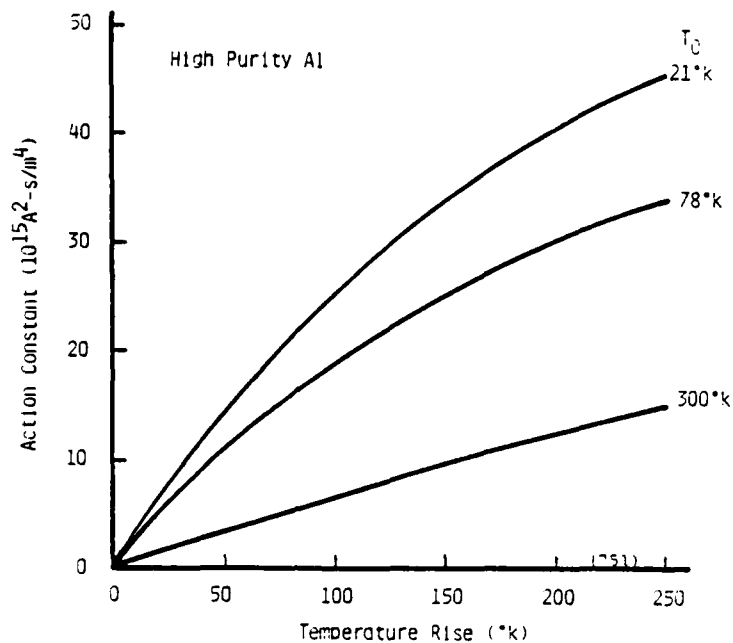


Figure C-6. Action Constant for Aluminum.

C.3.3.1.2 Active Cooling

Active cooling of a conductor can be characterized by equating the resistive dissipated power to the thermal transfer from the cooled surfaces. This may be written as:

$$I^2 \xi z / A = \dot{q} s z \quad (C-11)$$

where ξ = resistivity

\dot{q} = heat transfer rate

s = 'wetted' perimeter available for cooling.

Equation C-11 can be rewritten as:

$$A = I(\xi / \dot{q}(s/A))^{1/2} \quad (C-12)$$

The perimeter-to-area ratio, s/A , is a function of the geometry of the conductors. The cross-sectional area (and therefore, inductor mass) is reduced by reducing the resistivity (i.e., reducing conductor temperature),

designed as a thermal inertia. The conductor temperature is allowed to rise and the cross section is selected to keep the temperature rise acceptable for the required current level and the required conduction time. In the second approach, the conductors are actively cooled and the cross section is sized to permit steady-state transfer of the dissipated energy into the coolant. The approach which will provide the minimum-mass coil depends very strongly on the application. The tradeoffs and proper selection are made during computation.

C.3.3.1.1 Thermal Inertia

The required cross-sectional area for a thermal inertia design can be readily determined from the action integral:

$$\int I^2 dt = g_1 A^2 \quad (C-9)$$

where I = current

t = time of conduction

g_1 = action constant (dependent on temperature rise)

A = cross-sectional area.

The action constant, g_1 , is a function of the conductor material, the initial temperature, and the desired temperature rise. The values for aluminum are illustrated in Figure C-6.

Assuming a constant current, Equation C-9 can be rewritten as:

$$A = I(t/g_1)^{1/2} \quad (C-10)$$

The cross-sectional area, and therefore, the inductor mass, can be reduced by reducing the current or the pulse time or by increasing the action constant. The action constant can be increased by material selection, by increasing the allowable temperature rise, or by decreasing the initial temperature. Copper has a higher action constant than aluminum, however, that is more than compensated by the higher density of copper. Aluminum is usually the best overall material choice for minimum mass inductors.

C.4.6 CONDUCTION TIME

The specific energy is also a function of the conduction time and is shown in Figure C-13. In pulse-forming duty, time corresponds to the pulse time. In energy storage application, conduction is usually continuous or nearly so. For very short pulse times the inductor is sized as a thermal inertia. The minimum conductor cross section is then directly related to the pulse time. The specific energy of such inductors can be very high. As pulse time is increased the inductor must be actively cooled and the conductor cross section is independent of conduction time. The specific energy is usually lower for long-pulse actively-cooled inductors than for short-pulse thermal inertia designs.

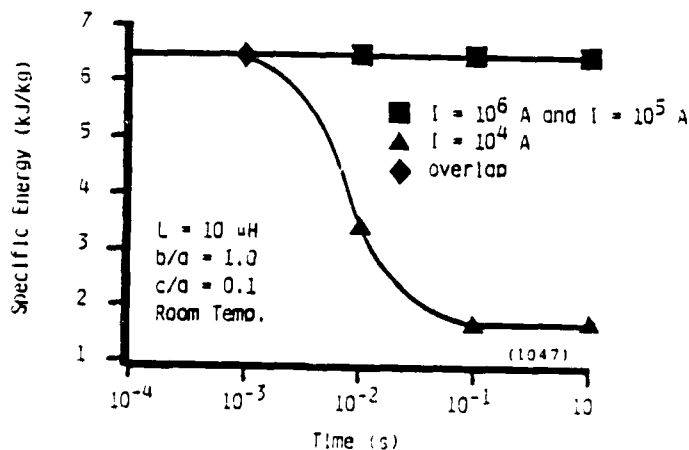


Figure C-13. Specific Energy vs. Conduction Time.

SECTION C.5

CONCLUSIONS

Several important conclusions can be drawn from this study of inductors. The conclusions are:

- (1) The specific energy of normal inductors is very attractive when compared to that of dielectric capacitors and is comparable to inertial stores.
- (2) Cryogenic operation has little effect on the specific energy of inductive stores. The mass of the cryogenic system must also be included to arrive at a system level conclusion. Cryogenic operation does, however, significantly reduce the inductor resistance.
- (3) The mass of an inductive store is a very complex function of material, operational, and application parameters. It is not possible to arrive at a single parameter (such as specific energy) which will completely characterize inductive energy stores for any application. The mass must be evaluated specifically for each application. The computational technique developed in this study meets this need.

BIBLIOGRAPHY

1. Grover, F. W. 'Inductance Calculations,' D. Van Nostrand Co., New York, 1946.
2. Wheeler, H. A., 'Inductance Formulas for Circular and Square Coils,' IEEE Proc., 70, pp. 1449-1450, 1982.

APPENDIX D

PARAMETRIC MODEL OF SUPERCONDUCTING ENERGY STORE
FOR SPACE PROPULSION

Report to IAP Research, Inc.

by

H.L. LAQUER Associates

Route 1, Box 445

Espanola, NM

87532

Revised

4 August 1983

TABLE OF CONTENTS

List of Symbols	ii
1. Overview	1
1.1 Components of Superconducting Energy Store	2
2. The Superconducting Inductor	2
2.1 Operating Considerations	2
2.2 Mass of Inductor	3
2.3 Surface Area of Inductor	4
2.4 Losses in the Inductor	6
2.5 Limitations on Fast Pulses	7
3. Current Leads	8
3.1 General Design Principles	8
3.2 Lead Refrigeration	8
3.3 Lead Resistance	9
3.4 Lead Mass	9
4. Dewars	10
4.1 Multilayer Insulation	11
5. Refrigerators	12
5.1 Refrigeration Alternatives	13
6. Example	13
7. References	16
8. List of Figures	17

List of Symbols

A_D	surface area of dewar
A_e	effective cross-sectional area of conductor
B	magnetic field strength
B_{dot}	Rate of field change
C_R	costs of refrigerator
D	geometry dependent coupling parameter
E_s	stored energy
J	current density averaged over coil structure
J_o	maximum operating current density in superconductor ($J_c/1.2$)
J_c	critical current density in superconductor proper
$J_c \times B$	flux pinning force in superconductor
L	$\rho \cdot k/T$, Lorenz ratio
M	mass, generic
M_D	mass of dewar
M_I	mass of insulation
M_I/E_s	specific mass for storing energy
M_L	mass of a pair of current leads
M_R	mass of refrigerator
M_S	mass of force containment structure
M_W	mass of conductor winding
P	rate at which a surface emits thermal radiation
P_o	refrigerator cooling capacity, 'frigiwatts'
P_a	refrigerator input power at ambient temperature
P_1	net exchange of radiant energy between two surfaces
P_2	heat conduction through solids
P_I	heat flux through insulation
P_{L1}	compressor power needed to refrigerate a pair of leads
P_{L2}	power dissipation in optimal leads
Q_o	hysteresis losses in superconductor
Q_R	rate dependent coupling losses in composite superconductor
$R_{L,opt}$	optimum resistance of a pair of leads
T_o	refrigerator output temperature
T_a	ambient temperature
T_p	triple point temperature

V	magnetic field volume (storing energy)
V_1	total conductor volume
V_0	volume of contained superconductor
V_R	volume of refrigerator
a	wire diameter
a_1	inner radius of solenoid
a_2	outer radius of solenoid
b	solenoid half length
d_0	diameter of superconducting filaments
d_1	winding thickness
d_s	density of structure
d_{avg}	average density
n	turns per unit length
ΔB	field change
λ	length
$\alpha = a_2/a_1$	ratio of outer to inner radius
$\beta = b/a_1$	ratio of half-length to inner radius
ϵ	emissivity
η_1	overall efficiency based on total power consumption,
η_2	conversion efficiency for 'high quality' pulse power
η_C	Carnot factor
η_R	combined thermal and mechanical efficiency of refrigerator
μ_0	$4 \cdot \pi \cdot 10^{-7}$, permeability of free space
ρ_{avg}	average resistivity over a temperature range
ρ_3	resistivity of high resistance web
σ	$5.67 \cdot 10^{-8}$ [$W \cdot m^{-2} \cdot K^{-4}$], radiation constant

APPENDIX D

PARAMETRIC MODEL OF SUPERCONDUCTING ENERGY STORE FOR SPACE PROPULSION

D.1 OVERVIEW

Superconducting inductive energy storage is an alternative method for long-term energy storage with the inherent advantage that the energy is immediately available in electrical form from a low impedance source. Compared to storage inductors made from normally conducting metals, superconducting inductors have no joule heating and an essentially infinite time constant. However, there are losses that vary with the rate of field change in the superconductor and there are refrigerator power demands that depend on these losses, on the surface area of the dewar, and on the currents that must flow from ambient to cryogenic temperatures. Maximum current densities and optimal field strengths are determined by the critical parameters of the superconductor. For large high-field systems, the mass and size of the force containment structure become the limiting factors. Temperature may be dictated by operational considerations or by refrigeration costs.

The objective of this note is to develop a simple parametric model of a superconducting energy store for space propulsion systems so as to permit a comparison with other storage methods in terms of system mass and energy efficiency. Presently envisaged systems require pulse energies from fractions of a kilojoule to half a megajoule, currents between 15 and 1200 kA, voltages generally below 1 kV, pulse lengths of 1 μ s to 6 ms, and pulse repetition frequencies between 0.4 and 19 Hz.

This comparison is somewhat complicated by the fact that two different types of energy efficiencies can be defined for a cryogenic system:

- (1) An overall efficiency, η_1 , based on total power consumption, including that of the refrigerator, and
- (2) A conversion efficiency, η_2 , which only looks at the 'high quality' pulse power inputs and outputs and disregards the power consumption of the refrigerator or the energy content of any 'used' cryogenic fluid.

The efficiency η_2 will be more or less constant for a given operation, but η_1 will decrease as the repetition rate decreases and when long periods of stand-by status are encountered.

D.1.1 Components of Superconducting Energy Store

The main components of a superconducting energy storage system are:

1. The superconducting inductor,
2. The current leads into the cryogenic region,
3. The dewar system, and
4. The refrigerator.

D.2 THE SUPERCONDUCTING INDUCTOR

D.2.1 Operating Considerations

To fully specify a superconducting storage system that will deliver a specified energy pulse at a specified repetition rate, requires a number of iterations on the following variables or parameters:

- Optimum field strength for minimum size and mass,
- Field shape and fringing as dictated by operational considerations,
- Ratio of stored to delivered energy,
- Type of superconductor and its operating temperature,
- Form and amount of stabilizer,
- Internal design of the conductor to minimize hysteresis and eddy current losses, and
- Coolant flow, plus location and sizing of the cooling channels.

Clearly, this is somewhat beyond the scope of the present analysis. However, it is always true that the highest possible field will give the most compact storage. Nevertheless, whenever high currents and high repetition rates are required in a self-sufficient environment, refrigeration economics, as determined by the Carnot factor, will push the system to the highest possible temperature.

Most superconducting magnets built to date operate at a temperature of about 4.2 K in liquid helium boiling at atmospheric pressure. Superconducting systems with dedicated closed cycle refrigerators permit operation at any temperature between 2 and 20 K. For the present task, an operating temperature of 13 K is suggested, in conjunction with a refrigerator output at 12 K. This is not a conventional choice for either magnets or storage inductors, but it is feasible as Stevenson (1973)¹ has reported a 5 T gas cooled solenoid operating at 13 K.

D.2.2 Mass of Inductor

In the following discussion the usual notation for solenoidal coils will be used. The ratio of outer to inner radius is

$$\alpha = a_2 / a_1 . \quad (2-1)$$

and the ratio of half-length to inner radius

$$\beta = b / a_1 . \quad (2-2)$$

Very large superconducting energy storage systems have been proposed over the past 15 years by Roger Boom and his associates at the University of Wisconsin. The latest of these reported by Eyssa, Boom, et al.² is a 100 kWh (360 MJ) study for NASA. It uses an earlier parametric analysis by Moses³ and suggests 10 T, 2 K coils at current densities of 250 to 500 A/mm². It also accepts the difficult task of non-uniform distribution of superconductor, as dictated by local field strengths, and proposes novel pure tension structures for force support. Since the design is not concerned about stray magnetic fields, it favors very short solenoids ($\beta = 0.3$), where most of the stored energy is outside the winding.

For smaller systems, one can afford to be somewhat less optimistic and consider longer coils with uniform current distributions. The mass of the inductor can be divided into three components: the superconductor, the stabilizer, and the structure providing force containment, support, and flow channels for the cryogen.

Realistic assumptions would be that the superconductor proper, with a density of 8 gm/cm³ will permit a current density, J_o , of 10⁹ A/m² (or 1000 A/mm²), and that the stabilizer and channel structure of density, d_s , will be present at an 'equivalent current density', J , of 1 to 5·10⁸ A/m² (100 to 500 A/mm²). The value of d_s would be 9000 kg/m³ for copper and stainless steel, and 2700 kg/m³ for aluminum and its alloys.

A still simpler approach can be based on an analysis of Lubell,⁴ who shows that for solenoids with uniform current density the specific mass, M/E_s , is proportional to the average density, d_{avg} , (usually close to d_s) divided by the square of the maximum field on the conductor, times some

(graphed) coefficients that depend on α and β . For small magnets ($E_s < 0.3$ MJ), the mass of the winding and coil mandrel predominates, and at $d_s = 9000$ kg/m³

$$M_W / (E_s \cdot B^2) = 45,000 [\text{kg} \cdot \text{MJ}^{-1} \cdot \text{T}^{-2}] , \text{ or} \quad (2-3)$$

$$M_W / (E_s \cdot B^2 \cdot d_s) = 5 [\text{m}^3 \cdot \text{MJ}^{-1} \cdot \text{T}^{-2}] . \quad (2-4)$$

For large magnets ($E_s > 3$ MJ), the mass of the force containment structure, M_S exceeds that of the conductor winding, M_W , and

$$(M_W + M_S) / (E_s \cdot B^2) = 8,500 [\text{kg} \cdot \text{MJ}^{-1} \cdot \text{T}^{-2}] , \text{ or} \quad (2-5)$$

$$(M_W + M_S) / (E_s \cdot B^2 \cdot d_s) = 1 [\text{m}^3 \cdot \text{MJ}^{-1} \cdot \text{T}^{-2}] . \quad (2-6)$$

For a mostly aluminum structure, $d_s = 3000$, and a field of 5 T these equations predict specific masses of 600 and 120 kg/MJ respectively.

It is worth noting that the minimum mass of the structure according to Levy's⁵ interpretation of the virial theorem comes to 11.5 kg/MJ for Armco 21-6-9 stressed to 200,000 psi. Lubell also graphs the specific masses for a number of coils between 0.05 and 20 MJ and shows values between 600 and 200 kg/MJ with a clear downtrend in the transition region, Fig. 1.

For space rated 0.5 to 1 MJ 5 T aluminum alloy solenoidal coils at 13 K, I would thus suggest a conservative design value of

$$(M_W + M_S) / E_s = 300 \text{ kg/MJ} . \quad (2-7)$$

D.2.3 Surface Area of Inductor

The following is not an inductor design by any means, but merely some rough assumptions to arrive at a plausible geometry and a conservative upper limit for the surface area. They are:

1. The inductor is a straight solenoid of rectangular cross-section, with an inner radius a_1 .
2. The length-to-diameter ratio β is 3. This approximates the energy density inside an infinite solenoid within 15%. The length is thus $6 \cdot a_1$, and the enclosed field volume is

$$V = 6 \cdot \pi a_1^3 . \quad (2-8)$$

3. All the field energy is contained within that volume so that the stored energy is

$$E_s = V \cdot B^2 / 2 \cdot \mu_0 , \text{ and} \quad (2-9)$$

$$a_1^3 = \mu_0 \cdot E_s / (3 \cdot \pi B^2) . \quad (2-10)$$

4. The average current density, J , in the winding volume is 100 A/mm², or 10⁸ A/m², so that the effective cross-sectional area of the conductor is

$$A_c = I / J . \quad (2-11)$$

5. The number of ampere turns per meter, $n \cdot I$, are obtained from the long solenoid formula as

$$n \cdot I = B / \mu_0 . \quad (2-12)$$

6. The winding thickness is

$$d_1 = n \cdot I / J = B / (\mu_0 \cdot J) , \text{ so that} \quad (2-13)$$

$$a_2 = a_1 + d_1 = a_1 + B / (\mu_0 \cdot J) \text{ and} \quad (2-14)$$

$$\alpha = 1 + B / (\mu_0 \cdot J \cdot a_1) . \quad (2-15)$$

7. There is a 50-mm space around the coil, so that

$$\text{Dewar Radius} = a_2 + 50 \text{ mm.} \quad (2-16)$$

8. End supports and plumbing take up 300 mm, so that

$$\text{Dewar Length} = 6 \cdot a_1 + 300 \text{ mm.} \quad (2-17)$$

D.2.4 LOSSES IN THE INDUCTOR

Changing fields cause energy dissipation in a superconductor. The magnitude of these losses is strongly dependent on the detailed internal layout of the conductor wire and cable. Fig. 2 shows the 'mixed matrix' structure for a composite superconductor specifically designed for millisecond pulse applications. The superconducting filaments are made as fine as possible to reduce hysteresis losses in the superconductor proper. Copper stabilizer is in close contact with each superconducting filament, but neighboring stabilizer elements are decoupled from each other by 'shields' of high resistivity Cu-Ni alloy. This reduces eddy currents in the copper stabilizer and, in conjunction with a wire twist, limits similar induced 'coupling' currents that are partly in the filaments and partly in the matrix.

The approximate relations from the previous section can also be used to estimate the total conductor volume as

$$V_1 = 6\pi a_1 d_1 \cdot (2a_1 + d_1) , \quad (2-18)$$

and that of the contained superconductor as

$$V_0 = V_1 J / J_0 . \quad (2-19)$$

Pinning centers are believed to enable superconductors to carry bulk supercurrents up to a critical current density J_c . For a wide range of fields the pinning force is constant, so that:

$$\text{Pinning Force} = J_c \times B . \quad (2-20)$$

The hysteresis losses per unit volume of superconductor represent the work done in pushing flux across pinning centers (Bean⁶), and are for each half-cycle (charge or discharge):

$$Q_0/V_0 = \Delta B J_c d_0 / 4 [J / m^3] , \quad (2-21)$$

where d_0 is the thickness of superconductor perpendicular to the changing field or the diameter of the superconducting filaments.

These losses are essentially independent of the rate of flux motion, and are only a function of the magnitude of the field change, ΔB , the critical current density, $J_c = 1.2 \cdot J_0$ (by design), and the filament diameter.

Most commercial superconducting materials are readily available with filament diameters down to 25 μm , and 5 μm is usually considered a practical limit. However, recent work by Larbalestier⁷ promises 1 μm filaments with improved current densities as well.

The rate dependent coupling losses in mixed matrix conductor that has been given the maximum practical twist pitch of eight wire diameters (Laquer⁸) are,

$$Q_R/(V_0) = (3\pi/8) \cdot a^2 \cdot \Delta B \cdot B\dot{}/(\rho_3 \cdot D) , \quad (2-22)$$

where:

a = Wire diameter, typically 0.5 mm

$B\dot{}$ = dB/dt , Rate of field change [T/s]

ρ_3 = ρ of high resistivity web, typically $10^{-7} \Omega \cdot \text{m}$

D = geometry dependent coupling parameter (0.148 max.).

In applying these equations we shall assume that the entire volume of superconductor is subject to the full ΔB and then divide by two in Eq (2-21) and by four in Eq (2-22). A more detailed analysis, again requiring a more complete coil design, would include integration of the losses over the actual field distribution.

D.2.5 Limitations on Fast Pulses

The above loss equations are probably valid for field change rates of up to several thousand Tesla per second. For faster rates and shorter pulses, however, one has to consider the distributed capacitance of the coil winding and the fact that the flux pinning mechanism, or its description breaks down for very high $B\dot{}$ values. If the repetition rates are not too high it might be possible to extract longer pulses and then shape them in a non-superconducting device.

AD-A152 244

ADVANCED ENERGY STORAGE SYSTEMS(U) IAP RESEARCH INC
DAYTON OH A CHALLITA ET AL JAN 85 IAP-TR-83-7
AFRPL-TR-84-099 F04611-82-C-0029

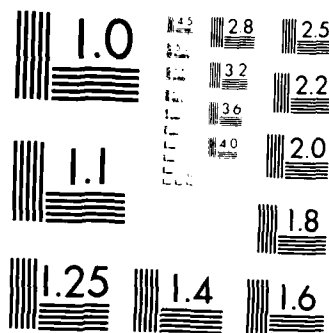
3/3

UNCLASSIFIED

F/G 21/3

NL





MICROCOPY RESOLUTION TEST CHART
 NATIONAL BUREAU OF STANDARDS-1963-A

D.3 CURRENT LEADS

D.3.1 General Design Principles

The function of cryogenic leads is to conduct a current from a power source at ambient temperature to an electrical device at cryogenic temperature. In doing so they also conduct heat between these temperatures, and generate I^2R losses. Since for a metal, thermal and electrical conductivities are fundamentally related, as shown by the near constancy of the Lorenz ratio, $L = \rho k/T$, there is no way to have one without the other.

The accepted procedure is to fabricate leads as 'counterflow' heat exchangers and size them so as to minimize the heat flow into the cryogenic environment at the rated current. If the cryoelectrical device operates in boiling liquid, all energy influx is taken up in the latent heat of vaporization of the cryogen. All of the boil-off can be channeled through the leads, and, provided the leads are thermally anchored in the cryogen, lead boil-off and flow can be self-regulating. No heat will be conducted directly to the device.

Minimum energy input from well-designed counterflow leads into boiling helium amounts to 1.2 watt/kA/lead, as shown empirically and from numerous analyses, e.g., Keilin and Klimenko⁹ and Efferson¹⁰

D.3.2 Lead Refrigeration

In an open system with boiling liquid, no use can be made of the sensible heat of the cold escaping gas. Most of the lead refrigeration is 'free'. However, in a closed system the sensible heat taken up by the lead flow gas in returning to ambient temperature also has to be produced by the refrigerator. The more gas is 'bypassed' into the current leads, from the normal return flow through the heat exchanger, the more difficult it becomes to maintain refrigerator efficiency.

Gerhold¹¹ has discussed the problem in general terms. Using his analysis together with some unpublished Los Alamos work, I suggest a provisional formula for the compressor power, P_{L1} , needed to refrigerate a pair of leads at a steady current

$$P_{L1} = 20 \cdot I / T_0 \text{ [MKS]} \quad (3-1)$$

where T_0 is the minimum gas temperature in the system. It should be noted that this formula assumes, in effect, 22% of Carnot efficiency. It is probably optimistic and needs to be examined in more detail. Nevertheless, it serves to point out the tremendous refrigeration penalty imposed by high-current leads. A pair of steady state 50 kA leads at 12 K would require 83 kW of compressor power.

For quickly varying and pulse currents, it should be possible to time-average the current by relying on the heat capacity of the lead. However, depending on pulse length and repetition rate, such a scheme could introduce flow and pressure instabilities and degrade the heat exchange efficiency of the lead.

D.3.3 Lead Resistance

Current leads optimized for minimum refrigeration have a resistance that produces a fixed voltage drop of about 45 mV at the design current. This optimum is quite independent of the material, its resistivity, the temperature coefficient of resistivity, or the length of the lead. Nor does it matter whether the lead is of constant cross-section or tapered toward the cold end. We thus have for the optimum resistance of a pair of leads:

$$R_{L, \text{opt}} = 0.09/I \text{ [MKS] } , \quad (3-2)$$

and for the corresponding power dissipation:

$$P_{L2} = 0.09 \cdot I \text{ [MKS] } . \quad (3-3)$$

A 50 kA current thus will dissipate 4.5 kW in a pair of leads.

D.3.4 Lead Mass

The length of each lead is usually set in the range of 0.5 to 1 m by space, mechanical, and insulation considerations. Since $R = \rho \cdot \lambda / A$, we get from eq'n (3-2) for each lead

$$(\lambda/A)_{\text{opt}} = 0.045 / (I \cdot \rho_{\text{avg}}) \text{ [MKS] } . \quad (3-4)$$

Clearly, a material with the lowest average resistivity, ρ_{avg} , over the relevant temperature range, i.e., a high purity metal such as Al or Cu, would then permit the lightest leads. Unfortunately, such leads are less stable and less tolerant of excess currents (more likely to burn out) than those made from less pure materials with higher resistivities and smaller temperature coefficients. The increased mass and heat capacity of alloy leads also improves their thermal inertia for pulse service, albeit at the expense of increased power dissipation when the current is increased above the optimum.

An extreme choice would be brass with a resistivity of $8 \cdot 10^{-8} \Omega \cdot m$ at 300 K and half that value at 10 K. If the lead is tapered for a constant ρ/A ratio along its length, λ , we get an average cross-sectional area

$$A_{avg} = 10 \cdot \rho_{avg} \cdot \lambda \cdot I = 6 \cdot 10^{-7} \cdot I \text{ [MKS]} . \quad (3-5)$$

For 0.5 m, 50 kA brass leads the average crosssection would be 300 cm^2 and the mass of two leads would be a massive 261 kg.

A better material would be Deoxidized High Phosphorus Copper (DHP) with a resistance ratio of 7 and an average resistivity of $1 \cdot 10^{-8} \Omega \cdot m$. A pair of DHP 50 kA leads would weigh 27 kg if straight with a 30 cm^2 cross-section, and 32 kg with a linear 5:1 taper from 12 to 60 cm^2 .

Information for aluminum alloy leads has not yet been collected, but similar resistivities are available. I therefore suggest an interim formula of

$$M_L = 0.2 \cdot I \text{ [kg / kA]} . \quad (3-6)$$

D.4 DEWARs

Dewar vessels are passive structures whose only purpose is to reduce the heat flow from ambient temperature to a cryogenic device, experiment, or fluid. In the vacuum of space two modes of heat transfer that are important in an atmospheric environment are absent. These are gas convection and gas conduction. Only radiation heat transfer between surfaces and conduction through solids remain.

The rate at which a surface of area, A , emits thermal radiation is given by the Stefan-Boltzmann relation

$$P = \sigma \cdot \epsilon \cdot A \cdot T^4 , \quad (4-1)$$

where: ϵ is the emissivity of the surface, and

$\sigma = 5.67 \cdot 10^{-8} \text{ [W} \cdot \text{m}^{-2} \cdot \text{K}^{-4} \text{]}$ the radiation constant.

The net exchange of radiant energy between two surfaces of equal (low) emissivity and equal area at T_1 and T_0 takes place at

$$P_1 = \sigma \cdot \epsilon \cdot A \cdot (T_1^4 - T_0^4) . \quad (4-2)$$

Clearly, radiative heat transfer is controlled almost entirely by the high temperature surface. A 300 K aluminum surface with $\epsilon=0.02$ will radiate 9.2 W/m^2 . The return radiation from a surface at 10 or 20 K is lower by four or five orders of magnitude, and therefore is insignificant in reducing the heat leak.

Conduction through solids, on the other hand, is expressed by the Fourier equation, which is linear in the temperature gradient:

$$P_2 = k \cdot A \cdot (T_1 - T_0) / \lambda . \quad (4-3)$$

Optimally designed dewars usually have equal heat losses through radiation and conduction. There is no sense in trying to make one heat leak orders of magnitude lower than the other. As a matter of fact, any significant additional energy losses in the system should also be considered when designing the dewar insulation.

D.4.1 Multilayer Insulation

The ideal insulation would consist of a number, N , of concentric, massless, low-emissivity, isothermal, floating radiation shields in a perfect vacuum. Such an arrangement would reduce the heat leak given by equation (4-2) by a factor of $N+1$.

Commercial multilayer insulation, known as 'super-insulation', tries to approximate the ideal by interleaving thin aluminum foils with fiberglass paper spacers or by using multiple wraps of crinkled aluminized mylar. The latter is the lighter option and also can be aluminized with strips or small squares so as to minimize eddy currents induced by changing magnetic fields.

The temperature profile in these insulations, however, is not as one might expect for a series of pure radiation shields, but becomes linear below 70 K. This indicates that conduction through contacts is predominant in the low temperature region, effectively shorting out the insulation that would be provided by the radiation shields. On the other hand, with the absence of gravity in a space dewar, it is conceivable that contact forces and the resulting heat flow could be reduced through proper design.

Aluminized mylar insulation is available in bulk form. Application data, published by National Research Corporation¹², suggest that the material is most effective when applied at 16 layers/cm (40 layers/inch) and then will have a heat flux between 300 K and 20 K of

$$P_I = 18.9 / N [W m^{-2} \cdot layers^{-1}] , \quad (4-4)$$

provided the number of layers, N , is between 30 and 150.

The mass of the insulation is

$$M_I = 8.94 \cdot 10^{-3} \cdot N [kg \cdot m^{-2} \cdot layers] . \quad (4-5)$$

As long as the dewar will only be operated in space, its inner aluminum alloy shell need be no more than 5 mm thick and its outer shell a mere 1 mm. This would give a mass of

$$M_D = 16.2 [kg \cdot m^{-2}] . \quad (4-6)$$

For short pulses, eddy currents in the dewar shell may be undesirable and a fiberglass epoxy dewar of similar mass may have to be used.

D.5 REFRIGERATORS

Information on space-rated refrigerators is rather scarce in the open literature, probably for classification and proprietary reasons. However, Strobbridge¹³ has done a thorough survey of cryogenic refrigerators. After taking out the inevitable Carnot factor

$$\eta_C = T_0 / (T_a - T_0) , \quad (5-1)$$

the combined thermal and mechanical efficiency, η_R , does not depend on the temperature, T_0 , between 1.8 and 90 K. Fig. 3 taken from his paper shows that it is only a function of the refrigeration capacity (frigiwatts), P_0 . For small refrigerators with large surface-to-volume ratios η_R is small. It reaches 15 % for kilowatt machines and levels off at about 33 % for megawatt units.

Strobridge also gives a relation for costs, C_R , (which have to be adjusted for inflation since 1969) as a function of the compressor power at ambient temperature, P_a

$$P_a = P_0 / (\eta_C \eta_R) \text{ and} \quad (5-2)$$

$$C_R = 48 \cdot P_a^{0.7} \text{ [1969 \$, watt]}. \quad (5-3)$$

Finally, we can extract the following relations from his plots of mass and volume against frigiwatts for refrigerators in the 10 to 30 K range:

$$M_R = 60 \cdot P_0^{0.7} \text{ [kg, watt]}, \text{ and} \quad (5-4)$$

$$V_R = 0.055 \cdot P_0^{0.85} \text{ [m}^3\text{, watt]}. \quad (5-5)$$

D.5.1 Refrigeration Alternatives

Stored cryogens present an alternative to mechanical refrigeration, but only for relatively short missions and low refrigeration powers. The latent heat of vaporization can be used effectively above the triple point temperature, T_p . Various cryogens have been used in this manner for cooling either equipment or radiation shields. For liquid hydrogen the cooling power amounts to about 450 kJ/kg. The triple point is at 13.8 K, mandating a slight increase in the operating temperature of the inductor or a short span (magnetic ?) refrigerator. Detailed analysis of these options is beyond the scope of this note.

D.6 EXAMPLE

We summarize the use of the parametric model with the example of a 500 kJ, 50 kA, 5 T superconducting storage inductor at 13 K and refrigeration at

12 K, recognizing that most of the numbers are intended to be conservative, i.e., on the high side.

From 2-7 we get the mass

$$M_W + M_S = 150 \text{ kg.}$$

From 2-10 Inner radius: $a_1 = 0.139 \text{ m}$

Coil length: $2 \cdot b = 6 \cdot a_1 = 0.832 \text{ m}$

From 2-13 Wind. thickness: $d_1 = 0.040 \text{ m}$

From 2-14 Outer radius: $a_2 = 0.139 + 0.040 = 0.179 \text{ m}$

From 2-16 Dewar radius: $a_2 + 0.05 = 0.229 \text{ m}$

From 2-17 Dewar length: $2 \cdot b + 0.3 = 1.132 \text{ m}$

Dewar surface: $A_D = 1.96 \text{ m}^2$

From 2-18 Cond. Volume: $V_1 = 3.33 \cdot 10^{-2} \text{ m}^3$

This does not include any structure and corresponds to a mass of about 100 kg compared to the above conservative value of 150 kg.

From 2-19 Supercond Volume

$$V_0 = 3.33 \cdot 10^{-3} \text{ m}^3$$

From 2-21 Hysteresis Loss for $\Delta B = 5 \text{ T}$

$$d_0 = 5 \text{ } \mu\text{m}$$

$$Q_0 = 21 \text{ J / half cycle}$$

if the entire conductor sees the full field change, otherwise divide by 2 and get 10.5 J.

At a rep rate of 1 Hz this dissipates

$$P_0 = 2 \cdot 10.5 = 21 \text{ frigiwatts.}$$

(Same loss for charge and discharge).

From 2-22 Coupling Loss for the given typical values and

$$\Delta B = 5 \text{ T}$$

$$\dot{B} = 5000 \text{ T/s (1 ms pulse)}$$

$$Q_R = 1660 \text{ J / discharge cycle}$$

if the entire conductor sees the full field change, otherwise divide by 4 and get 415 J.

At a rep rate of 1 Hz this dissipates

$$P_1 = 415 \text{ frigiwatts.}$$

(Assuming that \dot{B} for recharge is negligible).

From 3-1 Lead Refrigeration for 50 kA

$$P_{L1} = 83 \text{ kW Compressor Power}$$

Divide by 2 for average current of 25 kA.

$$P_{L1} = 42 \text{ kW}$$

From 3-3 Lead Dissipation for 50 kA

$$P_{L2} = 4.5 \text{ kW of Pulse Power}$$

Divide by 4 for average power dissipation.

From 3-6 Lead Mass for 50 kA

$$M_L = 10 \text{ kg}$$

Sum of average low temperature power dissipation from hysteresis and coupling (neglecting 'ordinary' eddy currents and deferring the lead problem)

$$P_0 + P_1 = 436 \text{ frigiwatts}$$

If these losses are present all the time, dewar losses would need be no less than 44 w.

From 4-4 Layers of Superinsulation to achieve 44 W

$$N = 18.9 \cdot A_D / 44 = 0.84 ,$$

or a single radiation shield.

A simple 40 layer insulation system would have a heat leak of

$$P_I = 18.9 \cdot A_D / 40 = 0.93 \text{ frigiwatts.}$$

This would minimize standby power requirements.

From 4-5 and 4-6 Dewar Mass

$$M_I + M_D = 0.7 + 31.8 = 32.5 \text{ kg.}$$

From 5-1 Carnot Factor at 12 K

$$\eta_C = 0.042 \text{ or } 4.2\%$$

From Fig. 3 Refrigerator Efficiency (iterated)

$$\eta_R = 0.13 \text{ or } 13\%$$

From 5-2 Compressor Power (neglecting leads)

$$P_a = 437 / (0.042 \cdot 0.13) = 80 \text{ kW}$$

Total Compressor Power

$$P_{L1} + P_a = 122 \text{ KW}$$

From 5-2 and 5-4 combined Refrigerator Mass

$$M_R = 5680 \text{ kg}$$

Total Mass

$$M_T = 150 + 10 + 32 + 5680 = 5872 \text{ kg}$$

To calculate efficiencies η_1 and η_2 more information is needed on operation and duty cycles and on the prime power supply.

Clearly, the biggest power and mass requirements are associated with the size of the refrigerator, which, in turn, is determined by the currents in the leads and the coupling (eddy current) losses in the composite superconductor.

D.7 REFERENCES

1. Stevenson, R., '50 kG Gas Cooled Superconducting Solenoid Operated at 13 k,' Cryogenics 13, 524-5 (1973).
2. Eyssa, Boom, McIntosh, and Li, 'A 100 kWh Energy Storage Coil for Space Applications,' IEEE Trans. MAG-19, 1081-5 (1983).
3. Moses, R. W. Jr., 'Configurational Design of Superconductive Energy Storage Magnets,' Adv. in Cryogenic Eng., 21, 140-8 (1976).
4. Lubell, M. S., 'The Specific Weight of Superconducting Magnets,' ORNL Eng. Sciences Memo No. 117 (1973).
5. Levy, R. H., J. Am. Rocket Soc. 32, 787- (1962).
6. Bean, C. P., 'Magnetization of Hard Superconductors,' Phys. Rev. Lett. 8, 250 (1962).
7. Larbalestier, D. C., Personal Communication, March 1983.
8. Laquer, H. L., 'Superconductivity, Energy Storage and Switching, in Energy Storage, Compression and Switching,' W. H. Bostick, V. Nardi and O. S. F. Zucker eds., Plenum Press, New York, (1976), pp. 279-305.
9. Keilin, V. E. and Klimenko, E. Yu., 'Investigation into High Current Leads in Liquid Helium Applications,' Cryogenics 6, 222-8 (1966).
10. Efferson, K. R., 'Helium Vapor Cooled Current Leads,' Rev. of Scient. Inst. 38, 1776-9 (1967).
11. Gerhold, J., 'Optimization of refrigerator-cooled current leads for superconducting devices,' Cryogenics, 16, 401-8 (1976).
12. National Research Corporation, NRC-2 Superinsulation, 4 pp (1967).
13. Strobridge, T. R., 'Refrigeration for Superconducting and Cryogenic

Systems,' IEEE Trans. NS-16, 1104-8 (1969).

D.8 LIST OF FIGURES

Fig. 1. Specific Mass of Superconducting Coils, from Lubell (1973)

Fig. 2. Mixed Matrix Superconductor Designed for Millisecond Pulse Applications, from Laquer (1976)

Fig. 3. Efficiency of Low Temperature Refrigerators as a Function of Refrigeration Capacity (Frigiwatts), from Strobridge (1969)

END

FILMED

5-85

DTIC